Hybrid additive and subtractive manufacturing of large-scale and multi-material parts

by

Eric Weflen

A dissertation submitted to the graduate faculty

in partial fulfillment of the requirements for the degree of

DOCTOR OF PHILOSOPHY

Major: Industrial Engineering

Program of Study Committee:
Frank Peters, Co-Major Professor
Matthew Frank, Co-Major Professor
Peter Collins
Michael Dorneich
David Eisenmann

The student author, whose presentation of the scholarship herein was approved by the program of study committee, is solely responsible for the content of this dissertation. The Graduate College will ensure this dissertation is globally accessible and will not permit alterations after a degree is conferred.

Iowa State University

Ames, Iowa

2023

DEDICATION

To my family, Dave, Cheri and Dan. Thank you for all of the support.

TABLE OF CONTENTS

LIST OF FIGURES

LIST OF TABLES

NOMENCLATURE

ABS	Acrylonitrile Butadiene Styrene
ABS-CF	ABS with Chopped Carbon Fiber Filler
AIC	Akaike Information Criterion
AM	Additive Manufacturing
ANOVA	Analysis of Variance
BAAM	Big Area Additive Manufacturing
BIC	Schwarz’s Bayesian Information Criterion
CAD	Computer Aided Design
CNC	Computer Numerical Control
CTA	Cognitive Task Analysis
DED	Directed Energy Deposition
DOA	Degree of Automation
DOE	Design of Experiments
FCAW	Flux Cored Arc Welding
FDM	Fused Deposition Modeling
FFF	Fused Filament Fabrication
FOM	Flat Top Overlapping Model
GMAW	Gas Metal Arc Welding
HDPE	High Density Polyethylene
HM	Hybrid Manufacturing
HTA	Hierarchical Task Analysis
LSAM	Large Scale Additive Manufacturing

MDF	Medium Density Fiberboard
MEX	Material Extrusion
MPI	Magnetic Particle Inspection
MSE	Mean Standard Error
NDE	Nondestructive Evaluation
PAUT	Phased Array Ultrasonic Testing
PP-GF	Polypropylene with chopped glass fiber
PQR	Process Qualification Record
ROS	Robot Operating System
SDM	Shape Deposition Modeling
TOM	Tangent Overlapping Model
TPU	Thermoplastic Urethane
UTS	Ultimate Tensile Strength
UX/UI	User Experience and User Interface
WAAM	Wire Arc Additive Manufacturing
WA-DED	Wire Arc Directed Energy Deposition
WPS	Welding Procedure Specification
YTS	Yield Tensile Strength

ACKNOWLEDGMENTS

I would like to thank my co-advisors, Dr. Frank Peters and Dr. Matt Frank along with my committee members, Dr. Peter Collins, Dr. Michael Dorneich, and Dr. David Eisenmann, for their guidance and support throughout the course of this research.

I would also like to thank the other advisors, collaborators and graduate students in the research lab, Dr. Iris Rivero, Dr. Srikanthan Ramesh, Dr. Sharon Lau, Dr. Jakob Hamilton, Dr. Ali Khorasani, Dr. Daniel Schimpf, Mohamed Eldakroury, Logan Beguhn, Jake Croghan, Jeff Tscherter, Landon Getting, Michael Ginther, Colton Richardson, Matt Janowicz, Carl Michellotti, and Randev Goonesekere. I learned so much working with each of you. Thanks to all of the undergraduate researchers, Moira Henderson, Katie Wyatt, Matt Bindel, Mitchell Black, Justin Nock, Michael De Jong, Peter Exley, Willem Potter, Nathan Pinto, and Luke Auderer who helped make sure the research projects could be completed. Thank you Dr. Barrett Caldwell for being my mentor in the IISE future faculty program. Special thanks to Aaron Jordan for fixing everything that I broke in the lab, and Emma Bailey for making endless test samples.

I would also like to thank Dr. Eric Johnson for providing direction and support on many research projects. Thanks to the members of the Steel Founders Society of America (SFSA), especially David Poweleit, Raymond Monroe for their support and guidance.

In addition, I would also like to thank my manager David Johnson, and my mentor Dr. Michael Benedict, along with the other friends, colleagues, and bozos at PARC.

Thanks to Dr. Kris Johansen for getting me involved in the entrepreneurship programs, and Judi Eyles, Peter Hong, and Ray Hansen for their continued support.

Finally, thanks to all my friends, colleagues, the department faculty and staff for making my time at Iowa State University a fantastic experience.

ABSTRACT

This research presents methods of improving manufacturing resilience and agility through the hybridization of multiple materials and multiple processes into a system. The increasing demand for product customization, expedited delivery times, and persistent supply chain disruptions highlight the importance of adopting versatile manufacturing systems for rapid production at the point of need. While traditional manufacturing consists of discrete, material-specific processes, automation and hybridization efforts are driving toward a convergence of processes and materials that allow for system adaptability to meet changing needs. However, the integration of traditionally incompatible or discrete processes and materials requires methods of interfacing them together which have not yet been developed.

The presented work is the development of interfaces between the machine and the part, material regions within a part, additive and subtractive processes within a machine, and between the operator and the machine. An emphasis is placed on high deposition rate processes for polymers and metals, paired with machining for dimensional accuracy and surface finish. A novel approach to bonding and releasing polymer parts to the build plate of a large-scale additive manufacturing system has been developed. Similar mechanically interlocking features to those used on the build plate are deployed to create multi-material parts consisting of metal and polymer composite regions. A new method of integrating robotic machining and metal additive manufacturing using advanced sensing is established to rework, repair, or upgrade metalcastings. An approach to integrating the operator into a complex system of robotic hybrid manufacturing processes is presented. This research contributes to realizing hybridized manufacturing processes that can produce heterogeneous, multi-material parts to improve manufacturing flexibility and resilience.

CHAPTER 1. GENERAL INTRODUCTION

1.1 Background

Humans are unique in the way they manufacture, use, and share improvements to complex tools to enhance their living conditions (Vaesen, 2012). Advances in production methods and tool usage accumulate over time, which has been attributed to social abilities to teach and pass down technological advancements across generations (Herrmann, Call, Hernández-Lloreda, Hare, & Tomasello, 2007; Richerson & Boyd, 2005). Manufacturing these tools and products to improve the quality of life is a crucial human activity, but limitations in manufacturing technologies impose constraints on achievable designs. A primary goal of manufacturing research should be eliminating such limits and constraints to allow for higher-performing designs.

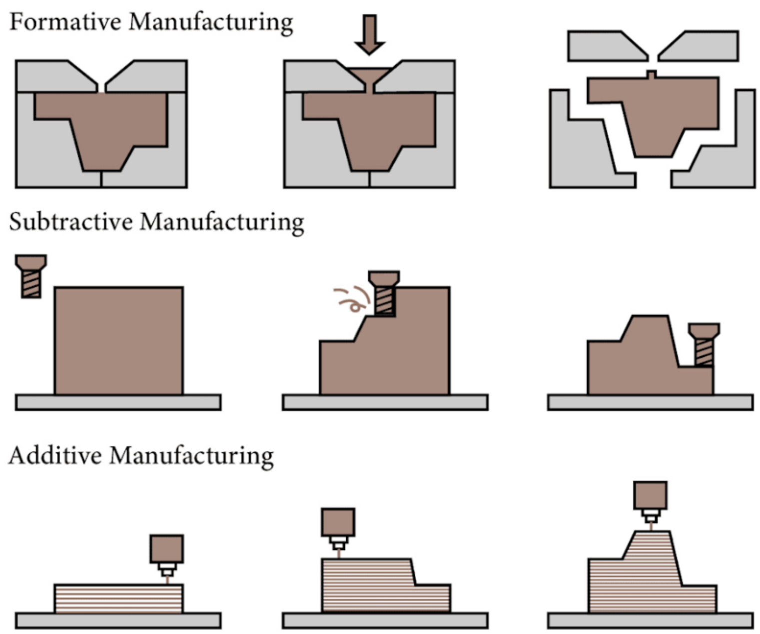

Figure 1. High-level categorization of manufacturing methods (Redwood et al., 2017)

Manufacturing methods can be broadly categorized into three groups: formative, subtractive, and additive (Figure 1) (Redwood, Schoöffer, & Garet, 2017). Typically, a discrete combination of these methods paired with assembly processes produces a product or component. Each category encompasses various manufacturing processes and techniques, each with its unique capabilities and limitations.

Forming processes, such as casting, injection molding, and forging, shape a material stock into the desired geometry. Although these processes can quickly generate intricate geometries, a forming tool is required, and it must be possible to release the object. Subtractive processes, like milling, turning, and grinding, remove material from a starting piece. However, the geometry is limited by the cutting tool's accessibility. While many processes, like welding or the application of coatings, are additive processes, modern additive manufacturing (AM) typically involves the layer-based deposition of a material using computer-based control and planning algorithms to automate the process. While AM can produce complex geometries with internal features, achieving the desired surface finish without sacrificing productivity through reduced layer height remains challenging, particularly for larger parts. This challenge is particularly pronounced as the size of the parts being produced grows. These processes typically focus on making parts of a single material. Each of these categories of manufacturing processes possesses strengths and weaknesses that can limit the designs that can be produced effectively.

Large-scale additive manufacturing systems are specifically designed to enable high deposition rates to quickly produce large parts on the scale of multiple meters in size. Sometimes referred to as big area additive manufacturing (BAAM), these technologies address several challenges conventional AM techniques face, which often struggle with size limitations and extended processing times when producing large parts (Love, Post, Noakes, Nycz, & Kunc, 2021). By utilizing high deposition rates up to 100x those of typical Fused Filament Fabrication (FFF) systems and polymer pellet feedstocks that are up to 10x cheaper, BAAM allows for the rapid production of sizable objects, surpassing the capabilities of traditional 3D printing methods (Post et al., 2016). This is often achieved through fused granulate fabrication (FGF) in polymers and through wire arc additive manufacturing (WAAM), a directed energy deposition (DED) approach, for metals. This technology has found application in various industries, such as automotive, aerospace, and construction, where large parts are often required in low production volumes (Pignatelli & Percoco, 2022). However, Large-scale AM systems can accumulate large residual stresses due to their size and lack of a temperature-controlled chamber, which can cause the part to distort or warp and peel off the print surface (Love et al., 2014). These systems also trade layer resolution to achieve these high levels of productivity.

Hybrid manufacturing (HM) processes that combine multiple approaches into a single process can overcome the limitations of a single manufacturing method and create a new process with capabilities beyond those of a single process (Lauwers et al., 2014). Out-of-envelope hybrid manufacturing (HM) processes combine processes in separate steps. In contrast, in-envelope hybrid manufacturing systems combine the processes into a single system that can allow for simultaneous or iterative application of multiple processes (Frank et al., 2017b). Hybridization of AM and subtractive machining has shown strong synergies because it can enable large layers to be deposited in the additive process

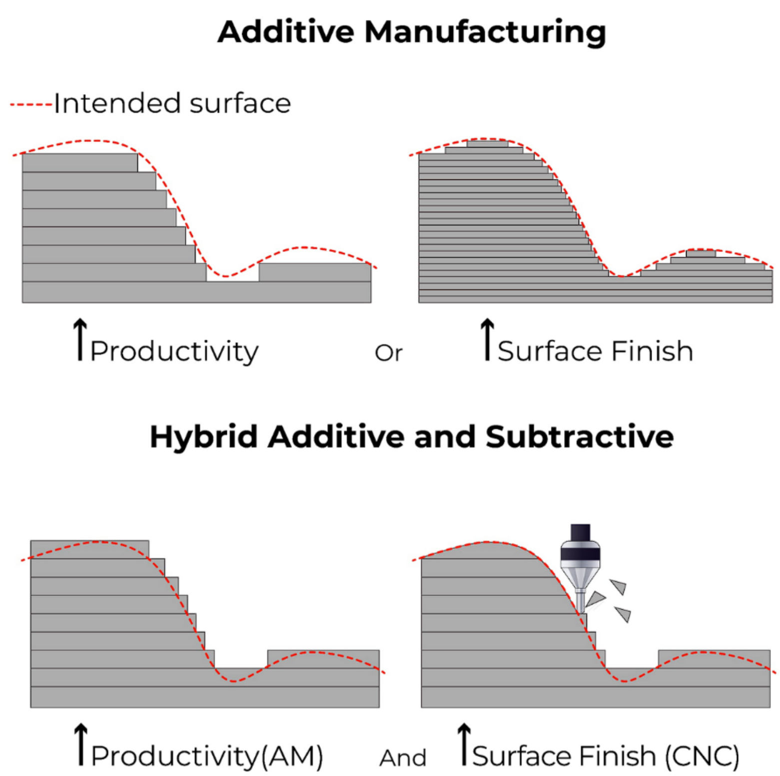

Figure 2. Typical AM systems improve surface finish by decreasing layer thickness, at the cost of productivity. HM processes can achieve the required surface finishes without sacrificing productivity.

to increase productivity, and machining is applied to achieve the required surface finish (Figure 2) (Jones, 2014). In a typical additive manufacturing process, there is an error between the intended surface described by the model and the actual surface caused by the stair-stepping error of the layers. To better reproduce the desired surface, a smaller layer thickness can be used, but at the expense of productivity. However, with hybrid additive and machining processes, large layers can be deposited in the additive process to increase productivity. For this reason, hybrid manufacturing can be beneficial when paired with the high deposition rates found in large-scale AM (Feldhausen, Heinrich, et al., 2022). Excess material is deposited to act as a machining allowance where needed. Milling can then be used to achieve the required surface finish. However, these additional machining forces and vibrations can further increase challenges bonding large-scale parts to the build plate.

Similar synergies to those found in HM can be achieved by hybridizing multiple materials to be used within a single part (Zheng, Williams, Spadaccini, & Shea, 2021). Each material has unique properties with advantages and disadvantages that may limit part functionality and performance when the designer must select a single material and a single manufacturing process. However, multi-material parts allow for further optimization of the material properties to better achieve the part’s function. Achieving these benefits through assemblies of parts can lead to additional complexities and processing steps to produce and assemble the parts. Today, multi-material parts in AM are often limited to similar materials that can be fused using the same approach used to build a single material part (Nazir et al., 2023a). However, materials with dissimilar material properties offer more opportunities to increase part performance by expanding the space for design optimization (Li & Kim, 2018). However, we lack robust interfaces for dissimilar material regions for hybrid manufacturing systems.

Increasing the range of materials that can be used to build multi-material parts would allow designs to be optimized beyond what can be achieved with a single material.

There is a drive to bring together hybrid materials and hybrid processes into a single platform to improve manufacturing process flexibility and resilience when faced with external influences like natural disasters, global pandemics, or conflicts (Bapat et al., 2022). Convergent manufacturing platforms promise to deliver multi-material parts using multiple processes to allow for on-demand production of parts at the point of need (National Academies of Sciences, 2022). However, bringing these technologies requires the development of integration methods at the interface between the materials and processes. Furthermore, the operators of these systems will face increasing complexity and need support to operate these systems effectively (Fillingim and Feldhausen 2023).

There is a need to develop methods of integrating additive and subtractive manufacturing processes and to improve the interface between material regions in dissimilar materials to move toward convergent manufacturing systems. These systems can help prevent supply chain challenges and expand available design space, allowing for better part performance. Progressing these hybrid manufacturing and hybrid material systems can reduce the limitations on existing designs. To achieve this overarching goal, it is critical that these systems are developed in a way that considers the user of the system. Otherwise, the novel approaches may fail to achieve the full potential they offer.

1.2 Research Problem and Objectives

This research works to solve the research problem that we lack methods for interfacing multiple processes, multiple dissimilar materials, and users into hybrid manufacturing systems for the production of large-scale and multi-material parts. It aims to advance towards the vision of convergent manufacturing by developing interfaces by meeting the four objectives:

Objective 1: Develop an adaptable build plate interface to fixture large-scale parts in a hybrid manufacturing system that can overcome warping and machining forces and release the part when processing is complete.

Objective 2: Develop a mechanical interface between dissimilar materials for hybrid additive and subtractive manufacturing processes compatible with various materials.

Objective 3: Develop a process and the associated parameters for integrating the formative matalcasting process with subtractive machining and additive wire-arc deposition in a hybrid manufacturing system.

Objective 4: Create a system architecture for implementing hybrid manufacturing in foundries that integrates advanced sensing and the operator's skills.

Developing an interface for a build plate to bond and fixture a polymer object in a hybrid manufacturing system during processing that can withstand warping and machining forces will enable the interleaving of the additive deposition and subtractive machining processes. The ability to release the object when processing is complete will reduce the time and cost of part removal. An interface between regions of dissimilar materials, such as metals and polymers, can expand the range of multi-material parts that can be produced in hybrid manufacturing systems. These new material combinations allow high-performance part designs that more effectively meet their functional requirements.

Harsh working conditions in steel foundries have led to a skilled labor shortage. Developing an approach to automating the production welding process of removing production anomalies and refilling them using arc welding can distance the worker from those harsh conditions. Developing an approach to integrating subtractive machining and wire-arc additive manufacturing into a single hybrid manufacturing system can enable this automation. However, the uniqueness of each production anomaly and the low production volumes in job shop foundries can make automation mean that rigid automation may not succeed. By integrating the user into the system and relying on the human ability to handle ambiguous situations, automation can succeed in this environment.

1.3 Dissertation Organization

Chapter two presents a review of relevant research and supporting literature. Chapter three discusses designing and evaluating mechanically interlocking features for a print surface that can withstand machining forces in hybrid manufacturing and resist distortion caused by residual stress in large-scale additive manufacturing applications. Chapter four presents research on creating mechanically interlocking interfacial features to produce parts consisting of dissimilar materials, such as metals and polymers. Chapter five describes the process for integrating hybrid additive and subtractive manufacturing into the steel foundry formative process and the investigation into the associated process parameters. Chapter six outlines the development of a hybrid manufacturing system using wire arc additive manufacturing (WAAM) and machining to automate low-volume welding of anomalies in steel casting. Chapter seven presents general conclusions and opportunities for further research, development, and innovation.

1.4 References

Bapat, S., Sealy, M. P., Rajurkar, K. P., Houle, T., Sablon, K., Malshe, A. P., … Applications, ". (2022). Applications of Hybrid Manufacturing during COVID-19 Pandemic: Pathway to Convergent Manufacturing . *Smart and Sustainable Manufacturing Systems* , *6*(1), 12–22. https://doi.org/10.1520/SSMS20210022

Feldhausen, T., Heinrich, L., Saleeby, K., Burl, A., Post, B., MacDonald, E., … Love, L. (2022). Review of Computer-Aided Manufacturing (CAM) strategies for hybrid directed energy deposition. *Additive Manufacturing*, *56*, 102900. https://doi.org/10.1016/J.ADDMA.2022.102900

Frank, M. C., Harrysson, O., Wysk, R. A., Chen, N., Srinivasan, H., Hou, G., & Keough, C. (2017). Direct Additive Subtractive Hybrid Manufacturing (DASH) Œ An Out of Envelope Method. *Solid Freeform Fabrication Symposium*. https://doi.org/10.7449/2017/MST_2017_366_368

Herrmann, E., Call, J., Hernández-Lloreda, M. V., Hare, B., & Tomasello, M. (2007). Humans have evolved specialized skills of social cognition: The cultural intelligence hypothesis. *Science*, *317*(5843), 1360–1366. https://doi.org/10.1126/SCIENCE.1146282

Jones, J. B. (2014). The synergies of hybridizing CNC and additive manufacturing. *Technical Paper - Society of Manufacturing Engineers*.

Lauwers, B., Klocke, F., Klink, A., Tekkaya, A. E., Neugebauer, R., & McIntosh, D. (2014). Hybrid processes in manufacturing. *CIRP Annals - Manufacturing Technology*. https://doi.org/10.1016/j.cirp.2014.05.003

Li, C., & Kim, I. Y. (2018). Multi-material topology optimization for automotive design problems. *Proceedings of the Institution of Mechanical Engineers, Part D: Journal of Automobile Engineering*, *232*(14), 1950–1969. https://doi.org/10.1177/0954407017737901/FORMAT/EPUB

Love, L. J., Kunc, V., Rios, O., Duty, C. E., Elliott, A. M., Post, B. K., … Blue, C. A. (2014). The importance of carbon fiber to polymer additive manufacturing. *Journal of Materials Research*, *29*(17), 1893–1898. https://doi.org/10.1557/JMR.2014.212

Love, L., Post, B., Noakes, M., Nycz, A., & Kunc, V. (2021). There's plenty of room at the top. *Additive Manufacturing*, *39*, 101727. https://doi.org/10.1016/J.ADDMA.2020.101727

National Academies of Sciences, E. and M. (2022). Convergent Manufacturing: A Future of Additive, Subtractive, and Transformative Manufacturing: Proceedings of a Workshop. *Convergent Manufacturing: A Future of Additive, Subtractive, and Transformative Manufacturing*. https://doi.org/10.17226/26524

Nazir, A., Gokcekaya, O., Md Masum Billah, K., Ertugrul, O., Jiang, J., Sun, J., & Hussain, S. (2023). Multi-material additive manufacturing: A systematic review of design, properties, applications, challenges, and 3D printing of materials and cellular metamaterials. *Materials and Design*, *226*. https://doi.org/10.1016/J.MATDES.2023.111661

Pignatelli, F., & Percoco, G. (2022). An application- and market-oriented review on large format additive manufacturing, focusing on polymer pellet-based 3D printing. *Progress in Additive Manufacturing*, *7*(6), 1363–1377. https://doi.org/10.1007/S40964-022-00309-3/FIGURES/10

Post, B., Lind, R., Lloyd, P., Kunc, V., Linhal, J., & Love, L. (2016). *The Economics of Big Area Additive Manufacturing*. Retrieved from https://repositories.lib.utexas.edu/handle/2152/89664

Redwood, B., Schoöffer, F., & Garet, B. (2017). The 3D Printing Handbook: Technologies, Design and Applications; 3D Hubs: Amsterdam, The Netherlands, 2017; ISBN 9789082748505. In *3D Hubs*. Retrieved from https://lib.hpu.edu.vn/handle/123456789/31395

Richerson, P. J., & Boyd, R. (2005). *Not by genes alone : how culture transformed human evolution*. 332.

Vaesen, K. (2012). The cognitive bases of human tool use. *Behavioral and Brain Sciences*, *35*(4), 203–218. https://doi.org/10.1017/S0140525X11001452

Zheng, X., Williams, C., Spadaccini, C. M., & Shea, K. (2021). Perspectives on multi-material additive manufacturing. *Journal of Materials Research*, *36*(18), 3549–3557. https://doi.org/10.1557/S43578-021-00388-Y/FIGURES/3

CHAPTER 2. REVIEW OF RELATED WORK

Over the past several decades, Additive Manufacturing (AM) has emerged as a transformative technology revolutionizing how products are designed, manufactured, and distributed. It offers the potential to create complex geometries, reduce waste, decrease process planning time, and enable mass customization. This literature review aims to provide a comprehensive understanding of various aspects of AM, focusing on large-scale additive manufacturing technologies, hybrid additive and subtractive (machining) processes, wire arc additive manufacturing, and multi-material parts. This review aims to establish the foundation and context for the proposed dissertation, which investigates the development of methods for producing large-scale and multi-material parts in hybrid manufacturing systems.

2.1 Additive Manufacturing

Commonly referred to as 3D printing or rapid prototyping, AM is a manufacturing process in which materials are typically deposited layer-by-layer to create three-dimensional objects in an automated fashion based on a 3D digital model (Wohlers et al., 2016). The term "additive" is used to distinguish this process from traditional "subtractive" manufacturing techniques, such as milling or turning, or “forming” processes, such as injection molding or metal casting. Modern AM was launched in the 1980s with the development of stereolithography (Patent No. US4575330A, 1984). Since then, AM has evolved into a diverse range of techniques, including seven technological and process categories (Gibson, Rosen, Stucker, & Khorasani, 2021). AM technology has tended to diverge into increasingly specialized processes to meet the unique needs of specific classes of parts or applications more efficiently.

The ISO/ASTM 52900 standard defines seven categories of AM processes: 1) Binder Jetting (BJT), 2) Directed Energy Deposition (DED), 3) Material Extrusion (MEX), 4) Material Jetting (MJT), 5) Powder Bed Fusion (PBF), 6) Sheet Lamination (SHL), and 7) Vat Photopolymerization (VPP) (Figure 3) (ISO/ASTM, 2021). These AM technologies have been used to process a wide range of materials, from polymers and metals to ceramics and even biological tissues, though research has focused primarily on single material systems or multi-material parts consisting of compatible materials (Gibson et al., 2021; Nazir et al., 2023a). AM research has demonstrated benefits such as design freedom, reduced material waste, and the possibility of creating multi-material and large-scale components, which has attracted the interest of various industries including aerospace (Blakey-Milner et al., 2021), construction (Pajonk, Prieto, Blum, & Knaack, 2022), biomedical (Rezvani Ghomi, Khosravi, Neisiany, Singh, & Ramakrishna, 2021), automotive (Salifu, Desai, Ogunbiyi, & Mwale, 2022), and others (Wohlers et al., 2022).

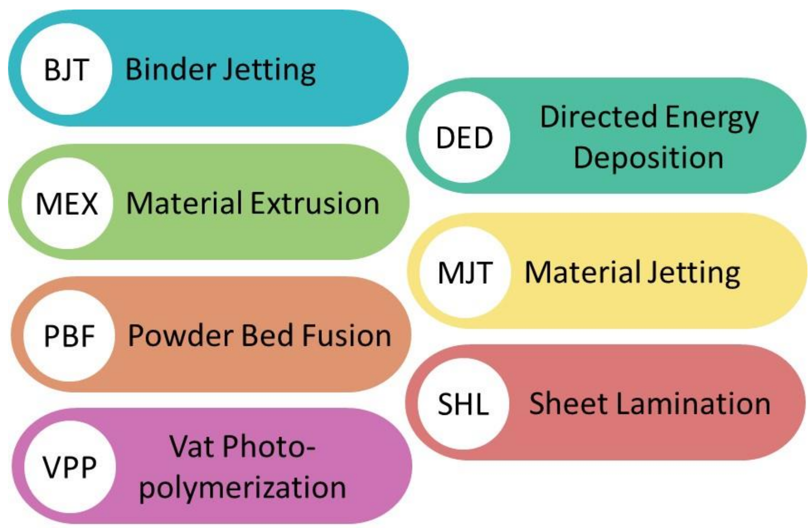

Figure 3. Seven categories of AM as defined by ISO/ASTM 52900.

However, despite its significant potential, research problems still exist for AM. Challenges include limitations in material properties, build size, surface finish, and the need for post-processing (Ngo, Kashani, Imbalzano, Nguyen, & Hui, 2018; Vafadar, Guzzomi, Rassau, & Hayward, 2021). As the field of AM continues to evolve, researchers work to develop solutions to overcome these challenges and expand the full potential of this technology to remove manufacturing-driven constraints on designers (Joshi et al., 2012).

2.2 Big Area Additive Manufacturing (BAAM)

Typical MEX Additive Manufacturing systems, often using Fused Filament Fabrication (FFF) technology, have build volumes that could produce parts smaller than one cubic meter. To expand the capabilities of MEX, Oak Ridge National Laboratory (ORNL) developed a system (Figure 4) in collaboration with Cincinnati Incorporated that could produce parts on the scale of multiple cubic meters (Curran et al., 2016; Duty et al., 2017; Holshouser et al., 2013; Love et al., 2015). This class of systems was named Big Area Additive Manufacturing (BAAM) but can also be referred to as Large Scale Additive Manufacturing (Chesser, Wang, Vaughan, Lind, & Post, 2022; Roschli et al., 2019). This system uses a screw extrusion system which allows for the use of polymer pellet feedstock common in the polymer processing industry that provides for a 2-10x reduction in material cost compared to the materials used in filament or plunger-fed MEX systems (Figure 5) (Love et al., 2021; Post et al., 2016). The screw extrusion system was paired with nozzles with diameters in the multiple millimeter scale, allowing material deposition to occur at a rate 100x greater than typical MEX systems, allowing faster part fabrication (Talagani et al., 2015). Due to the excessive energy consumption required to warm an area at that scale, the system forwent the traditional temperature-controlled build environment and used carbon fiber reinforcement

Figure 4. Fabricating a car chassis using a BAAM printer (Curran et al. 2016).

material to control the warping of parts (Love et al., 2014). As a testament to the innovation presented by this system, numerous manufacturers now sell and service BAAM systems, which now include Cincinnati Incorporated, Thermwood Corporation, Caracol AM, CEAD Group, DYZE Design, Cosine Additive, Loci Robotics, Massive Dimension, Titan Robotics (3D systems), REV3RD, Hybrid Manufacturing Technologies, CMS SpA, and others.

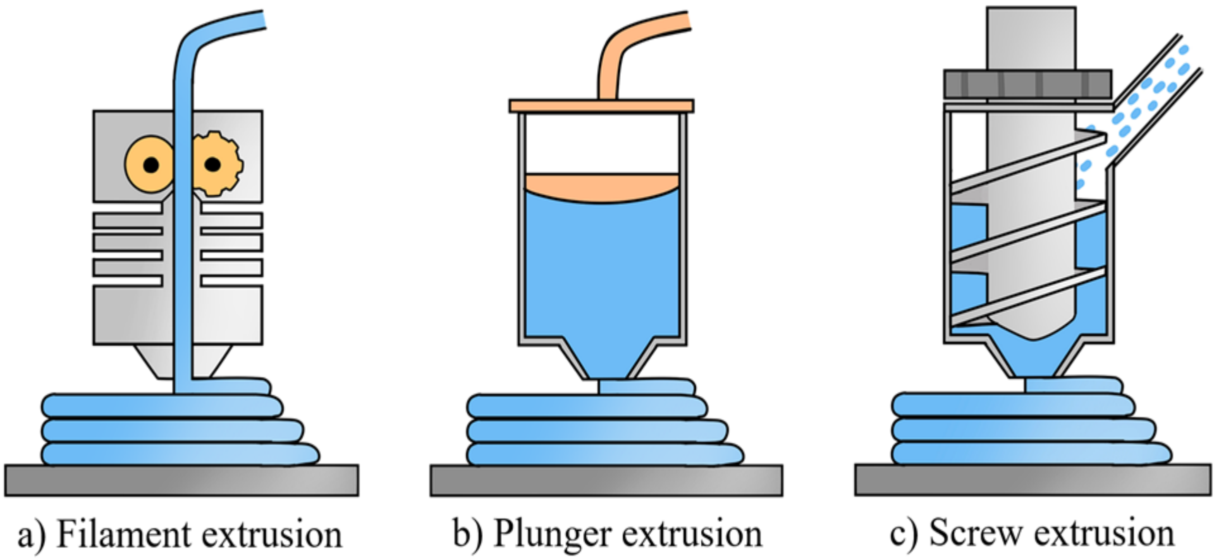

Figure 5. Typical MEX AM systems deposit material using a) filament-driven extrusion, b) plunger extrusion, or c) pellet-fed screw extrusion used on BAAM systems.

Despite these successes, open research problems exist for BAAM systems that can hamper adoption. One key challenge facing this industry is retaining the part during processing and removal when processing is complete (Roschli et al., 2022; Schroeder & Weaver, 2022). In MEX systems, the structure that supports the part is typically referred to as the build platform or plate, while the interface where the part bonds to the print bed is referred to as the build surface (ISO/ASTM, 2021). Build plate research attempts to achieve a bonded to the part while processing occurs and provide the structure to prevent the part from warping due to the buildup of residual stress (Roschli et al., 2022; Weflen, Peters, & Frank, 2022). However, a high bond between the part and the build plate can lead to challenges in removing the components (Figure 6).

Manufacturers of MEX systems have attempted to overcome this challenge through several methods. Those approaches include print surface materials with switchable chemical bond strengths, choosing a bond strength just above that needed for a successful print, using water-soluble raft material, and allowing for a peeling action for removal from the print surface and many other solutions (Goldschmidt, 2022). A key challenge of relying on chemical bonding between the parts is that the bond strength will depend on the material being used to produce the part, limiting materials that can be processed on that system (Govender, Kissi, Larsson, & Tho, 2021; Jeyachandran, Bontha, Bodhak, Balla, & Doddamani, 2021; Schirmeister, Hees, Licht, & Mülhaupt, 2019). While attempts have been made to apply several of these approaches to BAAM systems, the high forces due to residual stresses build up in the large parts produced in a non-controlled environment have proven to be challenging to overcome (Roschli et al., 2022; Schroeder & Weaver, 2022). ORNL uses thermal fusion to a polymer sheet of the same material being printed that is retained using a vacuum table (Roschli et al., 2022). However, the sheet can be challenging to remove from the part and can warp during processing, resulting in a loss of vacuum. Thermwood Corporation has

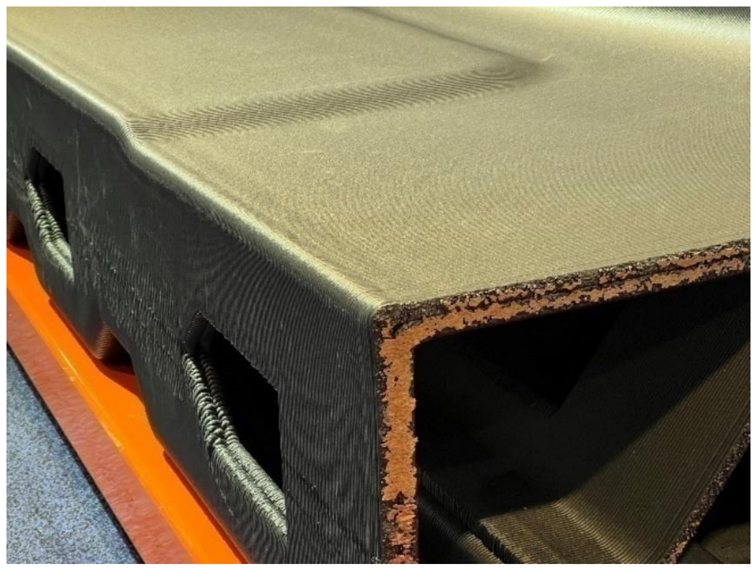

Figure 6. Pellets and MDF adhered to bottom face of a part made on a Thermwood LSAM system.

applied a medium-density fiberboard (MDF) where pellets of the same material being printed are adhered to the surface (Figure 4) to generate a high level of mechanical and thermal fusion bonding (Patent No. US10569523B2, 2017). The strong bond retains the part, but removal from the print surface can be challenging and often results in both pellets and wood attached to the bottom of the part (Figure 6). Thermwood has used the reduction in inter-layer bond strength caused by material cooling to tune the bond strength between the part and build plate to meet the needs of a specific application (Figure 7). However, this still results in a single bond strength for processing and part removal. CEAD Group has developed a mechanically interlocking print surface that releases the part by actuating a mechanism that releases the interlocking ("Print bed - CEAD | Large Scale Additive Manufacturing," 2023). Still, this system faces challenges with scaling to larger sizes. Mechanical cleating has been investigated for use on belt-style print beds that would release as the belt deflects as it moves over a roller (Shafer, Siddel, & Elliott, 2017). Other manufacturers of large-scale MEX systems currently rely on directly bonding the part to an MDF sheet, sometimes with adhesion-promoting chemicals or materials (Figure 8). This can require the use of a sizeable first-layer raft to achieve the needed bond strength to retain the part.


Figure 7. Separated first layer raft with reduced bond strength controlled by inter-layer cooling.

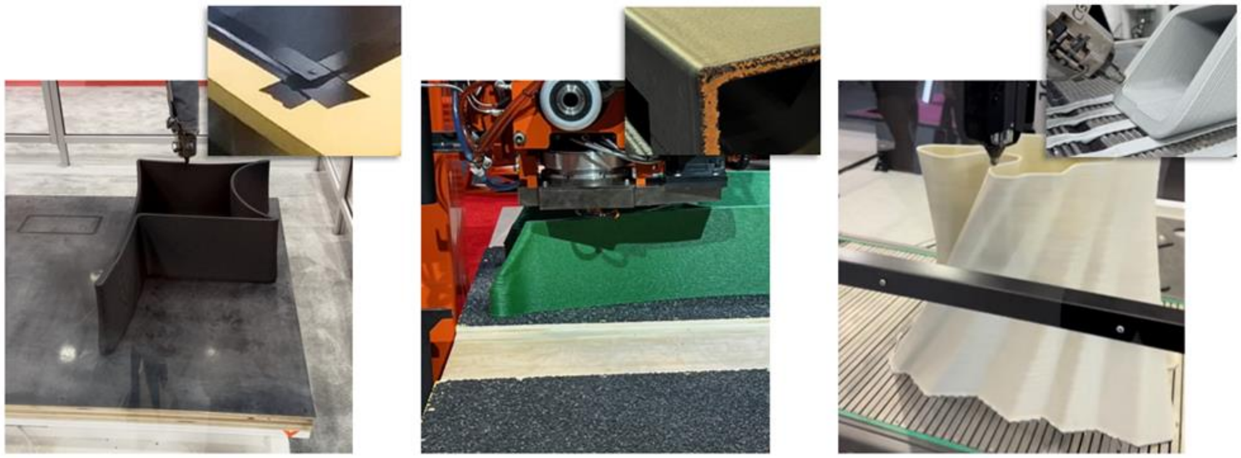

a) b) c)

Figure 8. Examples of current print surfaces for large-scale AM systems include a) a polymer sheet on a vacuum table, b) polymer pellets adhered to a fiberboard sheet, and c) an actuated mechanically interlocking surface.

2.3 Wire Arc Additive Manufacturing (WAAM)

Another large-scale AM process used to produce parts on the scale of multiple cubic meters is Wire Arc Additive Manufacturing (WAAM). While arc welding has always been an additive process (Patent No. US1533300A, 1920), WAAM adds automation to manual welding operations to rapidly produce geometry (Zhang & Li, 2001; Zhang, Chen, Li, & Male, 2003). WAAM is a Directed Energy Deposition (DED) process, also called wire-arc directed energy deposition (WA-DED). This process uses an arc welding process like Gas Metal Arc Welding (GMAW) paired with a 6-axis robot or multi-axis gantry for automated motion control to deposit metal material using a layer-by-layer approach (Greer et al., 2019). WAAM has been used for the production of large near-net-shape parts like those typically produced in the metalcasting industry, using high deposition rates similar to those used in BAAM (Cunningham, Flynn, Shokrani, Dhokia, & Newman, 2018; Wu et al., 2018). WAAM research has demonstrated the potential to reduce production lead times and bring down costs through high deposition rates and local, tool-free parts production (Love et al., 2021).

WAAM has been used in the production of end-use parts for several industries, including automotive, agriculture, and aerospace (Babu, Love, Peter, & Dehoff, 2016; Nycz et al., 2017; Omiyale, Olugbade, Abioye, & Farayibi, 2022). This process has been used to produce machining stock that reduced waste compared to standard stock material used in Computer Numerical Control (CNC) machining operations, which benefits parts made from high-cost materials by lowering the buy-to-fly ratio (Treutler, Wesling, Camacho, Chunhui, & Yang, 2021). Since a wire feedstock is used, parts consisting of high volatility materials like aluminum and magnesium have been produced instead of the powders used in many other metal AM processes (Treutler et al., 2021). WAAM has been applied to repair damaged parts, such as machine tools (Lee, Lee, & Kim, 2022).

Figure 9. Production welding of a steel casting using gas metal arc welding.

Arc welding is heavily used in the metalcasting industry for in-process welding on castings (Figure 9) (Monroe, 2019). Anomalies such as porosity, inclusions, or cracks can be removed using Arc-Air gouging or grinding, refilled using arc welding, and then surface grinding can be used to meet the customer’s surface requirements (Blair & Stevens, 1995; Branza, Deschaux-Beaume, Sierra, & Lours, 2009; David, Monroe, & Thomas, 2015). WAAM has demonstrated potential in this industry to automate the production welding process in a steel foundry (Weflen, Black, Frank, & Peters, 2021).

Despite the large number of successful applications of WAAM, the process faces several challenges. Overhang features can be difficult to produce with WAAM systems due to similar challenges that make out-of-position welding challenging (Greer et al., 2019; Yuan et al., 2021). This can limit the geometry that can be produced and make the build orientation a critical attribute of the process that must be considered in the design. The reliability of robotic WAAM systems can also be a limitation, with ORNL using dynamic tool-path assignments on a multi-robot system to improve system reliability and deposition rate (Bhatt, Nycz, & Gupta, 2022). Compared to other large-scale AM processes like BAAM, the scale of parts produced on WAAM systems has also been limited by the reach of robotic systems (Bhatt et al., 2022). It is yet to be seen if WAAM systems can produce parts on the same scale as castings. Furthermore, the operator burden and human factors considerations have been shown to be important and should be integrated into the system design when implementing an AM technology in novel applications (Elliott & Love, 2016).

2.4 Hybrid Additive and Subtractive Manufacturing

Research into hybrid manufacturing (HM) combines multiple processes in a way that allows for the strengths of each process to be emphasized while the weaknesses are avoided, resulting in a system that has unique capabilities beyond those of the individual processes (Figure 10) (Jones, 2014; Lauwers et al., 2014; Zhu, Dhokia, Nassehi, & Newman,

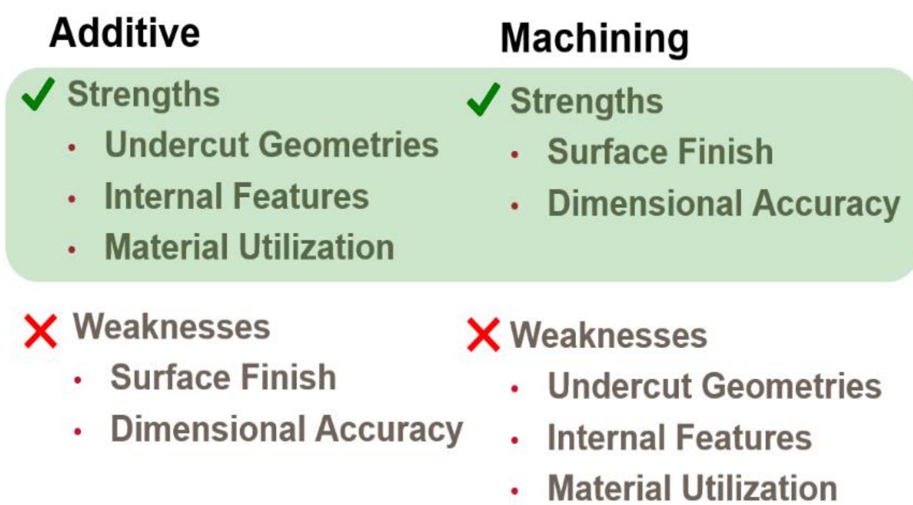

Figure 10. Comparison between the process strengths and weaknesses for Additive Manufacturing and Machining.

2013a). The processes can occur simultaneously, as done in laser-assisted machining (Ding and Shin 2010), or sequentially or iteratively (Zhu et al., 2013a). An HM process is considered in-envelope if the processes are integrated into a single system that allows processing to occur without removing the part. If the part must be transferred outside the system envelope, the HM process would be an out-of-envelope system (Frank, Croghan, Larson, & Beguhn, 2019; Frank et al., 2017a).

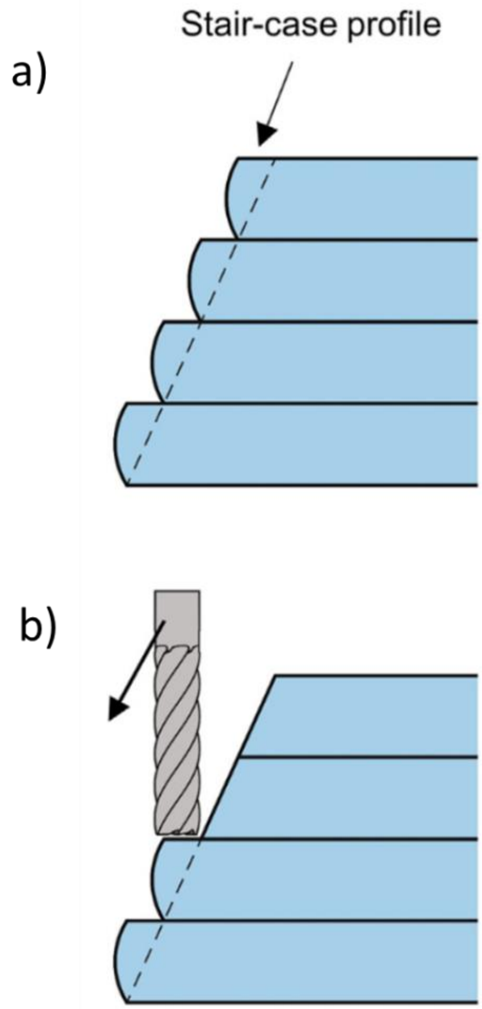

Figure 11. In HM, the a) AM produces a 2.5D staircase while b) machining finishes the surface (Pragana et al. 2021).

Two complementary processes that have emerged as a leading application for HM in literature have been additive manufacturing and subtractive machining (Grzesik, 2018). A Hybrid AM and machining process can take advantage of the AM's ability to produce undercut geometries and internal features with a high rate of material utilization (Figure 11) (Feldhausen, Heinrich, et al., 2022). These happen to be the weaknesses of a typical machining process. At the same time, the HM system can use the machining capabilities to produce a high-quality surface finish and produce parts with high dimensional accuracy, which are weaknesses of pure AM processes (Jones, 2016). This natural pairing has led to the emergence and adoption of hybrid additive and subtractive manufacturing

(Altıparmak, Yardley, Shi, & Lin, 2021; Korkmaz, Waqar, Garcia-Collado, Gupta, & Krolczyk, 2022; Pragana, Sampaio, Bragança, Silva, & Martins, 2021).

A typical additive process is 2.5D, with control in the x and y dimensions and a constant layer thickness. While 2.5D processing simplifies the process planning and allows for a high degree of automation by slicing parts into a series of layers, it results in a layer-based approximation of the desired surface geometry (Figure 11a) (Pragana et al., 2021). When AM is used to produce a near-net-shape material stock for a subsequent machining operation (Figure 11b), thicker layers can be used because they are no longer linked to the surface qualities of the part (Jones, 2014). An early example of hybrid additive/subtractive manufacturing was Shape Deposition modeling, which was used to deposit multiple different materials using AM approaches, then iteratively machine the part to achieve the required surface finishes (Merz, Ramaswami, Terk, & Weiss, 1994; Weiss et al., 1997). High deposition rate AM processes like BAAM or WAAM have been successfully paired with machining to produce an HM system because of lower material costs, and having fast deposition rates can improve economic feasibility while still meeting surface finish and geometric variability requirements through machining (Figure 12) (Dilberoglu, Gharehpapagh, Yaman, & Dolen, 2021; Li, Chen, Shi, Tian, & Zhao, 2017; Manogharan, Wysk, & Harrysson, 2016).

Figure 12. Polymer HM system being used to produce marine tooling (Nelson 2021).

HM has been applied heavily in the production of metal components for aerospace applications with costly or difficult-to-machine materials, where AM can deposit the stock material for machining, avoiding the high level of waste produced by machining (Frank et al., 2017b; Grzesik, 2018; Manogharan et al., 2016). It has also been used for repairing components, where machining can remove the defect, new material can be deposited, and the surface can be machined to meet requirements (Feldhausen, Kannan, et al., 2022; Jones, Mcnutt, Tosi, Perry, & Wimpenny, 2012). HM has been applied to large-scale polymer systems from nearly their inception (Figure 12) but can struggle to achieve the full benefit of HM due to the inability to interleave deposition and machining (Feldhausen, Raghavan, Saleeby, Love, & Kurfess, 2021; Love et al., 2015; Nelson, 2021). Polymer HM has challenges with weak interlayer bonding after resuming from machining due to the cool polymer surface reducing the ability for thermal fusion bonding to occur (Kishore et al., 2017; Weflen & Frank, 2021). Despite this limitation, polymer HM has been used to produce end-use parts (Li et al., 2016) but has found many applications for tooling (Barera & Pegoretti, 2023; Kunc, Hassen, Lindahl, & Kim, 2017; Kunc et al., 2016; Northrup, Weaver, & George, 2021; Post et al., 2018). While HM systems using WAAM and machining have typically been used to produce end-use parts, they have also been used for repair or re-work processes (Figure 13) (Feldhausen, Kannan, et al., 2022; Zhang et al., 2019).

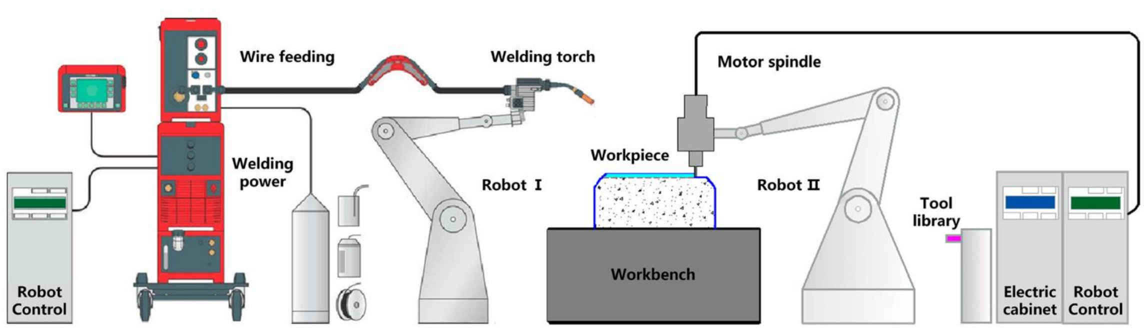

Figure 13. Hybrid manufacturing system incorporating robotic WAAM and machining (Zhang et al. 2019).

2.5 Multi-Material Components

Components designed to leverage the distinctive advantages of multiple different materials have resulted in reduced weight, improved structural performance, reduced assembly complexity, and reduced the need to compromise on material selection to meet competing functional requirements (Hasanov et al., 2021). Multi-material parts are produced extensively in the injection molding industry using an over-molding process to make parts of flexible and rigid or different colors (Goodship & Love, 2002). Multi-material components have also been produced using regions of dissimilar materials, such as polymers, metals, ceramics, or a combination (Nazir et al., 2023a).

Automated design techniques such as generative design and topology optimization bring the potential for including multiple materials and the associated properties into the optimization problem (Figure 14) (Jiang, Chen, & Gu, 2019; Zuo & Saitou, 2017). Researchers have demonstrated the ability for weight reductions beyond those achievable when a single material system is used (Li & Kim, 2018; Wang, Luo, & Yan, 2022). Researchers have evaluated applying these techniques to large-scale structures (Yu Li et al., 2022). To improve the optimization problem's results, multi-material systems using materials with unique properties are needed (Huang & Li, 2021).

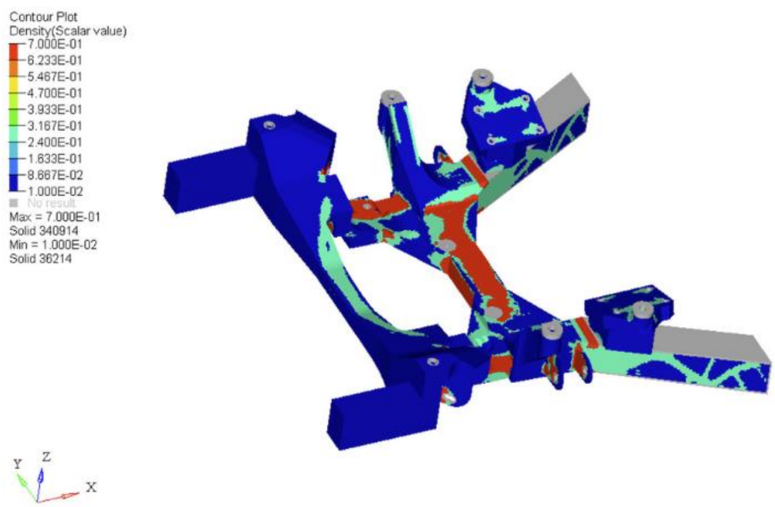

Figure 14. Topology optimized engine cradle consisting of two materials (C. Li and Kim 2018).

In the development of multi-material parts, particularly those involving dissimilar materials, achieving a strong bond between different regions is critical to ensure structural integrity and performance. The primary methods of bonding these dissimilar materials include chemical bonding, thermal fusion, and mechanical bonding (Martinsen, Hu, & Carlson, 2015). While each bonding method has advantages and challenges, thermal fusion and chemical bonding can be particularly challenging to implement when attempting to create multi-material parts from dissimilar materials (Wang et al., 2022).

The ability to produce multi-material components has been expanded by AM, enabling more ways for designers to integrate dissimilar materials within a single part with complex geometries (Nazir et al., 2023a; Zheng, Zhang, Lopez, & Ahmad, 2021). Mechanical interlocking (Figure 15) has been used to improve the bond strength of multi-material parts produced using AM. These mechanically interlocking features, such as dovetails and t-slots have been used to improve performance of multi-material parts consisting of similar and dissimilar polymeric materials (Dairabayeva, Perveen, & Talamona, n.d.; Kakaraparthi, Tatara, & Chen, 2022; Ribeiro, Sousa Carneiro, & Ferreira da Silva, 2019; Weflen, Ginther, Eldakroury, & Frank, 2021). Mechanical interlocking features can also be applied to metal-polymer components by using a laser powder bed fusion system to print the metal

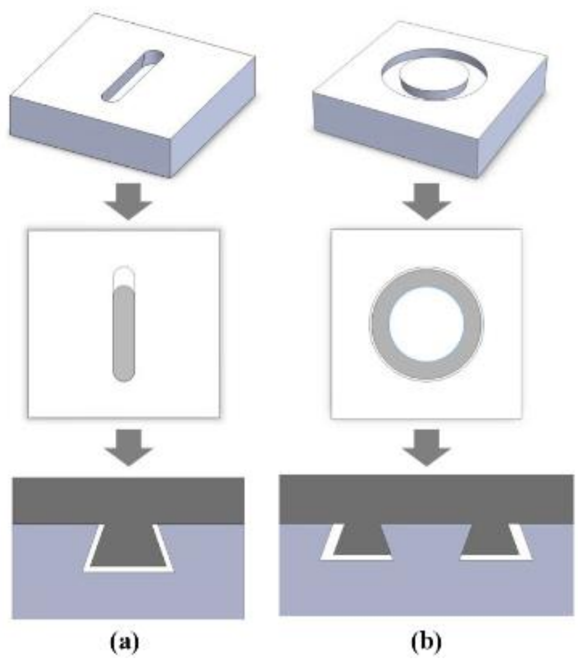

Figure 15. Metal-polymer multi-material parts produced using an undercut feature struggle to maintain interlocking due to shrinking of the polymer as it solidifies and cools.

region and an interface on interlocking features, then have polymer material compression molded or injection molded over the surface to achieve metal-polymer components (Verma, Yang, Lin, & Jeng, 2022). It is also possible use MEX systems to deposit the polymer material on overhanging features produced in powder bed system to form a mechanical interlocking (Englert et al., 2022). In a powder bed based AM system for the production of metal-polymer parts by allowing for selective deposition of both copper and nylon, it was found that mechanical interlocking was occurring due to the rough surface produced during laser scanning on the copper substrate (Chueh et al., 2020a). Multi-material parts consisting of metals and polymers have been made in a hybrid manufacturing environment but struggled to maintain a structural, mechanical bond due to the contracting of the polymer during the solidification and cooling processes (Figure 15) (Weflen & Frank, 2021). Still, the literature shows that mechanically interlocking has a strong potential for forming bonds between regions on dissimilar materials in AM, which may translate to HM approaches (Chueh et al., 2020a; Englert et al., 2022; Ribeiro et al., 2019).

2.6 Conclusions

Hybrid additive and subtractive manufacturing of large-scale and multi-material parts is gaining interest in academia and traction in industry. However, the new technology still faces challenges that limit its application. Process improvements are needed in the area of part bonding and removal from the print bed, developing new interfacial bonding methods for multi-material parts consisting of dissimilar materials, and there are opportunities to deploy HM-based technologies into a broader range of applications in industry to automate tasks.

To address these challenges, future research should focus on developing approaches to implementing mechanical bonding in ways suitable to the capabilities of the HM system. Additionally, innovative strategies for part removal and support structures could streamline the

HM and large-scale additive process and improve overall efficiency. Furthermore, by integrating human factors in the design and implementation of hybrid manufacturing systems, a human-centered approach can be applied across various industries, leading to improved user engagement and the likelihood of automation succeeding in achieving its goals.

By addressing these challenges and capitalizing on the opportunities presented by HM, advancements in large-scale and multi-material part production can be achieved. This will ultimately pave the way for more widespread adoption of HM technologies and drive innovation across the aerospace, defense, automotive, and other industries.

2.7 References

Altıparmak, S. C., Yardley, V. A., Shi, Z., & Lin, J. (2021). Challenges in additive manufacturing of high-strength aluminium alloys and current developments in hybrid additive manufacturing. *International Journal of Lightweight Materials and Manufacture, 4*(2), 246–261. https://doi.org/10.1016/J.IJLMM.2020.12.004

Babu, S., Love, L. J., Peter, W., & Dehoff, R. (2016). *Report on Additive Manufacturing for Large-Scale Metals Workshop*. Retrieved from http://www.osti.gov/scitech/

Baker, R. (1920). *Patent No. US1533300A*. Retrieved from https://patents.google.com/patent/US1533300A/en

Barera, G., & Pegoretti, A. (2023). Screw Extrusion Additive Manufacturing of Carbon Fiber Reinforced PA6 Tools. *Journal of Materials Engineering and Performance*, 1–19. https://doi.org/10.1007/S11665-023-08238-0/FIGURES/19

Bhatt, P. M., Nycz, A., & Gupta, S. K. (2022). Optimizing Multi-Robot Placements for Wire Arc Additive Manufacturing. *Proceedings - IEEE International Conference on Robotics and Automation*, 7942–7948. https://doi.org/10.1109/ICRA46639.2022.9812318

Blair, M., & Stevens, T. L. (1995). *Steel castings handbook* (6th ed.; M. Blair & T. L. Stevens, eds.) [Book]. Materials Park, OH: Steel Founders' Society of America.

Blakey-Milner, B., Gradl, P., Snedden, G., Brooks, M., Pitot, J., Lopez, E., … du Plessis, A. (2021). Metal additive manufacturing in aerospace: A review. *Materials & Design*, *209*, 110008. https://doi.org/10.1016/J.MATDES.2021.110008

Branza, T., Deschaux-Beaume, F., Sierra, G., & Lours, P. (2009). Study and prevention of cracking during weld-repair of heat-resistant cast steels. *Journal of Materials Processing Technology*, *209*(1), 536–547. https://doi.org/10.1016/J.JMATPROTEC.2008.02.033

Chesser, P. C., Wang, P. L., Vaughan, J. E., Lind, R. F., & Post, B. K. (2022). Kinematics of a Cable-Driven Robotic Platform for Large-Scale Additive Manufacturing. *Journal of Mechanisms and Robotics*, *14*(2). https://doi.org/10.1115/1.4052010/1115505

Chueh, Y. H., Zhang, X., Ke, J. C. R., Li, Q., Wei, C., & Li, L. (2020). Additive manufacturing of hybrid metal/polymer objects via multiple-material laser powder bed fusion. *Additive Manufacturing*, *36*. https://doi.org/10.1016/J.ADDMA.2020.101465

Cunningham, C. R., Flynn, J. M., Shokrani, A., Dhokia, V., & Newman, S. T. (2018). Invited review article: Strategies and processes for high quality wire arc additive manufacturing. *Additive Manufacturing*, *22*, 672–686. https://doi.org/10.1016/J.ADDMA.2018.06.020

Curran, S., Chambon, P., Lind, R., Love, L., Wagner, R., Whitted, S., … Keller, M. (2016). Big Area Additive Manufacturing and Hardware-in-the-Loop for Rapid Vehicle Powertrain Prototyping: A Case Study on the Development of a 3-D-Printed Shelby Cobra. *SAE Technical Papers*, *2016-April*(April). https://doi.org/10.4271/2016-01-0328

Dairabayeva, D., Perveen, A., & Talamona, D. (n.d.). *Investigation on the mechanical performance of mono-material vs multi-material interface geometries using fused filament fabrication*. https://doi.org/10.1108/RPJ-07-2022-0221

David, D., Monroe, R., & Thomas, E. (2015). Exploring the Need to Include Cast Carbon Steels in Welding Procedure Specifications. *Welding Journal*, *94*(10), 56–58.

Dilberoglu, U. M., Gharehpapagh, B., Yaman, U., & Dolen, M. (2021). Current trends and research opportunities in hybrid additive manufacturing. *The International Journal of Advanced Manufacturing Technology 2021 113:3*, *113*(3), 623–648. https://doi.org/10.1007/S00170-021-06688-1

Duty, C. E., Kunc, V., Compton, B., Post, B., Erdman, D., Smith, R., … Love, L. (2017). Structure and mechanical behavior of Big Area Additive Manufacturing (BAAM) materials. *Rapid Prototyping Journal*. https://doi.org/10.1108/RPJ-12-2015-0183

Elliott, A. M., & Love, L. J. (2016). Operator Burden in Metal Additive Manufacturing. *Proceedings of the 27th Annual International Solid Freeform Fabrication Symposium*, 1890–1899. Retrieved from http://energy.gov/downloads/doe-public-

Englert, L., Heuer, A., Engelskirchen, M. K., Frölich, F., Dietrich, S., Liebig, W. V., … Schulze, V. (2022). Hybrid material additive manufacturing: interlocking interfaces for fused filament fabrication on laser powder bed fusion substrates. *Https://Doi.Org/10.1080/17452759.2022.2048228*, *17*(3), 508–527. https://doi.org/10.1080/17452759.2022.2048228

Feldhausen, T., Heinrich, L., Saleeby, K., Burl, A., Post, B., MacDonald, E., … Love, L. (2022). Review of Computer-Aided Manufacturing (CAM) strategies for hybrid directed energy deposition. *Additive Manufacturing*, *56*, 102900. https://doi.org/10.1016/J.ADDMA.2022.102900

Feldhausen, T., Kannan, R., Saleeby, K., Fillingim, B., Kurfess, R., Nandwana, P., & Post, B. (2022). Hybrid Manufacturing Approaches for the Production and Repair of Industrial Tooling. *International Conference on Nuclear Engineering, Proceedings, ICONE*, *1*. https://doi.org/10.1115/ICONE21-16472

Feldhausen, T., Raghavan, N., Saleeby, K., Love, L., & Kurfess, T. (2021). Mechanical properties and microstructure of 316L stainless steel produced by hybrid manufacturing. *Journal of Materials Processing Technology*, *290*, 116970. https://doi.org/10.1016/J.JMATPROTEC.2020.116970

Frank, M. C., Croghan, J., Larson, S., & Beguhn, L. (2019). Integration Challenges with Additive/Subtractive In-Envelope Hybrid Manufacturing. *Proceedings of the 30th Annual International Solid Freeform Fabrication Symposium*. https://doi.org/10.26153/TSW/17258

Frank, M. C., Harrysson, O., Wysk, R. A., Chen, N., Srinivasan, H., Hou, G., & Keough, C. (2017a). Direct Additive Subtractive Hybrid Manufacturing (DASH) – An Out of Envelope Method. *Proceedings of the 28th Annual International Solid Freeform Fabrication Symposium*. https://doi.org/10.26153/TSW/16910

Frank, M. C., Harrysson, O., Wysk, R. A., Chen, N., Srinivasan, H., Hou, G., & Keough, C. (2017b). Direct Additive Subtractive Hybrid Manufacturing (DASH) Œ An Out of Envelope Method. *Solid Freeform Fabrication Symposium*. https://doi.org/10.7449/2017/MST_2017_366_368

Gibson, I., Rosen, D., Stucker, B., & Khorasani, M. (2021). Additive Manufacturing Technologies. In *Additive Manufacturing Technologies*. https://doi.org/https://doi.org/10.1007/978-3-030-56127-7

Goldschmidt, B. (2022). 3D Printer Bed Adhesion: All You Need to Know | All3DP. Retrieved May 6, 2023, from https://all3dp.com/2/3d-printer-bed-adhesion-all-you-need-to-know/

Goodship, V., & Love, J. C. (2002). *Multi-material injection moulding*. Shrewsbury, U.K: Rapra Technology.

Govender, R., Kissi, E. O., Larsson, A., & Tho, I. (2021). Polymers in pharmaceutical additive manufacturing: A balancing act between printability and product performance. *Advanced Drug Delivery Reviews*, *177*, 113923. https://doi.org/10.1016/J.ADDR.2021.113923

Greer, C., Nycz, A., Noakes, M., Richardson, B., Post, B., Kurfess, T., & Love, L. (2019). Introduction to the design rules for Metal Big Area Additive Manufacturing. *Additive Manufacturing*, *27*, 159–166. https://doi.org/10.1016/J.ADDMA.2019.02.016

Grzesik, W. (2018). Hybrid additive and subtractive manufacturing processes and systems: a review. *Journal of Machine Engineering*, *18*(4), 5–24. https://doi.org/10.5604/01.3001.0012.7629

Hasanov, S., Alkunte, S., Rajeshirke, M., Gupta, A., Huseynov, O., Fidan, I., … Rennie, A. (2021). Review on Additive Manufacturing of Multi-Material Parts: Progress and Challenges. *Journal of Manufacturing and Materials Processing 2022, Vol. 6, Page 4*, *6*(1), 4. https://doi.org/10.3390/JMMP6010004

Holshouser, C., Newell, C., Palas, S., Love, L. J., Kunc, V., Lind, R. F., … Dehoff, R. R. (2013). Out of bounds additive manufacturing. *Advanced Materials and Processes*, *171*(3), 15–17. Retrieved from https://www.osti.gov/biblio/1068744

Huang, X., & Li, W. (2021). A new multi-material topology optimization algorithm and selection of candidate materials. *Computer Methods in Applied Mechanics and Engineering*, *386*, 114114. https://doi.org/10.1016/J.CMA.2021.114114

Hull, C. W. (1984). *Patent No. US4575330A*. United States.

ISO/ASTM. (2021). ISO/ASTM 52900:2021(en), Additive manufacturing — General principles — Fundamentals and vocabulary. *ASTM International*. https://doi.org/10.1520/F3177-21

Jeyachandran, P., Bontha, S., Bodhak, S., Balla, V. K., & Doddamani, M. (2021). Material extrusion additive manufacturing of bioactive glass/high density polyethylene composites. *Composites Science and Technology*, *213*, 108966. https://doi.org/10.1016/J.COMPSCITECH.2021.108966

Jiang, L., Chen, S., & Gu, X. D. (2019). Generative Design of Multi-Material Hierarchical Structures via Concurrent Topology Optimization and Conformal Geometry Method. *Proceedings of the ASME Design Engineering Technical Conference*, *2*A-*2019*. https://doi.org/10.1115/DETC2019-97617

Jones, J. B. (2014). The synergies of hybridizing CNC and additive manufacturing. *Technical Paper - Society of Manufacturing Engineers*.

Jones, J. B. (2016). Repurposing mainstream CNC machine tools for laser-based additive manufacturing. *SPIE LASE*, *9738*(6), 151–161. https://doi.org/10.1117/12.2217901

Jones, J., Mcnutt, P., Tosi, R., Perry, C., & Wimpenny, D. (2012). Remanufacture of turbine blades by laser cladding, machining and in-process scanning in a single machine. *Proceedings of 23rd Annual International Solid Freeform Fabrication Symposium*, 821–827.

Joshi, P. C., Dehoff, R. R., Duty, C. E., Peter, W. H., Ott, R. D., Love, L. J., & Blue, C. A. (2012). Direct digital additive manufacturing technologies: Path towards hybrid integration. *FIIW 2012 - 2012 Future of Instrumentation International Workshop Proceedings*, 39–42. https://doi.org/10.1109/FIIW.2012.6378353

Kakaraparthi, S., Tatara, R. A., & Chen, N. (2022). A new boundary interlock geometry design pattern to strengthen FDM part multi-material interface. *Manufacturing Letters*, *33*, 664–669. https://doi.org/10.1016/J.MFGLET.2022.07.082

Kenneth Susnjara, & Scott Vaal. (2017). *Patent No. US10569523B2*. United States.

Kishore, V., Ajinjeru, C., Nycz, A., Post, B., Lindahl, J., Kunc, V., & Duty, C. (2017). Infrared preheating to improve interlayer strength of big area additive manufacturing (BAAM) components. *Additive Manufacturing*. https://doi.org/10.1016/j.addma.2016.11.008

Korkmaz, M. E., Waqar, S., Garcia-Collado, A., Gupta, M. K., & Krolczyk, G. M. (2022). A technical overview of metallic parts in hybrid additive manufacturing industry. *Journal of Materials Research and Technology*, *18*, 384–395. https://doi.org/10.1016/J.JMRT.2022.02.085

Kunc, V., Hassen, A. A., Lindahl, J., & Kim, S. (2017). *LARGE SCALE ADDITIVELY MANUFACTURED TOOLING FOR COMPOSITES Additive Manufacturing Coatings View project AMIE 1.0 View project 15 TH JAPAN INTERNATIONAL SAMPE SYMPOSIUM AND EXHIBITION*. Retrieved from http://energy.gov/downloads/doe-

Kunc, V., Lindahl, J. M., Dinwiddie, R. B., Post, B. K., Love, L. J., Duty, C., … Hassen, A. A. (2016). Investigation of In-Autoclave Additive Manufacturing Composite Tooling. *CAMX*. Retrieved from https://www.osti.gov/biblio/1366373

Lauwers, B., Klocke, F., Klink, A., Tekkaya, A. E., Neugebauer, R., & McIntosh, D. (2014). Hybrid processes in manufacturing. *CIRP Annals - Manufacturing Technology*. https://doi.org/10.1016/j.cirp.2014.05.003

Lee, J. H., Lee, C. M., & Kim, D. H. (2022). Repair of damaged parts using wire arc additive manufacturing in machine tools. *Journal of Materials Research and Technology*, *16*, 13–24. https://doi.org/10.1016/J.JMRT.2021.11.156

Li, C., & Kim, I. Y. (2018). Multi-material topology optimization for automotive design problems. *Proceedings of the Institution of Mechanical Engineers, Part D: Journal of Automobile Engineering*, *232*(14), 1950–1969. https://doi.org/10.1177/0954407017737901/FORMAT/EPUB

Li, F., Chen, S., Shi, J., Tian, H., & Zhao, Y. (2017). Evaluation and Optimization of a Hybrid Manufacturing Process Combining Wire Arc Additive Manufacturing with Milling for the Fabrication of Stiffened Panels. *Applied Sciences 2017, Vol. 7, Page 1233*, *7*(12), 1233. https://doi.org/10.3390/APP7121233

Li, L., Tirado, A., Nlebedim, I. C., Rios, O., Post, B., Kunc, V., … Paranthaman, M. P. (2016). Big Area Additive Manufacturing of High Performance Bonded NdFeB Magnets. *Scientific Reports 2016 6:1*, *6*(1), 1–7. https://doi.org/10.1038/srep36212

Li, Y., Lai, Y., Lu, G., Yan, F., Wei, P., & Xie, Y. M. (2022). Innovative design of long-span steel–concrete composite bridge using multi-material topology optimization. *Engineering Structures*, *269*, 114838. https://doi.org/10.1016/J.ENGSTRUCT.2022.114838

Love, L. J., Duty, C. E., Post, B. K., Lind, R. F., Lloyd, P. D., Kunc, V., … Blue, C. A. (2015). Breaking Barriers in Polymer Additive Manufacturing. *United States*. Retrieved from https://www.osti.gov/biblio/1185467

Love, L. J., Kunc, V., Rios, O., Duty, C. E., Elliott, A. M., Post, B. K., … Blue, C. A. (2014). The importance of carbon fiber to polymer additive manufacturing. *Journal of Materials Research*, *29*(17), 1893–1898. https://doi.org/10.1557/JMR.2014.212

Love, L., Post, B., Noakes, M., Nycz, A., & Kunc, V. (2021). There's plenty of room at the top. *Additive Manufacturing*, *39*, 101727. https://doi.org/10.1016/J.ADDMA.2020.101727

Manogharan, G., Wysk, R. A., & Harrysson, O. L. A. (2016). Additive manufacturing-integrated hybrid manufacturing and subtractive processes: Economic model and analysis. *International Journal of Computer Integrated Manufacturing*, *29*(5), 473–488. https://doi.org/10.1080/0951192X.2015.1067920

Martinsen, K., Hu, S. J., & Carlson, B. E. (2015). Joining of dissimilar materials. *CIRP Annals - Manufacturing Technology*. https://doi.org/10.1016/j.cirp.2015.05.006

Merz, R., Ramaswami, Terk, K., & Weiss, M. (1994). Shape Deposition Manufacturing. *The Solid Freeform Fabrication Symposium*.

Monroe, R. (2019). Welding Steel Castings. *Steel Founders' Society of America*.

Nazir, A., Gokcekaya, O., Md Masum Billah, K., Ertugrul, O., Jiang, J., Sun, J., & Hussain, S. (2023). Multi-material additive manufacturing: A systematic review of design, properties, applications, challenges, and 3D printing of materials and cellular metamaterials. *Materials and Design*, *226*. https://doi.org/10.1016/J.MATDES.2023.111661

Nelson, D. (2021). A talk with Thermwood's CEO, author of a new book on large-scale 3D printing. *The Fabricator*. Retrieved from https://www.thefabricator.com/additivereport/article/additive/a-talk-with-thermwoods-ceo-author-of-a-new-book-on-large-scale-3d-printing

Ngo, T. D., Kashani, A., Imbalzano, G., Nguyen, K. T. Q., & Hui, D. (2018). Additive manufacturing (3D printing): A review of materials, methods, applications and challenges. *Composites Part B: Engineering*, *143*, 172–196. https://doi.org/10.1016/J.COMPOSITESB.2018.02.012

Northrup, N., Weaver, J., & George, A. (2021). Vacuum Infusion of Composites: Durability of Hybrid Large Area Additive Tooling for Vacuum Infusion of Composites. *SAMPE Journal*, 52. Retrieved from https://scholarsarchive.byu.edu/facpub/5870

Nycz, A., Noakes, M. W., Richardson, B., Messing, A., Post, B., Paul, J., … Love, L. (2017). *Challenges in Making Complex Metal Large-Scale Parts for Additive Manufacturing: A Case Study Based on the Additive Manufacturing Excavator*. https://doi.org/10.26153/16923

Omiyale, B. O., Olugbade, T. O., Abioye, T. E., & Farayibi, P. K. (2022). Wire arc additive manufacturing of aluminium alloys for aerospace and automotive applications: a review. *Https://Doi.Org/10.1080/02670836.2022.2045549*, *38*(7), 391–408. https://doi.org/10.1080/02670836.2022.2045549

Pajonk, A., Prieto, A., Blum, U., & Knaack, U. (2022). Multi-material additive manufacturing in architecture and construction: A review. *Journal of Building Engineering*, *45*, 103603. https://doi.org/10.1016/J.JOBE.2021.103603

Post, B. K., Chesser, P. C., Lind, R. F., Roschli, A., Love, L. J., Gaul, K. T., … Wu, S. (2018). Using Big Area Additive Manufacturing to directly manufacture a boat hull mould. *Https://Doi.Org/10.1080/17452759.2018.1532798*, *14*(2), 123–129. https://doi.org/10.1080/17452759.2018.1532798

Post, B., Lind, R., Lloyd, P., Kunc, V., Linhal, J., & Love, L. (2016). *The Economics of Big Area Additive Manufacturing*. Retrieved from https://repositories.lib.utexas.edu/handle/2152/89664

Pragana, J. P. M., Sampaio, R. F. V., Bragança, I. M. F., Silva, C. M. A., & Martins, P. A. F. (2021). Hybrid metal additive manufacturing: A state–of–the-art review. *Advances in Industrial and Manufacturing Engineering*, *2*, 100032. https://doi.org/10.1016/J.AIME.2021.100032

Print bed - CEAD | Large Scale Additive Manufacturing. (2023). Retrieved May 6, 2023, from https://ceadgroup.com/solutions/technology-components/print-bed/

Rezvani Ghomi, E., Khosravi, F., Neisiany, R. E., Singh, S., & Ramakrishna, S. (2021). Future of additive manufacturing in healthcare. *Current Opinion in Biomedical Engineering*, *17*, 100255. https://doi.org/10.1016/J.COBME.2020.100255

Ribeiro, M., Sousa Carneiro, O., & Ferreira da Silva, A. (2019). Interface geometries in 3D multi-material prints by fused filament fabrication. *Rapid Prototyping Journal*, *25*(1), 38–46. https://doi.org/10.1108/RPJ-05-2017-0107/FULL/PDF

Roschli, A., Gaul, K. T., Boulger, A. M., Post, B. K., Chesser, P. C., Love, L. J., … Borish, M. (2019). Designing for Big Area Additive Manufacturing. *Additive Manufacturing*, *25*, 275–285. https://doi.org/10.1016/J.ADDMA.2018.11.006

Roschli, A., Post, B. K., Atkins, C., Stevens, A. G., Chesser, P., & Zaloudek, K. (2022). Build Plate Design for Extrusion-Based Additive Manufacturing. *Proceedings of the 33rd Annual International Solid Freeform Fabrication Symposium*, 1079–1090.

Salifu, S., Desai, D., Ogunbiyi, O., & Mwale, K. (2022). Recent development in the additive manufacturing of polymer-based composites for automotive structures—a review. *International Journal of Advanced Manufacturing Technology*, *119*(11–12), 6877–6891. https://doi.org/10.1007/S00170-021-08569-Z/TABLES/2

Schirmeister, C. G., Hees, T., Licht, E. H., & Mülhaupt, R. (2019). *3D printing of high density polyethylene by fused filament fabrication*. https://doi.org/10.1016/j.addma.2019.05.003

Schroeder, A., & Weaver, J. (2022). Optimizing Build Plate Adhesion of Polymers in Fused Granule Fabrication Processes. *Faculty Publications*. Retrieved from https://scholarsarchive.byu.edu/facpub/5873

Shafer, C. S., Siddel, D. H., & Elliott, A. M. (2017). Cleated Print Surface for Fused Deposition Modeling. *Journal of Mechanics Engineering and Automation*, *7*(1), 1359–1365. https://doi.org/10.17265/2159-5275/2017.01.005

Talagani, M., DorMohammadi, S., Dutton, R., Godines, C., Baid, H., Abdi, F., … Blue, C. (2015). Numerical Simulation of Big Area Additive Manufacturing (3D Printing) of a Full Size Car Virtual Integrated Battery Environment View project Solidification Microstructure Control in Electron Beam Additive Manufacturing View project. *Sampe Journal*, *51*(4), 27–36. Retrieved from www.mgc-a.com

Treutler, K., Wesling, V., Camacho, A. M., Chunhui, R. (, & Yang,). (2021). The Current State of Research of Wire Arc Additive Manufacturing (WAAM): A Review. *Applied Sciences 2021, Vol. 11, Page 8619*, *11*(18), 8619. https://doi.org/10.3390/APP11188619

Vafadar, A., Guzzomi, F., Rassau, A., & Hayward, K. (2021). Advances in Metal Additive Manufacturing: A Review of Common Processes, Industrial Applications, and Current Challenges. *Applied Sciences 2021, Vol. 11, Page 1213*, *11*(3), 1213. https://doi.org/10.3390/APP11031213

Verma, S., Yang, C. K., Lin, C. H., & Jeng, J. Y. (2022). Additive manufacturing of lattice structures for high strength mechanical interlocking of metal and resin during injection molding. *Additive Manufacturing*, *49*, 102463. https://doi.org/10.1016/J.ADDMA.2021.102463

Wang, D., Liu, L., Deng, G., Deng, C., Bai, Y., Yang, Y., … Han, C. (2022). Recent progress on additive manufacturing of multi-material structures with laser powder bed fusion. *Https://Doi.Org/10.1080/17452759.2022.2028343*, *17*(2), 329–365. https://doi.org/10.1080/17452759.2022.2028343

Wang, Y., Luo, Y., & Yan, Y. (2022). A multi-material topology optimization method based on the material-field series-expansion model. *Structural and Multidisciplinary Optimization*, *65*(1), 1–15. https://doi.org/10.1007/S00158-021-03138-0/METRICS

Weflen, E., Black, M., Frank, M., & Peters, F. (2021). Wire Arc Additive Manufacturing of Low Carbon Steel for Casting Applications. *Proceedings of the 33rd Annual International Solid Freeform Fabrication Symposium*, 170–177.

Weflen, E., & Frank, M. C. (2021a). Hybrid additive and subtractive manufacturing of multi-material objects. *Rapid Prototyping Journal*, *27*(10), 1860–1871. https://doi.org/10.1108/RPJ-06-2020-0142/FULL/PDF

Weflen, E., & Frank, M. C. (2021b). Hybrid additive and subtractive manufacturing of multi-material objects. *Rapid Prototyping Journal*, *ahead-of-print*(ahead-of-print). https://doi.org/10.1108/RPJ-06-2020-0142

Weflen, E.D., Ginther, M. C., Eldakroury, M. A., & Frank, M. C. (2021). *Mechanical Interface for Iterative Hybrid Additive and Subtractive Manufacturing*. https://doi.org/10.26153/TSW/17676

Weflen, Eric D., Peters, F. E., & Frank, M. C. (2022). THERMALLY SWITCHABLE BUILD TABLE BY MECHANICAL INTERLOCKING FOR ADDITIVE MANUFACTURING. *Proceedings of the 33rd Annual International Solid Freeform Fabrication Symposium*.

Weiss, L. E., Merz, R., Prinz, F. B., Neplotnik, G., Padmanabhan, P., Schultz, L., & Ramaswami, K. (1997). Shape Deposition Manufacturing of Heterogeneous Structures. *Journal of Manufacturing Systems*. https://doi.org/10.1016/S0278-6125(97)89095-4

Wohlers, T., Gornet, T., Mostow, N., Campbell, I., Diegel, O., Kowen, J., … Peels, J. (2016). History of Additive Manufacturing. *SSRN Electronic Journal*. https://doi.org/10.2139/SSRN.4474824

Wohlers, T. T., Campbell, I., Diegel, O., Huff, R., Kowen, J., & Wohlers Associates (Firm). (2022). *Wohlers report 2022 : 3D printing and additive manufacturing global state of the industry*. Retrieved from https://wohlersassociates.com/product/wohlers-report-2022/

Wu, B., Pan, Z., Ding, D., Cuiuri, D., Li, H., Xu, J., & Norrish, J. (2018). A review of the wire arc additive manufacturing of metals: properties, defects and quality improvement. *Journal of Manufacturing Processes*, *35*, 127–139. https://doi.org/10.1016/J.JMAPRO.2018.08.001

Yuan, L., Pan, Z., Ding, D., Yu, Z., van Duin, S., Li, H., … Norrish, J. (2021). Fabrication of metallic parts with overhanging structures using the robotic wire arc additive manufacturing. *Journal of Manufacturing Processes*, *63*, 24–34. https://doi.org/10.1016/J.JMAPRO.2020.03.018

Zhang, S., Zhang, Y., Gao, M., Wang, F., Li, Q., & Zeng, X. (2019). Effects of milling thickness on wire deposition accuracy of hybrid additive/subtractive manufacturing. *Https://Doi.Org/10.1080/13621718.2019.1595925*, *24*(5), 375–381. https://doi.org/10.1080/13621718.2019.1595925

Zhang, Y M, & Li, P. J. (2001). MODIFIED ACTIVE CONTROL OF METAL TRANSFER AND PULSED GMAW OF TITANIUM. *Welding Journal*, *80*(2), 54–61.

Zhang, Yu Ming, Chen, Y., Li, P., & Male, A. T. (2003). Weld deposition-based rapid prototyping: a preliminary study. *Journal of Materials Processing Technology*, *135*(2–3), 347–357. https://doi.org/10.1016/S0924-0136(02)00867-1

Zheng, Y., Zhang, W., Lopez, D. M. B., & Ahmad, R. (2021). Scientometric Analysis and Systematic Review of Multi-Material Additive Manufacturing of Polymers. *Polymers 2021, Vol. 13, Page 1957*, *13*(12), 1957. https://doi.org/10.3390/POLYM13121957

Zhu, Z., Dhokia, V. G., Nassehi, A., & Newman, S. T. (2013). A review of hybrid manufacturing processes – state of the art and future perspectives. *Https://Doi.Org/10.1080/0951192X.2012.749530*, *26*(7), 596–615. https://doi.org/10.1080/0951192X.2012.749530

Zuo, W., & Saitou, K. (2017). Multi-material topology optimization using ordered SIMP interpolation. *Structural and Multidisciplinary Optimization*, *55*(2), 477–491. https://doi.org/10.1007/S00158-016-1513-3/METRICS

CHAPTER 3. INTERLOCKING BUILD SURFACE WITH THERMALLY SWITCHABLE BOND FOR BIG AREA ADDITIVE MANUFACTURING

Eric Weflen, Frank E. Peters, Matthew C. Frank

Industrial and Manufacturing Systems Engineering Department, Iowa State University,

Ames, Iowa 50011, USA

Modified from a manuscript to be submitted to the journal *Additive Manufacturing*

3.1 Abstract

Additive Manufacturing of large-scale objects on the scale of multiple meters using pellet-fed screw extrusion systems has grown in popularity and is gaining industrial adoption. While part adhesion and removal from the build surface can be challenging on many material extrusion AM systems, the challenges are even more pronounced on large-scale systems due to the large force required to overcome warping forces, the lack of heated build environments, and the weight of printed parts intensifying the difficulty in part removal. This work demonstrates a build surface for Big Area Additive Manufacturing (BAAM) systems using mechanical interlocking features to lock the part to the build surface during processing and then release the complete part through rapid heating. Dovetail undercut features are machined into an aluminum build surface with integrated resistance heating. A model for pin geometry design is established to guide system design. A design of experiments is conducted to build a relationship between the undercut area, undercut angle, and undercut pin height, the resulting retention force, and the force required to remove the part once it has been released. This study demonstrates an improved retention strength that is greater than the carbon fiber-reinforced polymer material being printed, while the operator can manually remove the parts when released. These findings can reduce the processing difficulty of large-scale objects by eliminating print-bed related post-processing steps.

3.2 Introduction

Large-scale polymer additive manufacturing (AM) has gained rapid adoption for applications such as tooling, architectural products, and end-use parts (Altıparmak, Yardley, Shi, & Lin, 2022; Kalle, Joni, Alexander, & Juhani, 2023; Love et al., 2021). Sometimes referred to as fused granulate fabrication (FGF), these systems use screw extrusion systems to process low-cost polymer pellets deposit at rates up to 45 kg/hr (Post et al., 2016). However, retaining parts to the build plate during processing can be challenging due to warping forces caused by a buildup of residual stress from differential cooling of layers (Love et al., 2014; Talagani et al., 2015). Furthermore, removing the large parts from the build plate after processing can require substantial effort, partially due to the higher bond needed to retain the part (Roschli et al., 2022; Shafer et al., 2017). Ideally, the part would be locked to the surface during processing and released when processing is complete. However, we lack a method of producing a build plate for large-scale AM with these properties.

The abundance and variety of proposed solutions for bonding a part to the build plate may be a symptom of the continued challenges faced by the industry (Figure 16). Early solutions implemented in the Manufacturing Demonstration Facility at Oak Ridge National Lab (ORNL) and commercialized by companies such as Cincinnati Incorporated and Loci Robotics relied on a thermal fusion bond between the hot material deposited and a polymer sheet retained to the build surface (Roschli et al., 2022). However, there can be challenges retaining the sheet to the build plate or the part delaminating during production. The company Thermwood holds a patent on a method of bonding polymer granules to a build plate, often plywood, that may form a more robust thermal fusion bond along with some mechanical interlocking (Patent No. US 10,569,523 B2, 2020). Still, removal of the part often damages this build plate and may require additional processing to clean the areas of the part in contact. CEAD B.V. has developed a build plate the relies primarily on mechanical bonding to retain the part during processing, then releases the part using a mechanism causing a motion that relieves the interlock ("Print bed - CEAD | Large Scale Additive Manufacturing," 2023). Yet, the complexity of this approach makes scaling to large-scale systems a challenge. While numerous variations of the build plates presented here are available in the market, they do not meet the need for a large-scale polymer AM build plate that locks to the part during processing while releasing it when complete.

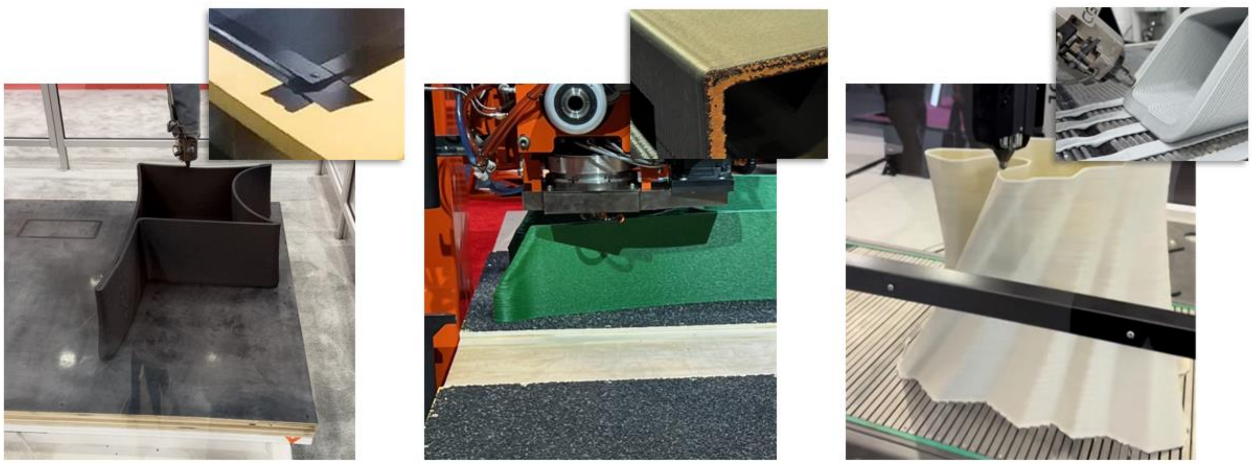

a) b) c)

Figure 16. Standard methods for large-scale AM build plate bonding are a) thermal fusion to a polymer sheet, b) thermal and mechanical bonding to a polymer granule, and c) mechanical bonding and releasing through motion.

Joining substrates can be achieved through thermal fusion, chemical bonding, mechanical bonding, or a hybrid combination of these processes (Martinsen et al., 2015). Thermal fusion to a build plate would require the material thermal properties to be similar, while chemical bonding would be material dependent. Research into the fabrication of multi-material parts that consist of dissimilar materials has demonstrated the use of mechanical bonding to structurally join a wide range of materials (Verma et al., 2022; Weflen & Frank, 2021). Using a build plate material like aluminum that is distinct from the polymer used in the AM process can allow the mechanical bond to be released through heating.

This work presents a method of producing a build plate for large-scale AM that meets the requirement of locking the part to the surface during processing and releasing the part when processing is complete. A model is produced for evaluating and nesting mechanical interlocking features on the surface of a build palate. The relationship between the geometry of these interlocking features and the resulting in-process and removal strengths are experimentally investigated. A multiple linear regression model is produced to predict the bond strength achieved by interlocking features to guide the practical implementation of the build plate. A demonstration build plate is created for a medium-scale FGF hybrid additive and subtractive manufacturing system to evaluate the build plate's ability to produce tooling and the potential for scaling to larger AM systems. The presented method can reduce scrap due to parts delaminating from the build plate during processing and can save processing time and challenges related to part removal and post-processing. Furthermore, improving the understanding of mechanical bonding and releasing in dissimilar material parts can be applied to other applications, such as multi-material parts.

3.3 Solution Overview

The proposed method forms a mechanical bond using milled undercut geometry in an aluminum build plate produced using Computer Numerical Control (CNC) machining (Figure 17). The molten polymer is deposited on the build plate that has been preheated, filling the void under the overhanging features (Figure 18a and b). The build plate is typically allowed to cool to ambient temperatures after depositing the first polymer layer. Upon solidification of the polymer, a mechanical interlock is formed with the build plate. This

Figure 17. Interlocking build plate.

mechanical bond must be strong enough to withstand the forces developed during additive processing and, in some applications, machining. The part must sufficiently cool before machining (Figure 18c). When the processing on the part is complete, it can be removed by rapid heating of the print bed, which softens the polymer along the metal-polymer interface (Figure 18d and e). When the polymer within the small undercut region softens sufficiently, the mechanical interlocking is relieved, allowing easy part removal (Figure 18f). Using a dovetail pin-shaped feature with a small undercut angle allows a slight deformation in the polymer to release the part from the build plate.

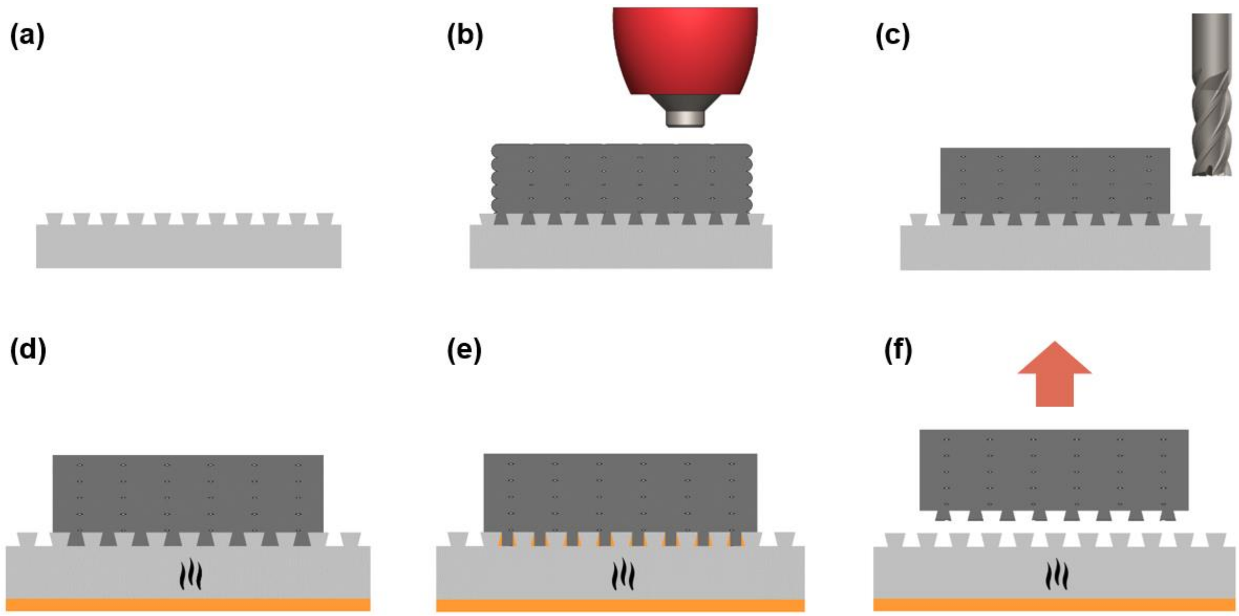

Figure 18. The process steps for the proposed print bed are: a) preheating the print bed, b) depositing the polymer material, c) machining of surfaces, d) rapid heating of print bed, e) polymer softening in the undercut region, and f) removal of the completed object.

Using a protruding pin feature ensures that as the polymer shrinks during solidification and cooling, it forms a tight bond to the aluminum pin feature (Figure 19a). The polymer is retained by the small amount of material under the overhang created by the dovetail geometry (Figure 19b). The retention area will be small compared to the overall cross-section of the part, so it is expected that the strength of the mechanical bond will be lower than the thermal fusion bond formed between the succeeding layers of deposited polymer. When heating is applied to the bottom of the build plate (Figure 19c), thermal conduction transfers that heat to the polymer, softening the polymer (Figure 19d). The thermal conductivity of the aluminum build plate will typically be substantially greater than the polymer, even when conductive fillers like carbon fibers are used (Weflen, Peters, & Frank, 2022). This disparity will allow for the rapid heating of the build plate and the controlled softening of the polymer part, allowing for removal while only softening a layer of polymer material around a tenth of a millimeter.

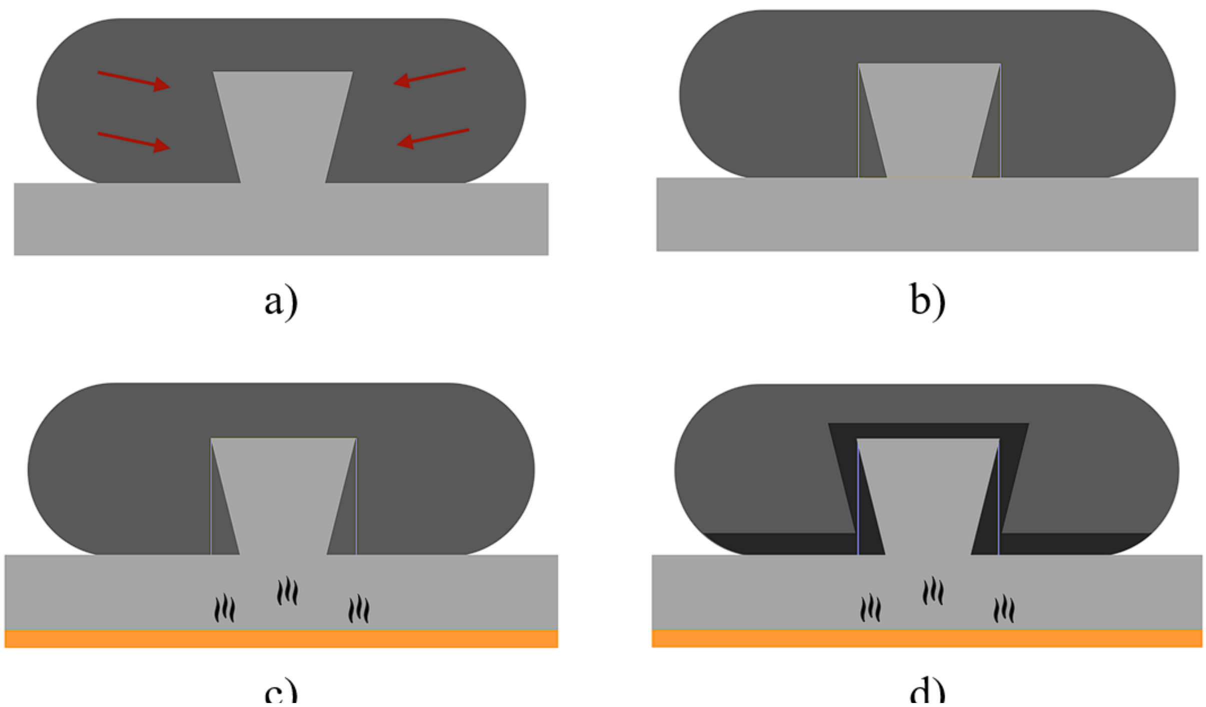

Figure 19. Mechanical bonding and releasing is achieved through a) thermoplastic solidifying around the protruding pins on the print bed, b) an undercut region around the pins retain the part during processing, c) rapid heating of the aluminum print bed heats the thermoplastic from the bottom, and d) the part is released when the thermoplastic in the undercut region softens.

3.4 Methodology

3.4.1 Hybrid Manufacturing System

A Haas UMC 750 5-axis machining center was upgraded to work with Hybrid Manufacturing Technologies' pellet-fed screw extrusion AM tool. The build volume of the system is approximately 450 x 450 x 300 mm. A nozzle diameter of 3 mm is used to produce a 9 mm wide bead with a 2 mm thickness. Both neat Acrylonitrile butadiene styrene (ABS) polymer and an ABS reinforced with 20% carbon fiber (ABS/CF) are deposited. However, the thickness of the first layer is modified to be 0.5mm taller than the undercut geometry to ensure the undercut geometry is adequately filled. A build plate made from 12.7 mm thick aluminum 6061 T6 is retained to the platter using the integrated T-slots, with adequate spacing for resistance heating elements.

3.4.2 Mechanically Interlocking Feature Design

The mechanically interlocking feature is in the shape of a dovetail pin, with an undercut formed using a specialized undercutting milling tool (Figure 20). A repeating unit cell consisting of the dovetail pin and the surrounding machining path forms the build surface. Defining the unit cell allows for evaluating properties through an engineering mechanics approach and optimization, aiming to inform the design of future systems. The key feature of the unit cell that leads to the retention of the polymer region is the undercut geometry. While the effect of the undercut area is evaluated by testing various undercut angles and pin heights, the length of the undercut, defined as the perimeter at the top of the pin feature, can be evaluated mathematically. Additionally, the structural properties of the aluminum pin feature can be assessed to ensure that

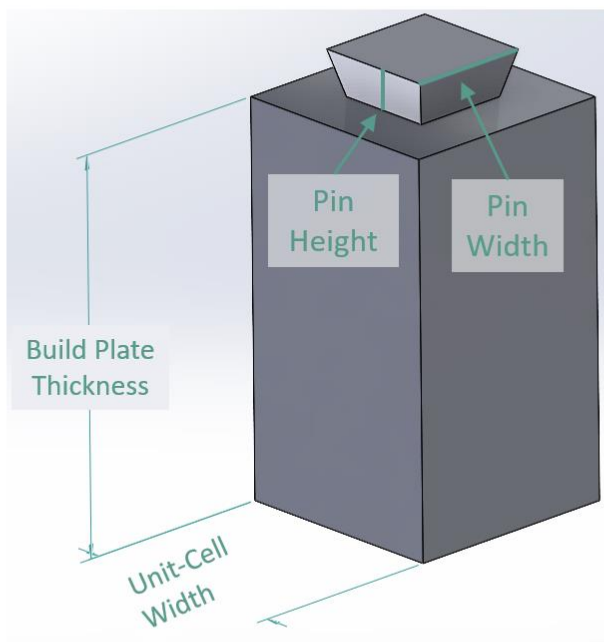

Figure 20. Unit-cell of the mechanical interlocking feature on the build plate.

the pin will not deform, even if the polymer region is removed from the print surface forcefully while it is still locked in place.

3.4.3 Characterizing Bonding and Release Properties

The structural performance of the mechanically interlocking interface was evaluated. The holding force during processing and the force to remove the part after completion were assessed for various pin lengths and undercut angles. A Design of Experiments (DOE) was conducted to elucidate the contributions of the pin height, angle, and their interactions on the holding characteristics of the build plate. The three factors in the DOE are quantitative factors of pin height, the undercut angle, and the categorical factor of build plate temperature. The build plate temperature is a categorical factor because, at ambient lab temperature, the polymer is solid, while after heating the build plate to 141°C, the polymer near the build plate will soften. In the ambient state, the polymer can be considered rigid or "locked" to the build plate, while in the heated condition, it is "released" or softened. To test the tensile properties of the mechanical bond between the polymer region and the build plate, tensile adhesion samples were produced similar to those used in ASTM D897-08.

Materials

Sample build plates were produced from 12.7 mm thick plates of aluminum alloy 6061 with a T6 heat treatment. Acrylonitrile butadiene styrene (ABS) pellets with 20 wt. % carbon fiber loading (ABS/CF) (HM Technologies, McKinney, TX, USA) was used to produce the tensile samples. The ABS/CF material was dried for at least 4 hours at 75°C in a dehydrator (National Presto Industries, Eau Clair, WI, USA) before processing in the material extrusion system.

Tensile Sample Fabrication

Dovetail pins were machined into a 305 x 76 mm aluminum plate on a 5-axis HAAS machining center using a carbide dovetail endmill (Harvey Tool Company, Rowley, MA, USA) (Figure 21). A 3.2 mm diameter carbide flat endmill was used to machine slots at a 0.5, 1.0, or 1.5 mm depth into the aluminum plate in a cross-hatch pattern, leaving 3.2 mm square pins remaining on the surface (Figure 22a-c). Undercut features were machined into the remaining pins using a dovetail cutting tool with an included angle of 10, 20, or 30 degrees (Figure 22d). All combinations of machining depths and included angle of the overhang are presented in Table 1, along with the categorical factor of build plate temperature.

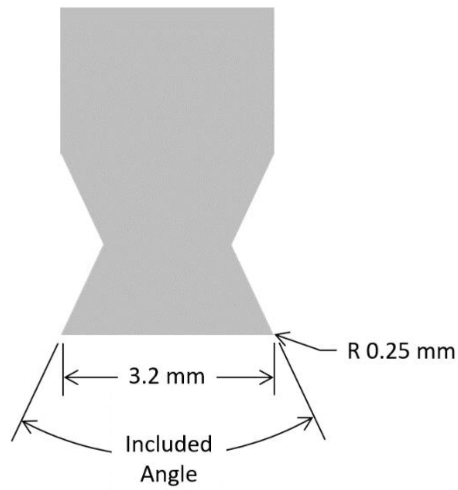

Figure 21. Dovetail cutting tool dimensions.

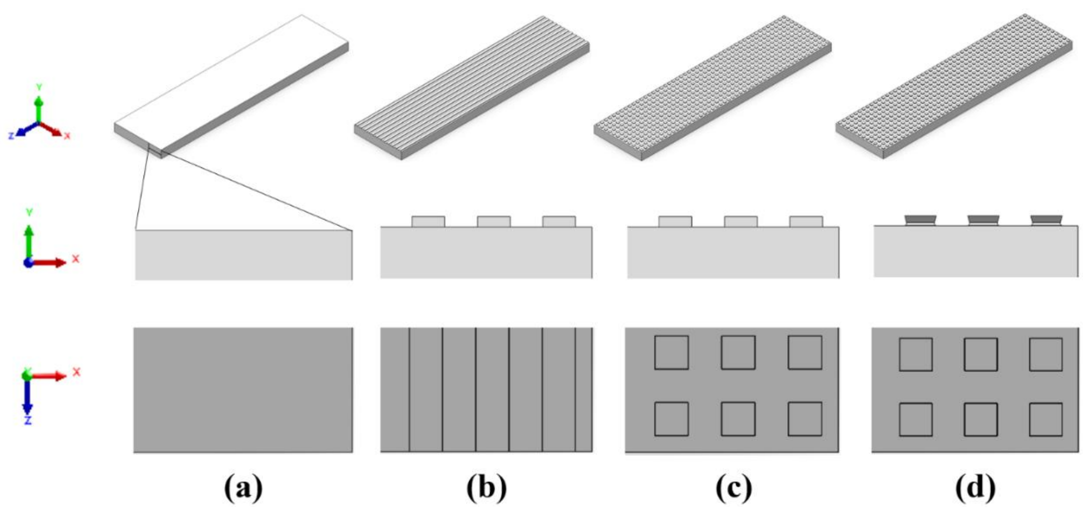

Figure 22. Processing steps for machining undercut geometry test samples: a) aluminum stock, b) slot milling with a flat end mill, c) slot milling in a second orientation with a flat end mill, d) machining with a dovetail cutting tool.

The AMBIT XTRUDE screw extrusion tool (HM Technologies, McKinney, TX, USA) was positioned 0.5 mm above the tops of the pins and deposited a 9 mm wide bead of ABS/CF material in a cross-hatch pattern with a +45/-45 path until the entire surface was covered. Then, ten subsequent 2 mm thick layers of material were deposited to achieve a thickness of 20.5 mm above the top surface of the pins (Figure 23a & b). The end of the part was milled and inspected under an optical microscope to ensure adequate filling occurred in the undercut regions. A 12.7 mm shoulder was machined into the sample to allow for clamping in the tensile testing fixture (Figure 23c). Four adhesion testing samples were cut from the center of the sample on a horizontal bandsaw, leaving a 50.8 mm square by 20.5 mm tall region of ABS/CF on the sample (Figure 23d). An aluminum fixture was attached to the top of the polymer region using West Systems 650-8 G/flex epoxy (Gougeon Brothers, Inc., MI, USA), which has a tensile strength significantly greater than the printed ABS/CF material (Figure 23e).

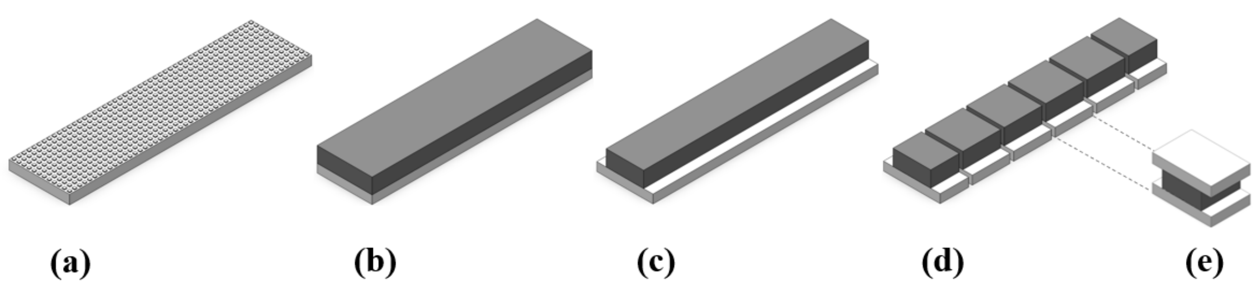

Figure 23. Sample preparation steps: a) prepare build plate, b) deposit ABS/CF, c) machine shoulder on edges, d) cut tensile samples, e) adhere tensile fixture.

Table 1. Experimental matrix for the build plate adhesion DOE.

Pin Length (mm)	Dovetail Angle (Degrees)	Build Plate Temperature (Categorical State)	Sample Quantity	Sample Set ID
0.5	10	25°C (Locked)	4	$A1_L$
0.5	10	141°C (Released)	4	$A1_R$
0.5	20	25°C (Locked)	4	$A2_L$
0.5	20	141°C (Released)	4	$A2_R$
0.5	30	25°C (Locked)	4	$A3_L$
0.5	30	141°C (Released)	4	$A3_R$
1.0	10	25°C (Locked)	4	$A4_L$
1.0	10	141°C (Released)	4	$A4_R$
1.0	20	25°C (Locked)	4	$A5_L$
1.0	20	141°C (Released)	4	$A5_R$
1.0	30	25°C (Locked)	4	$A6_L$
1.0	30	141°C (Released)	4	$A6_R$
1.5	10	25°C (Locked)	4	$A7_L$
1.5	10	141°C (Released)	4	$A7_R$
1.5	20	25°C (Locked)	4	$A8_L$
1.5	20	141°C (Released)	4	$A8_R$
1.5	30	25°C (Locked)	4	$A9_L$
1.5	30	141°C (Released)	4	$A9_R$

Release Temperature Tensile Testing

Samples were conditioned in the lab environment of 34% Humidity and 25°C for 24 hours before testing. A screening test was conducted on a portion of the experimental matrix to evaluate the release temperature for the subsequent tensile testing. A single sample from the sample sets $A2_R$, $A4_R$, $A5_R$, $A6_R$, and $A8_R$ with a reduced cross-section of 50.8 x 25.4 mm was loaded with 14 kPa with a spring scale, then gradually heated with a power input of 30 Watts until the ABS/CF released from the aluminum print bed. The temperature at release was recorded to evaluate how the pin geometry could affect the release temperature under a constant force. The release temperature of 141°C for the sample from set $A5_R$, at the center of the experimental matrix, was used in the following tensile testing experiment.

Release Force Tensile Testing DOE

Samples were conditioned in the lab environment of 34% Humidity and 25°C for 24 hours before testing. Tensile specimens underwent tensile testing on a Shimadzu universal testing machine at a strain rate of 2.54 mm/min using a custom fixture (Figure 24). The samples from the “locked” sample sets, designated by the “L” in the sample set ID, were pulled at ambient conditions. The Samples in the “released” state, represented by an “R” in the sample set ID, were placed on a hot plate set to 250°C until a k-type thermocouple inserted into the side of the aluminum build plate section signaled that the sample reached 141°C, then immediately transferred and tested on the universal testing machine.

Figure 24. Universal testing machine with custom fixture.

Model Development

The results were modeled in R Studio (Posit PBC, Boston, MA, USA) with the goal of better understanding the effect of the different pin design parameters on the bond formed in the locked condition and the force needed to release the part in the unlocked condition. A secondary goal of the model was for use in tuning future applications of the interlocking dovetail pins to meet various customer requirements. The performance of several models was compared against the additional complexity and the ability to understand and explain the factors and interactions.

3.4.4 Demonstration Build Plate Production

A print bed was fabricated using the dovetail interlocking features on the build surface. Implementing this new print bed into the system will allow for evaluation of the integrated system and any potential performance issues. The build plate must also be thick enough to provide adequate stiffness to maintain flatness, even under load caused by the weight of the part and warping. It must also be thick enough to act as a heat spreader to maintain an approximately even temperature across the top surface, even though the heat is locally applied on the bottom. A prototype print bed was produced from a 38 mm thick aluminum plate with a length of 444 mm and a width of 483 mm. Intersecting grooves at 0 ° and 90 ° were machined with a slot width and spacing of 3.2 mm and at a depth of 1.0 mm using a carbide flat end mill. A specialty dovetail undercut end mill was used to mill a 20° included angle undercut into the sides of the resulting pin features, matching the pin geometry of the A5 sample sets. Two 457 x 152 mm glass fiber reinforced adhesive-backed silicone heaters were mounted to the bottom of the build table with a total heat output of 2,160 watts. The heaters and a k-type thermocouple were wired to a custom temperature and process controller that used a proportional-integral-derivative (PID) control loop to reach the set temperature. The build plate and the interlocking build surface were evaluated by printing four bead-wide strips of ABS and ABS/CF material running the length of the build plate to assess the ability to resist the bow caused by a buildup of residual stress. The strips were machined to see if the vibratory loading of the cutting tool would affect the bond between the part and the plate. Finally, a casting pattern on the size scale of the build plate was produced using hybrid manufacturing to assess the suitability of the build plate for the production of parts.

3.5 Results and Discussion

3.5.1 Mechanically Interlocking Feature Design

A dovetail geometry was chosen for the mechanical interlocking features, as the shallow slope will facilitate easy removal of the part when printing is complete, taking inspiration from reversible snap feature design approaches used in injection molding. Since different applications will have unique adhesion requirements for the build plate, a model is developed that can be used as a design guide. However, there are several common design considerations. A Mechanical interlock should be formed even if only a single bead of material is deposited, so the unit-cell X-Y dimensions of the unit cell should ideally be less than the polymer bead width, in this case, 9 mm (Figure 25). Since these undercut features are machined in this application, the cutting tool diameter determines the minimum distance between pins. This cutting tool diameter is related to the material removal rate, so a balance must be struck between the minimum pin spacing and the machining time, and thus cost, to produce the geometry. For this application, a 3.2mm diameter flat end mill was selected. Similarly, the pin height should be less than the thickness of the first layer deposited, in this case, 2 mm, though it is expected to use a different thickness for the first layer than for subsequent layers. This is especially true when the layers used are thin relative to the flatness of the build plate.

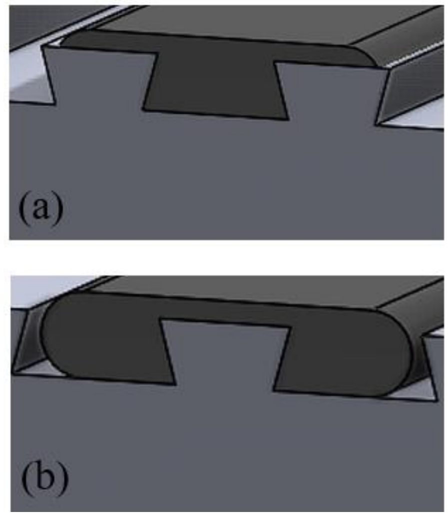

Figure 25. Mechanical interlocking formed when a) bead is centered between pins or b) bead is centered on a row of pins.

As shown in Figure 19, the undercut region retains the part during printing and machining. Maximizing the area of undercut region per unit area on the build plate should maximize the bond strength, retaining the part during processing. This can be accomplished by increasing the undercut angle, increasing the pin height (depth of cut), or maximizing the pin perimeter distance, increasing the length of the undercut region. This study will experimentally evaluate the undercut angle and pin height. The length of the undercut can be assessed mathematically using eqs. 1 and 2. Where A_{uc} is the Area of the unit cell, W_p is the width of the pin, which can also be thought of as the edge length, and D_t is the diameter of the cutting tool used to produce the groove, which is 3.2 mm in this instance. Equation 2 can be used to calculate the density of undercut edge length per unit area ρ_u. When values for ρ_u are plotted for each potential pin diameter, a maximum value can be found at a pin diameter of 3.2 mm.

$$A_{uc} = \left(W_p + D_t\right)^2 \tag{1}$$

$$\rho_u = \frac{4W_p}{A_{uc}} \tag{2}$$

The dovetail pin feature should not be a failure point, so it should be designed to be stronger than the polymer material it will retain. That would ensure that if a failure were to occur, it would damage the printed part and not the build plate. This is accomplished by comparing the Yield Tensile Strength (YTS) at the base of the aluminum pin, 276 MPa for 6061 T6, to the Ultimate Tensile Strength (UTS) of the ABS/CF that is deposited across the entire unit cell cross-section, which is approximately 16.9 MPa (E. Weflen & Frank, 2021). Yield strength is selected for the build plate because plastic deformation of the pin would be considered a failure. On the other hand, the UTS is used for the polymer region to ensure that the part can break away without damaging the build plate. To further safeguard against failure, a conservative factor of safety of two is applied. Equation 3 shows the relationship between the pin area, A_p, and the YTS of the aluminum YTS_{al} with the Area of the unit cell, A_{uc}, the UTS of the ABS/CF, $UTS_{ABS/CF}$, and a safety factor of two, SF. The area of the unit cell, A_{uc}, is related to the diameter of the cutting tool, D_t, and the area of the width of the pin feature, W_p (eq. 4). Finally, the relation between the width of the pin and the area of the pin from eq. 5 results in three equations with three unknowns.

$$A_p \times YTS_{Al} = A_{uc} \times UTS_{\frac{ABS}{CF}} \times SF \tag{3}$$

$$A_{uc} = \left(D_t + W_p\right)^2 \tag{4}$$

$$A_p = {W_p}^2 \tag{5}$$

Solving eqs. 3-5 simultaneously results in a minimum pin diameter of 1.7 mm. Figure 26 highlights the region between the minimum pin diameter needed to avoid the potential for pin damage and the maximum density of undercut edge per area on the print surface. This area ranges from 1.7 mm to 3.2 mm. There may be reasons to reduce the pin size, which could potentially allow for the entire pin to be buried in a single bead of material. Reducing the pin size may also aid in part removal. In this study, a pin width of 3.2 mm will be held constant while the pin height and undercut angle are evaluated for their effect on retention while processing and when the part is thermally released.

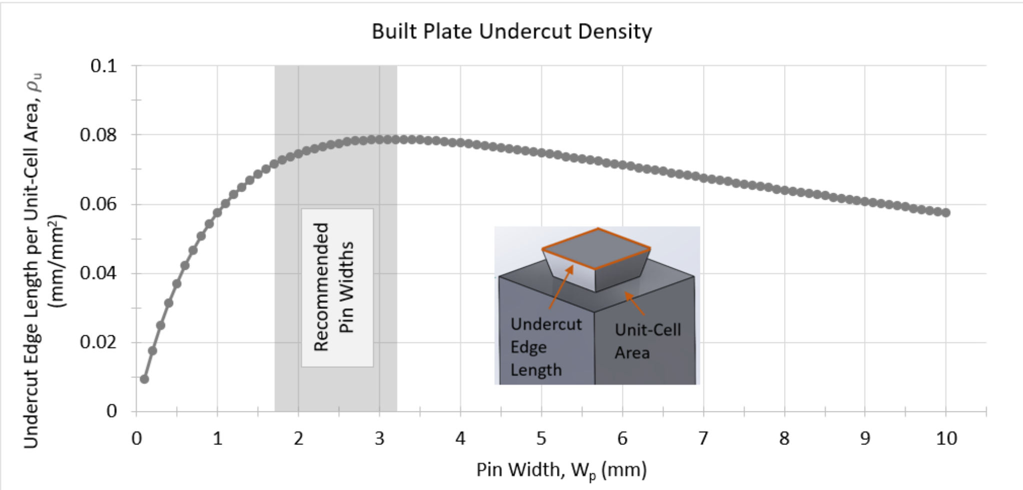

Figure 26. The ratio of undercut edge length per unit-cell area is plotted for various pin diameters with a maximum value found with pin diameters of 3.2 mm. The smallest acceptable pin diameter based on engineering mechanics calculations is 1.7 mm.

3.5.2 Characterization of bonding and release properties

The Temperatures at which the ABS/CF is released from the sample build plates with various dovetail pins are summarized in Figure 27. For dovetail pins with an included angle of 20°, increasing the pin length from 0.5 to 1.5 mm resulted in a 45% increase in the temperature needed to release the part under a constant load of 14 kPa. Similarly, increasing the included angle from 10° to 30° on a 1.0 mm pin increased the temperature needed to release the part by 20%. In both cases, the increase in release temperature corresponds to an increase in the undercut depth. A constant, rapid rate of heating is applied to the aluminum with a relatively high thermal conductivity compared to the ABS/CF. The release temperature in all cases is less than the 230° C temperature at which the polymer was processed, suggesting that only a moderate degree of softening is needed to release the parts from the dovetail-shaped pins. This is expected due to the limited polymer material in the undercut region retaining the part paired with the gradual slope of the dovetail pin.

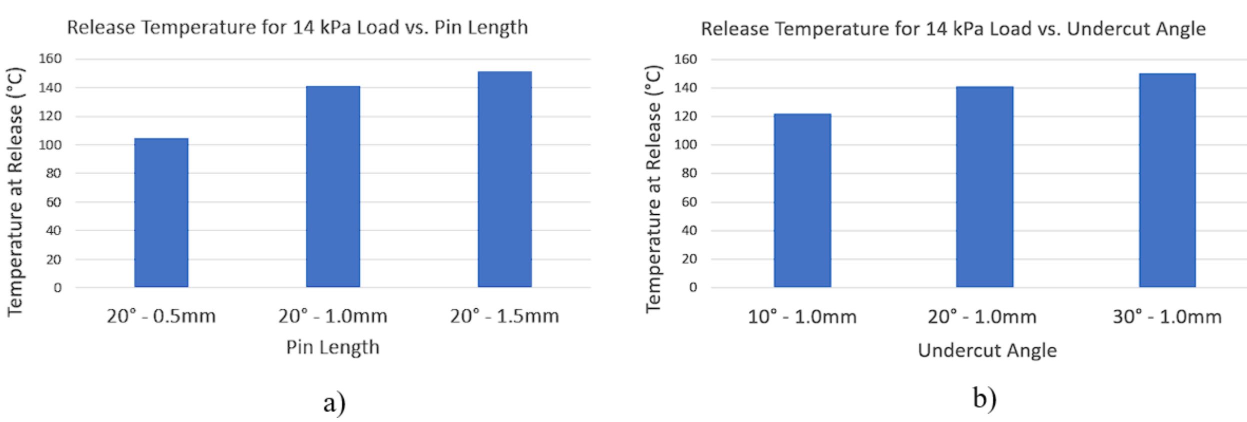

Figure 27. Release temperatures for ABS/CF printed simulated build plates with various interlocking pin geometries at a constant load for a) increasing pin length and b) increasing undercut included angles.

The ultimate tensile strength of the mechanical interlocking between the aluminum build plate specimens and the ABS/CF polymer resulted in two failure modes (Figure 28). While some samples pulled off the interlocking print surface, others experienced a delamination failure within the polymer region, leaving a single layer of polymer attached to the build plate. The tensile strengths of the samples in ambient conditions produced with various pin geometries are presented (Figure 29). Sample sets that experienced the delamination failure are marked with a star. A general trend is observed of increasing the pin length or the undercut angle, resulting in an increase in the sample's ultimate tensile strength (UTS).

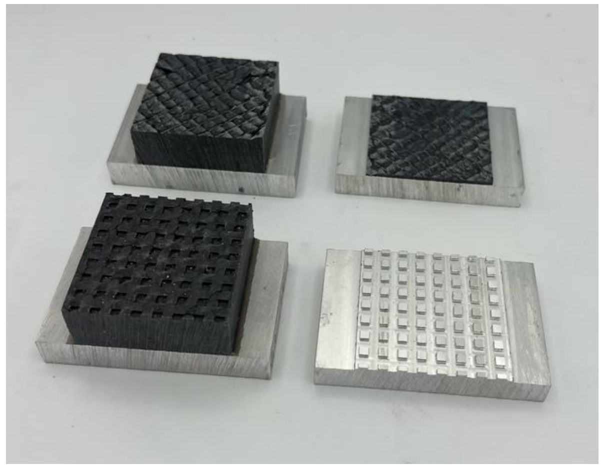

Figure 28. Failure modes of tensile samples at ambient temperatures.

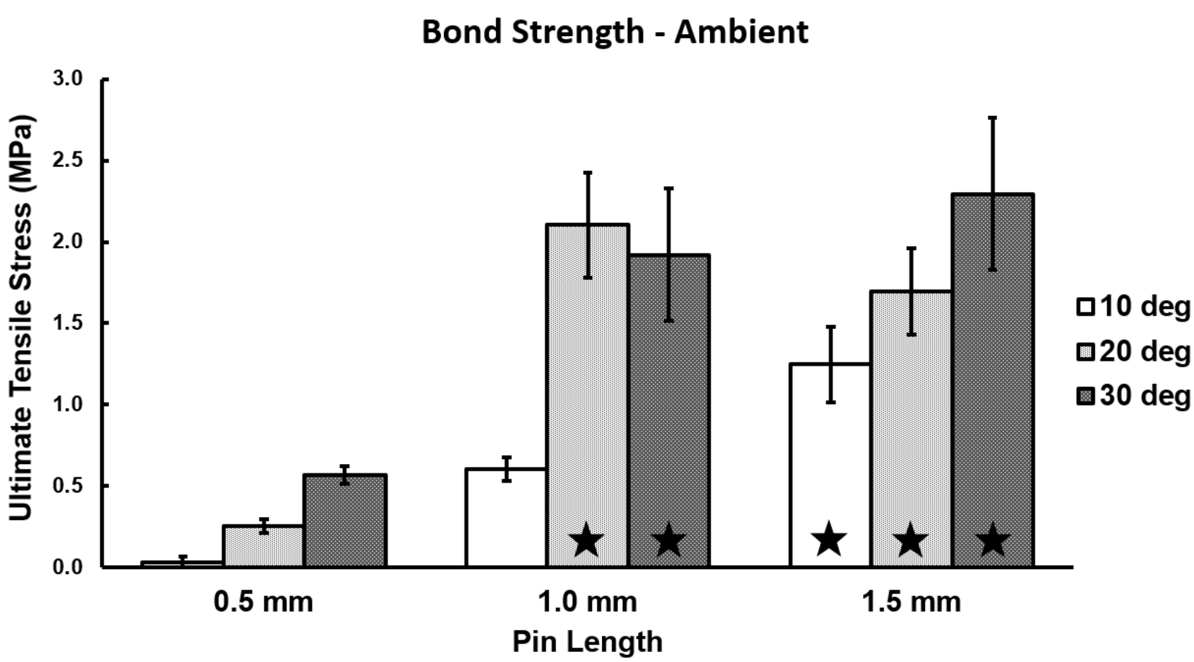

Figure 29. Tensile bond strength at ambient conditions for various interlocking pin geometries. Error bars represent one standard deviation. Stars denote an inter-layer delamination failure within the polymer region.

When the samples are heated to 141° C before tensile testing, the strength drops substantially, requiring the scale of the y-axis to be reduced by a factor of ten to observe the trends in the data (Figure 30). While the magnitude of the UTS is reduced, the general trend remains that increasing the pin length and the undercut angle both appear to increase the resulting strength of the bond. All of these samples were tested at the same release temperature, but adjusting the release temperature would change the release force, allowing for tuning of the parameter to meet the needs of a specific application. In this experiment, the release temperature was selected that would be expected to result in a 14 kPa strength in the samples with pin lengths of 1.0 mm, and undercut included angles of 20° (Figure 27). However, the results show a mean strength of 34 kPa, suggesting that the samples may have experienced some cooling during the tensile test. No instances of the polymer region inter-layer delamination failure mode occurred on samples tested at the elevated temperature.

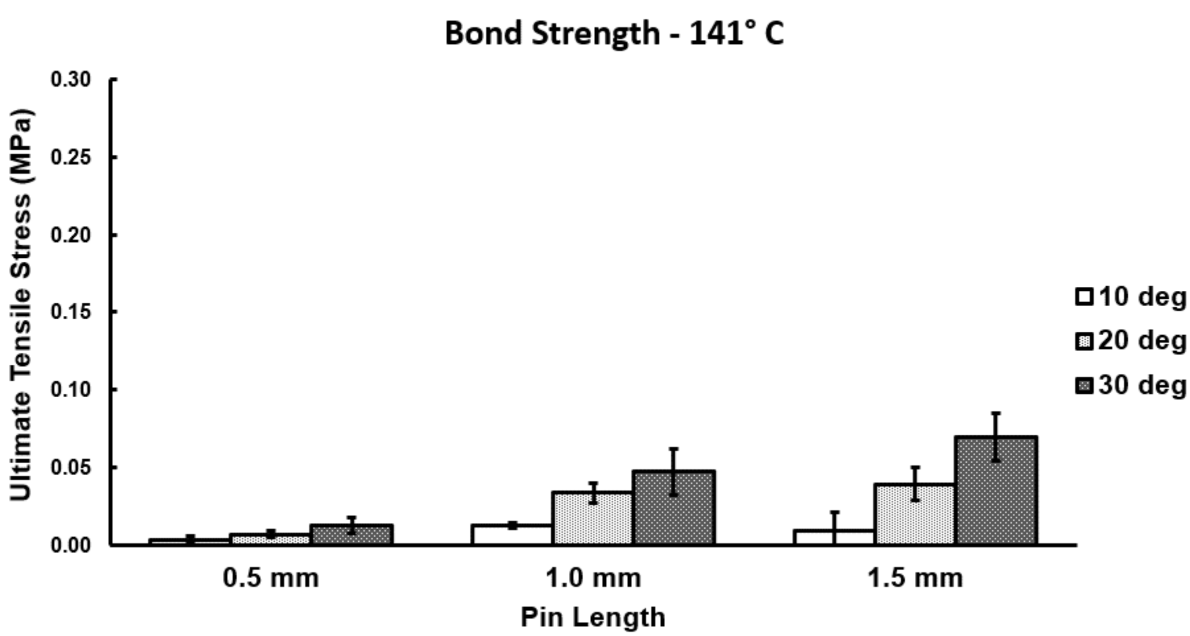

Figure 30. Tensile bond strength at elevated temperature for various interlocking pin geometries. Error bars represent one standard deviation.

To assist in the practical application of the print bed based on the data from this study, a linear regression model is produced using RStudio. This model will allow a user to enter their requirements for retention or removal load and receive a prediction for a pin design that meets those requirements. It also can be used to predict the retention and release strength for a given pin geometry. Four linear regression models were compared to balance complexity and accuracy (Table 2). The independent variables from the study, including the angle of the pin (*A*), pin length (*L*), and temperature (*T*), were considered along with two-way and three-way interactions for their ability to predict the dependent variable of bond strength.

Table 2. Four linear models are considered for prediction.

Model	Type	Independent Variables	Two-Way Interactions	Three-Way Interactions
M_1	Linear	*A*, *L*, *T*	n/a	n/a
M_2	Linear	*A*, *L*, *T*	*T*A*, *T*L*	n/a
M_3	Linear	*A*, *L*, *T*	*T*A*, *T*L*, *L*A*	n/a
M_4	Linear	*A*, *L*, *T*	*T *A*, *T*L*, *L*A*	*T*L*A*

The significance of the terms in each model is checked using ANOVA. All terms in M_1 and M_2 are significant ($\alpha < 0.05$). The two-way interaction between length and angle included in M_3 did not meet the significance threshold, suggesting that there is little benefit gained by the added complexity of that model compared to model M_2. The three-way interaction term also did not meet the threshold for significance. Furthermore, the model performance and complexity were compared using four metrics: the mean squared error (MSE), adjusted R^2, Akaike Information Criterion (AIC), and Schwarz's Bayesian Information Criterion (BIC) (Table 3). Multiple approaches were used to guide model selection because each has unique approaches to calculating the model performance and penalizing additional model complexity, allowing for increased confidence if the criteria agree and providing good information to guide selection even if they disagree (Kuha, 2004). The model selection is essential because the goal is not simply to select the model that best fits the data but to select the simplest model that adequately describes the data while avoiding overfitting.

Table 3. Model selection criterion.

Model	MSE	Adjusted R^2	AIC	BIC
M_1	0.230	0.691	100.2	111.4
M_2	0.105	0.863	48.3	63.9
M_3	0.104	0.853	48.5	66.4
M_4	0.105	0.853	49.5	69.6

Comparing the MSE for each model, where a lower value is desirable, there is a substantial drop in the MSE between M_1 and M_2 but little further reduction from the added complexity in M_3 and M_4. For the adjusted R^2, model M_2 provides the value closest to the ideal value of one. M_2 also achieves the lowest value for both AIC and BIC, signifying that the model does better than the other models at predicting the values when a penalty for added complexity is considered. The greater differentiation in BIC values between M2 and M3 than AIC values is likely due to BIC tending to penalize added complexity more heavily than AIC. Model M2 is chosen to represent the data based on the selection criterion. A residual plot suggests heteroskedasticity, which may be partially driven by greater variance in the samples tested at ambient temperatures. The Breusch-Pagan test evaluates the null hypothesis that heteroskedasticity exists in the data (Table 4). However, we fail to reject the null hypothesis since the p-value is not less than the threshold of 0.05. Yet, the p-value is close to the threshold, so care should be taken when using the model for predictions, and there may be a need to correct heteroskedasticity if the model were to be expanded to a broader design space.

Table 4. Results of Breusch-Pagan heteroskedasticity test.

Statistic	p-value	Parameter	Method
10.623	0.0594	5	Breusch-Pagan test

The selected multiple linear regression model M_2 is presented for the prediction of the bond strength ($\hat{Y}$) in MPa of ABS/CF to the aluminum build plate based on the pin height (length), the included angle of the undercut (angle), and the temperature of the build plate (temperature). A significant regression equation was found ($F(5,63) = 79.14$, $p < 2.2e-16$), with an adjusted R^2 of 0.863. Predicted bond strength is given by equation 6, with coefficients presented in (Table 5), where temperature is coded as a categorical variable, length is measured in mm, and angle is measured in degrees. Angle, length, temperature, and the two-way interactions between temperature and angle and between temperature and length were significant predictors of strength.

$$\begin{aligned}\hat{Y} = \beta_0 + \beta_1 \times angle + \beta_2 \times length + \beta_3 \times temperature \\ + \beta_4 \times temperature \times length \\ + \beta_5 \times temperature \times angle \qquad (6)\end{aligned}$$

Table 5. Coefficients for model M_2.

	Estimate	Std. Error	T Value	Pr (>|t|)	
Intercept	-1.235	0.195	-6.332	2.87E-08	***
A	1.461	0.133	11.026	2.42E-16	***
L	0.048	0.007	7.283	6.41E-10	***
T	1.195	0.284	4.201	8.53E-05	***
T:L	-1.423	0.194	-7.329	5.32E-10	***
T:A	-0.047	0.010	-4.800	1.02E-05	***

3.5.3 Evaluating the Demonstration Build Plate

The build plate was designed to minimize the disruption to the bottom of the part caused by the pins while maintaining a bond strength that led to interlayer delamination as the failure mode. The data show that the 1.0 mm tall pins with a 20° included angle achieve this objective. A rectangular build plate was fit to the size of the HAAS UMC750 machining center used for hybrid manufacturing in the lab, with the surface machined from aluminum stock (Figure 31). However, it was also designed to scale up to large-scale AM systems using a modular architecture, where pins may be placed only where needed for a build (Figure 32). This built plate is used to evaluate the ability to retain large-scale parts during their AM deposition, cooling, and machining operations.

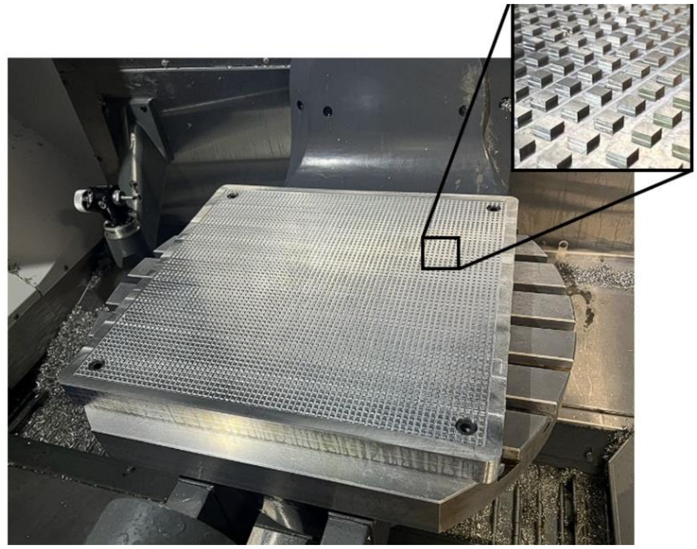

Figure 31. Fabrication of demonstration build plate with mechanically interlocking surface.

To evaluate the ability of the build surface to withstand warping loads, test strips were printed that span the width of the build surface. The test strips printed in neat ABS and an ABS/CF composite performed well during the processing evaluation. Parts remained firmly attached throughout

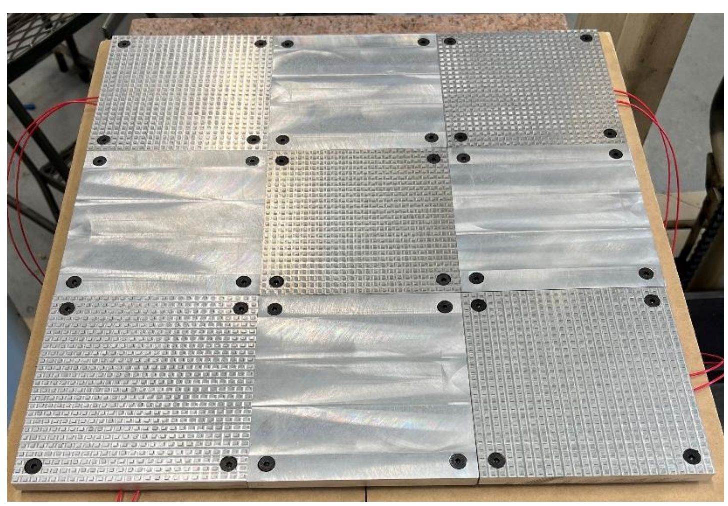

Figure 32. Modular Build plate for large-scale AM.

the additive extrusion process (Figure 33a), a cooling period of one hour, and the subsequent machining operation (Figure 33b). Samples remained affixed to the build plate during an aggressive machining operation with a 12.7 mm diameter flat end mill taking a 4.5 mm radial depth of cut with a 0.25 mm chip load. The samples were removed by heating the print bed to 141° C, at which point the operator could pull the samples off without needing tools.

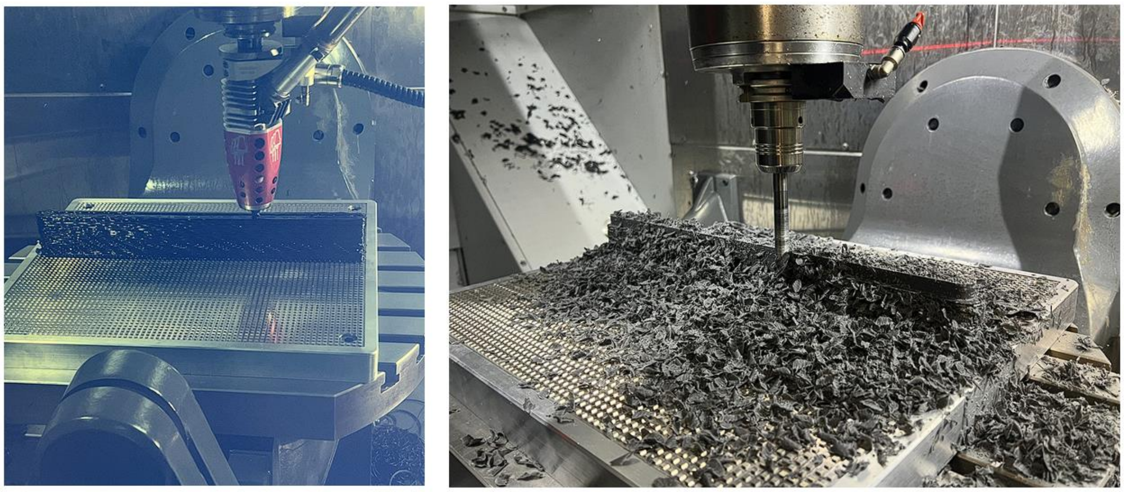

(a) (b)

Figure 33. Bow resistance and retention testing involved a) deposition using the Ambit Xtrude and b) machining after cooling.

When evaluated on a calibrated granite surface plate, the samples did not exhibit any significant signs of distortion (e.g., curling/bowing), potentially due to remaining retained to the built plate during cooling and machining (Figure 34). ABS without a filler material has traditionally been challenging to print on large-scale systems due to the shrink that occurs during solidification and cooling, leading to a buildup of residual stress,

Figure 34. ABS (bottom) and ABS/CF (top) parts on a granite surface plate.

resulting in bowing (Love et al., 2014). While the interlocking build plate may be able to retain a part printed in unfilled ABS, the thermally induced inter-bead shear stresses could lead to the formation of cracking (Talagani et al., 2015). The neat ABS sample showed signs of deformation immediately around the areas where the undercut pins were removed, potentially a sign that the neat ABS may have been overheated, reinforcing the desire to minimize the pin height (Figure 35). The release temperature testing should be conducted on each new material to prevent overheating. This experiment successfully demonstrates the print bed's ability to 1) withstand the forces produced during the additive and subtractive manufacturing operations and 2) allow rapid removal without needing tools.

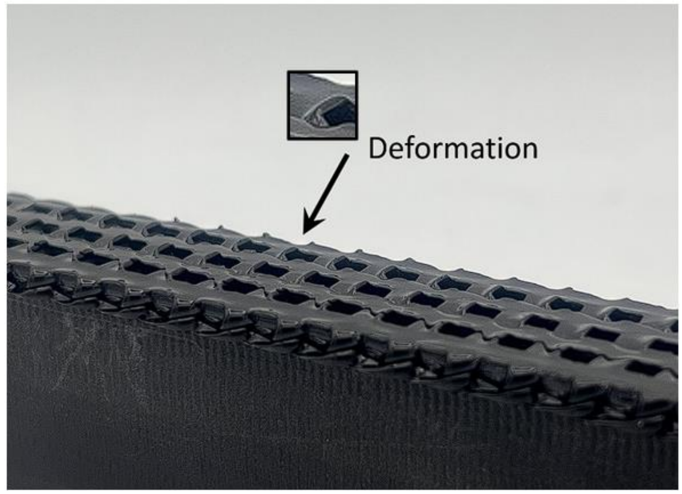

Figure 35. Example of deformation around pin locations seen only on the ABS sample.

A casting pattern was produced on the build plate using the ABS/CF material. The build plate was preheated to 100°C, then turned off when printing began. Since the overall height of the part exceeded the maximum tool extension of 76 mm, the pattern was partially printed to a height less than the tool reach (Figure 36a & b). Dovetail pin features were machined into the interface to potentially reduce the reduction in strength caused by cooling (Weflen, Ginther, Eldakroury, & Frank, 2021). The remaining geometry of the part was printed, allowed to cool, and then machined (Figure 36c & d). Once completed, the print bed was turned on, and the part was removed when the print bed reached 141°C (Figure 36e). It was noted that this larger part had to dwell at the removal temperature for a few minutes before it could be removed.

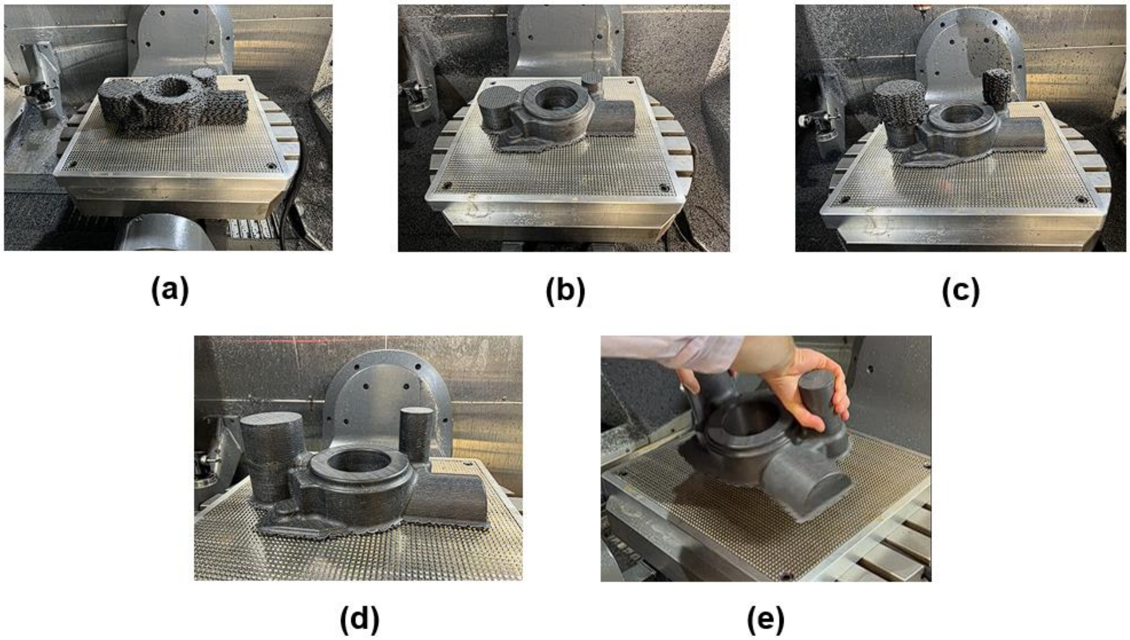

Figure 36. A casting pattern is produced by a) depositing ABS/CF material, b) machining the surfaces, c) continuing material deposition, d) final machining of the pattern, and e) removal from the build plate.

Since mechanical bonding primarily retains the part during printing instead of a chemical bond or thermal fusion, a wide range of materials can be used on the build plate. A small part was produced using high-density polyethylene (HDPE) to demonstrate part retention (Figure 37). While HDPE is one of the most common polymers used in traditional manufacturing, it has been a challenge for AM due to shrinkage-related bowing and challenges adhering to common print surfaces (Daniele, Armoni, Dul, & Alessandro, 2023). Overcoming the challenges related to printing HDPE can open new applications for material extrusion AM, ranging from the broader use of reclaimed material to

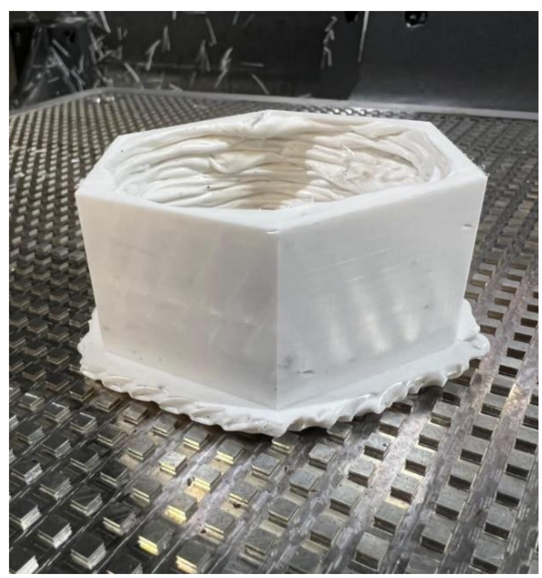

Figure 37. HDPE part produced using hybrid manufacturing.

the production of biomedical implants (Jeyachandran et al., 2021; Mejia et al., 2020). The ability to use a single build plate for a broad range of materials expands the applications where hybrid manufacturing can be effectively used.

The interlocking features presented in this work are designed for applications in large-scale AM systems. However, there is an opportunity to scale down the mechanical bonding and releasing approach to work with standard Fused Filament Fabrication (FFF) AM systems (**Error! Reference source not found.**). The research into effective design approaches for mechanically bonding and releasing build plates for smaller-scale AM systems may be able to achieve similar benefits as those achieved in large-scale systems.

The high bond strength presents a potential for this approach to be applied to end-use parts comprising metals and polymers (Figure 38). Multi-material parts benefit from local material selection, improving performance through greater design freedom. Demonstrations of multi-material parts consisting of aluminum and polymer regions were produced. Undercut dovetail features with the same specifications as those used on the print bed were nested on the interface between the aluminum and polymer materials from a structural bond. There is a need to optimize further the undercut geometry for multi-material parts to form a permanent bond between the dissimilar materials. Expanding the range of materials that can be combined into a single component within a hybrid manufacturing system moves us closer to achieving the goals of convergent manufacturing (National Academies of Sciences, 2022).

Figure 38. Multi-material parts produced using mechanical interlocking features.

3.6 Conclusions

This work presented a novel build plate for large-scale AM using mechanical interlocking to form a bond and rapid heating to release the part. The build plate with dovetail pin features demonstrated the ability to meet bonding requirements during processing and release the bond when processing is complete. An engineering mechanics and undercut feature density optimization model was presented that can be used to inform the design of systems for a broad range of applications and materials, including hybrid additive and subtractive manufacturing systems or multi-material parts. The relationship between the dovetail pin length and undercut angle was established, and a model was developed. This model can predict the retention and release strength that will be achieved based on a given dovetail pin design. It can also guide the design of the dovetail pin features to meet bond strength requirements. A demonstration build plate was produced to evaluate performance. Long test parts spanning the length of the build plate showed the ability to retain the part as residual stress builds up, even without a filler material, which has traditionally been required to reduce warping in ABS in open-environment large-scale additive manufacturing systems. The concept of the print bed has also shown initial promise in making multi-material parts, where the mechanical interlocking would be optimized for permanent bonding. The improvements made to the build plate can help expand the potential feasible applications for large-scale AM by making the processes more robust and reducing cost.

The proposed method of producing a thermally switchable print bed bond showed the potential for improving the manufacturing process for large-scale AM parts. However, there are still opportunities for refining this method and demonstrating its application on a broad spectrum of AM materials. Each material will require establishing appropriate release temperatures and may require a unique design of the dovetail pin feature to achieve optimal performance. There may also be materials that will chemically bond to the aluminum build plate, making part release challenging. Scaling this print bed up to a larger scale AM system will uncover additional challenges that must be solved. This approach of nesting the undercut geometry on end-use multi-material parts of dissimilar materials warrants further investigation. Mechanically interlocking interfaces can enable the production of tooling and end-use multi-material parts that traditionally are challenging to produce due to dissimilar material characteristics.

3.7 Acknowledgement

The authors thank Emma Bailey for help producing test samples. The authors would also like to thank Dr. Kris De Brabanter and Hao Wang for advice on the statistical analysis.

3.8 References

Altıparmak, S. C., Yardley, V. A., Shi, Z., & Lin, J. (2022). Extrusion-based additive manufacturing technologies: State of the art and future perspectives. *Journal of Manufacturing Processes, 83*. https://doi.org/10.1016/j.jmapro.2022.09.032

Daniele, R., Armoni, D., Dul, S., & Alessandro, P. (2023). From Nautical Waste to Additive Manufacturing: Sustainable Recycling of High-Density Polyethylene for 3D Printing Applications. *Journal of Composites Science 2023, Vol. 7, Page 320*, *7*(8), 320. https://doi.org/10.3390/JCS7080320

Jeyachandran, P., Bontha, S., Bodhak, S., Balla, V. K., & Doddamani, M. (2021). Material extrusion additive manufacturing of bioactive glass/high density polyethylene composites. *Composites Science and Technology*, *213*, 108966. https://doi.org/10.1016/J.COMPSCITECH.2021.108966

Kalle, J., Joni, K., Alexander, S., & Juhani, O. (2023). Potential and Challenges of Fused Granular Fabrication in Patternmaking. *International Journal of Metalcasting*, *17*(4), 2469–2476. https://doi.org/10.1007/S40962-023-00989-9/FIGURES/11

Kuha, J. (2004). *AIC and BIC Comparisons of Assumptions and Performance*. https://doi.org/10.1177/0049124103262065

Love, L. J., Kunc, V., Rios, O., Duty, C. E., Elliott, A. M., Post, B. K., … Blue, C. A. (2014). The importance of carbon fiber to polymer additive manufacturing. *Journal of Materials Research*, *29*(17), 1893–1898. https://doi.org/10.1557/JMR.2014.212

Love, L., Post, B., Noakes, M., Nycz, A., & Kunc, V. (2021). There’s plenty of room at the top. *Additive Manufacturing*, *39*, 101727. https://doi.org/10.1016/J.ADDMA.2020.101727

Martinsen, K., Hu, S. J., & Carlson, B. E. (2015). Joining of dissimilar materials. *CIRP Annals - Manufacturing Technology*. https://doi.org/10.1016/j.cirp.2015.05.006

Mejia, E. B., Al-Maqdi, S., Alkaabi, M., Alhammadi, A., Alkaabi, M., Cherupurakal, N., & Mourad, A. H. I. (2020). Upcycling of HDPE waste using additive manufacturing: Feasibility and challenges. *2020 Advances in Science and Engineering Technology International Conferences, ASET 2020*. https://doi.org/10.1109/ASET48392.2020.9118269

National Academies of Sciences, E. and M. (2022). Convergent Manufacturing: A Future of Additive, Subtractive, and Transformative Manufacturing: Proceedings of a Workshop. *Convergent Manufacturing: A Future of Additive, Subtractive, and Transformative Manufacturing*. https://doi.org/10.17226/26524

Post, B., Lind, R., Lloyd, P., Kunc, V., Linhal, J., & Love, L. (2016). *The Economics of Big Area Additive Manufacturing*. Retrieved from https://repositories.lib.utexas.edu/handle/2152/89664

Print bed - CEAD | Large Scale Additive Manufacturing. (2023). Retrieved May 6, 2023, from https://ceadgroup.com/solutions/technology-components/print-bed/

Roschli, A., Post, B. K., Atkins, C., Stevens, A. G., Chesser, P., & Zaloudek, K. (2022). Build Plate Design for Extrusion-Based Additive Manufacturing. *Proceedings of the 33rd Annual International Solid Freeform Fabrication Symposium*, 1079–1090.

Shafer, C. S., Siddel, D. H., & Elliott, A. M. (2017). Cleated Print Surface for Fused Deposition Modeling. *Journal of Mechanics Engineering and Automation*, *7*(1), 1359–1365. https://doi.org/10.17265/2159-5275/2017.01.005

Susnjara, K. J., & Vaal, S. G. (2020). *Patent No. US 10,569,523 B2*. Retrieved from https://patentimages.storage.googleapis.com/bc/af/b6/e204bc5f1bd0b3/US10569523.pdf

Talagani, M., DorMohammadi, S., Dutton, R., Godines, C., Baid, H., Abdi, F., … Blue, C. (2015). Numerical Simulation of Big Area Additive Manufacturing (3D Printing) of a Full Size Car Virtual Integrated Battery Environment View project Solidification Microstructure Control in Electron Beam Additive Manufacturing View project. *Sampe Journal*, *51*(4), 27–36. Retrieved from www.mgc-a.com

Verma, S., Yang, C. K., Lin, C. H., & Jeng, J. Y. (2022). Additive manufacturing of lattice structures for high strength mechanical interlocking of metal and resin during injection molding. *Additive Manufacturing*, *49*, 102463. https://doi.org/10.1016/J.ADDMA.2021.102463

Weflen, E. D., Ginther, M. C., Eldakroury, M. A., & Frank, M. C. (2021). Mechanical Interface for Iterative Hybrid Additive and Subtractive Manufacturing. *Proceedings of the 32nd Annual International Solid Freeform Fabrication Symposium*, 1676–1682. https://doi.org/http://dx.doi.org/10.26153/tsw/17676

Weflen, E. D., Peters, F. E., & Frank, M. C. (2022). Hybrid Additive and Subtractive Manufacturing of Direct-Heated Tooling. *Proceedings of the 33rd Annual International Solid Freeform Fabrication Symposium*. https://doi.org/10.26153/TSW/44652

Weflen, E., & Frank, M. C. (2021a). Hybrid additive and subtractive manufacturing of multi-material objects. *Rapid Prototyping Journal*, *27*(10), 1860–1871. https://doi.org/10.1108/RPJ-06-2020-0142/FULL/PDF

Weflen, E., & Frank, M. C. (2021b). Hybrid additive and subtractive manufacturing of multi-material objects. *Rapid Prototyping Journal*, *ahead-of-print*(ahead-of-print). https://doi.org/10.1108/RPJ-06-2020-0142

CHAPTER 4. HYBRID ADDITIVE/SUBTRACTIVE MANUFACTURING OF MULTI-MATERIAL PARTS USING MECHANICALLY INTERLOCKING FEATURES

Eric Weflen, Frank E. Peters, Matthew C. Frank

Industrial and Manufacturing Systems Engineering Department, Iowa State University,

Ames, Iowa 50011, USA

Modified from a manuscript to be submitted to *Additive Manufacturing Letters*

4.1 Abstract

This work presents mechanically interlocking interfaces for the production of multi-material parts using an integrated hybrid additive and subtractive manufacturing system to move towards the convergence of multiple materials and processes in a single manufacturing system. Multi-material parts have a long history of use in the injection molding industry and are gaining popularity as a method of reducing design constraints, allowing for further design optimization that can be achieved with a single material. However, we lack a method for creating multi-material parts of dissimilar materials in hybrid additive and subtractive manufacturing systems. These hybrid manufacturing systems integrating polymer material extrusion and machining take advantage of the strengths of each process while avoiding their weaknesses. A mechanically interlocking interface is developed that produces a structural bond by machining undercut geometry into the interface between dissimilar material regions of a heterogeneous part. A mechanical bond is formed as the deposited molten polymer region solidifies on the interface. Undercut geometries are created using dovetail and t-slot specialty milling tools and are evaluated for their ability to withstand tensile loading conditions. The results presented in this work expand the applications of multi-material components produced in hybrid manufacturing systems, resulting in designs that more effectively meet customer requirements.

4.2 Introduction

There is industry demand to move away from traditional serialized manufacturing systems with discrete processes and materials to improve manufacturing and supply chain resilience and agility (National Academies of Sciences, 2022). The convergence of hybridized manufacturing processes and hybrid materials systems into a single platform presents an alternative, integrated approach to manufacturing functional parts at the point of use (Bapat et al., 2022). Interleaving of additive manufacturing (AM) and subtractive machining processes results in synergistic benefits that allow for novel geometries to be produced with higher productivity and better surface finish (Feldhausen, Heinrich, et al., 2022; J. B. Jones, 2014). Similar synergistic performance gains can be made possible by bringing multi-material capabilities to these systems.

Research into hybrid additive and subtractive manufacturing processes has often focused on producing single-material parts more effectively (Dávila, Neto, Noritomi, Coelho, & da Silva, 2020). Still, research into multi-material AM parts has grown over the past several years, with researchers demonstrating the potential for improved performance and functionality from heterogeneous parts (Nazir et al., 2023b; Zhang et al., 2019). Using traditional manufacturing approaches, Tesla and Mercedes have achieved weight reductions using hybrid metal-polymer cross-car beams produced by ElringKlinger (Albert et al., 2019). However, AM research has concentrated on bringing together compatible materials, emphasizing metal-metal or polymer-polymer combinations, which may be due to challenges with the interface between dissimilar materials. Dissimilar materials in hybrid parts offer the potential for advanced design optimization to reduce cost and weight with improved performance (Hiller & Lipson, 2009; Li & Kim, 2018). A method for joining regions of dissimilar materials is needed to move existing hybrid manufacturing systems toward the goals of convergent manufacturing.

Material regions in parts can be joined using chemical bonding, thermal fusion, mechanical joining, or a combination of these approaches (Martinsen et al., 2015). Parts with dissimilar metal-polymer materials produced using AM processes have successfully employed mechanical interlocking features to form structural interfacial bonds (Chueh et al., 2020b; Englert et al., 2022; Ribeiro et al., 2019). Mechanical bonding has shown potential for use in producing multi-material parts in hybrid manufacturing (Weflen & Frank, 2021). Still, a more general solution is needed for compatibility with a broad range of materials and interface geometries.

A method for joining dissimilar metal-polymer and polymer-polymer regions in multi-material parts using mechanically interlocking features is presented. Undercut pin features are milled using simple facing toolpaths on the interface between materials to form a mechanical bond. The structural performance of the interface is evaluated for two interlocking interface geometries on four combinations of materials. Multi-material parts are produced using two different metals and four different polymers to demonstrate the potential of mechanical interlocking to form structural bonds with a broad range of materials.

4.3 Solution Overview

Mechanical interlocking will be formed using undercut or overhanging geometry to retain a polymer material region (Figure 39). When producing a multi-material part in a hybrid manufacturing system, one material region will first either be machined from stock material or deposited using AM. An overhanging feature can be created in this primary material region (Figure 39a). A second material can be deposited in molten form, filling the area under the overhanging geometry (Figure 39b). As most materials solidify and cool, they will contract. It is critical to consider material contraction when designing the undercut feature to ensure that a rigid interlock will be produced. Pin features are used in this approach to ensure the polymer will pull tight to the protruding dovetail feature as it shrinks. After cooling, the material under the overhang is solid, producing a mechanical interlock that joins the two regions (Figure 39c).

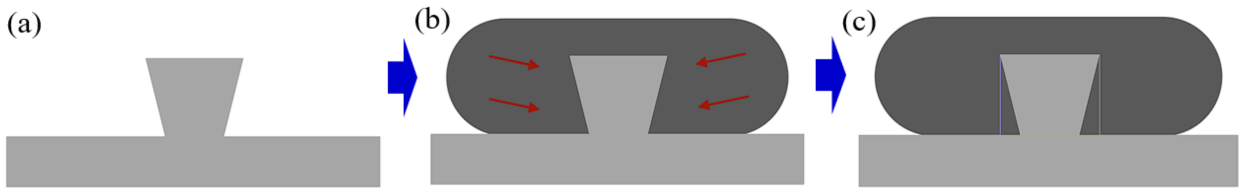

Figure 39. A detail view of the mechanical interlocking produced by a) forming an overhanging feature in the interface, b) molten polymer fills the volume under the overhand and pulls tight upon solidification and cooling, and c) solidified material under the overhang joins the dissimilar material regions.

A wide range of strategies can be used to form overhanging geometry in a hybrid manufacturing system depending on the process capabilities, so opportunities may exist to further optimize the mechanical bond strength (Figure 40). Undercutting tools or multi-axis toolpaths can be used to mill the features into the primary substrate. Various additive processes can be used to deposit material to form undercut geometry. The appropriate approach to creating the geometry will depend on the requirements of the part being produced and the manufacturing system's capabilities.

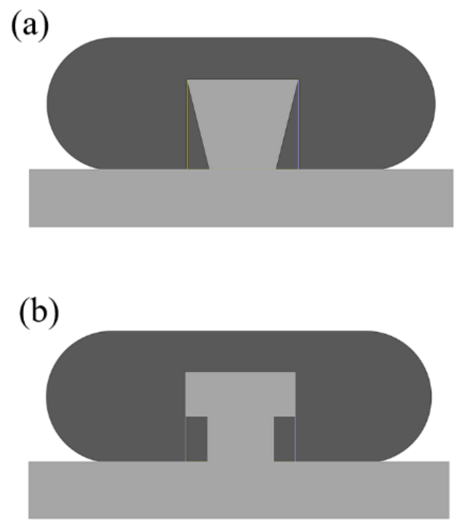

Figure 40. A wide range of geometries exist that will result in interlocking, including a) dovetail and b) t-slot features.

A multi-material part can be produced by nesting these features into the interface between material regions. A primary material stock, such as aluminum or steel, can be used, and the required part geometry can be machined into that substrate (Figure 41a and b). An undercutting machine tool can create repeating pin features with overhanging geometry in the area where a secondary material, such as a polymer composite, will be deposited. An additive process can deposit the secondary material (Figure 41c). Upon solidification, the machining of the part produces the final part geometry (Figure 41d). This process can be repeated in multiple setup orientations or with numerous different materials depending on the system capabilities and the requirements of the part.

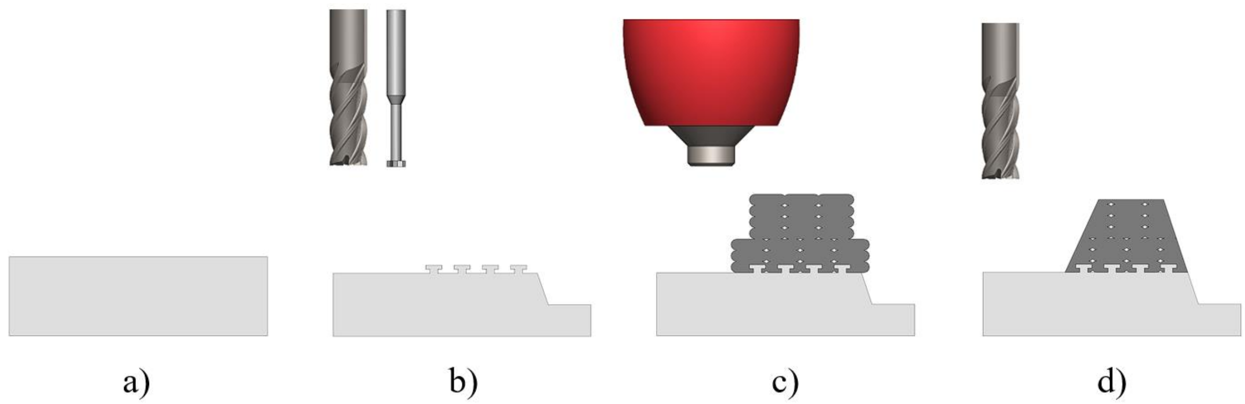

Figure 41. A multi-material part is produced through the steps of a) selecting a primary substrate, b) machining part geometry and creating retaining features in the material interface, c) depositing secondary material using AM, and d) machining final part geometry.

This approach is implemented in a HAAS UMC750 5-axis machining center modified by Hybrid Manufacturing Technologies to include polymer and metal AM. A cylindrical aluminum stock has an array of dovetail pin features machined in three locations (Figure 42a). Undercut dovetail pins were machined using a specialty dovetail-cutting tool. The AMBIT Xtrude pellet extruder prints a machining stock of Acrylonitrile Butadiene Styrene (ABS) (Figure 42b). A ball end mill is used to machine the final geometry in the ABS and blend the interface between the material regions (Figure 42c).

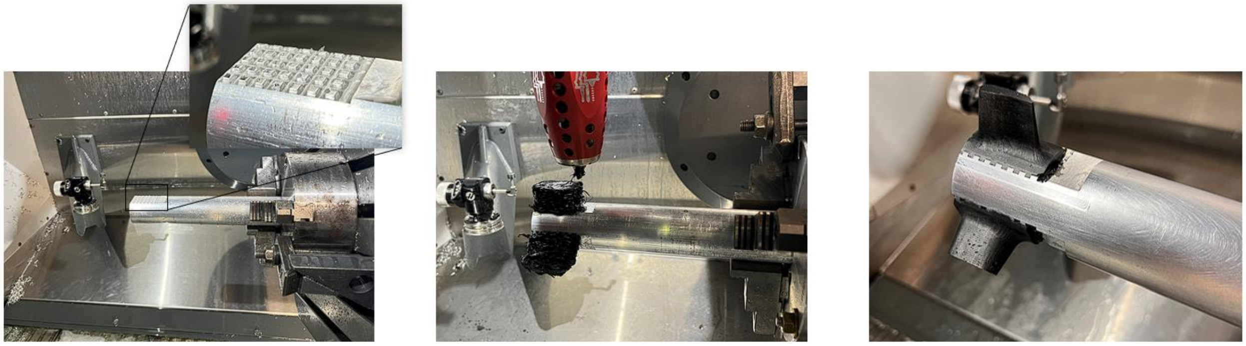

(a) (b) (c)

Figure 42. A multi-material part is produced by a) machining interlocking features, b) depositing polymer machining stock, and c) final machining after cooling.

4.4 Methodology

To investigate the structural performance of mechanically interlocking interfaces, they were evaluated in both metal-polymer and polymer-polymer material systems. Dovetail and t-slot pin features with the same undercut depth were investigated to determine how the geometry influenced the mechanical properties. Samples were produced in a HAAS UMC750 5-axis machining center with AMBIT Xtrude tooling made by Hybrid Manufacturing Technologies (Figure 43).

Figure 43. HAAS 5-axis hybrid manufacturing system.

4.4.1 Metal-Polymer Bond Strength

This experiment investigated two metal-polymer material systems, each with three different interface geometries (Table 6). Aluminum primary material was paired with an ABS secondary material. In addition, low-carbon steel was paired with a composite ABS containing a 20% chopped carbon fiber content. Three interfaces were tested: a control, t-slot pins, and dovetail pins. A flat-surfaced control interface was tested with a solvent-cast ABS film to promote adhesion. However, samples using the control interface broke during processing due to the weak bond and were not able to be tested. Dovetail or t-slot pins were machined into a 305 x 76 mm aluminum or steel plate with a spacing of 3.2 mm (Figure 44a). The pin length and width measured 3.2 mm, while the height was only 1 mm. A 3.2 mm diameter dovetail cutting tool with a 20° included angle and a 3.2 mm diameter t-slot cutter with a slot height of 0.5 mm were used to mill the undercut geometry.

Table 6. Experimental matrix for metal-polymer multi-material interfaces.

ID	Primary Material	Secondary Material	Interface	Quantity Tested
M1	Aluminum - 6061	ABS	Control	0
M2	Aluminum - 6061	ABS	T-Slot Pins	5
M3	Aluminum - 6061	ABS	Dovetail Pins	5
M4	Steel - 1020	ABS-CF	Control	0
M5	Steel - 1020	ABS-CF	T-Slot Pins	4
M6	Steel - 1020	ABS-CF	Dovetail Pins	5

The ABS and ABS-CF polymer was deposited using the AMBIT Xtrude screw extrusion system (Figure 44b). The 3 mm nozzle was positioned 0.5 mm over the top of the pins for the first layer, and 9 mm wide beads were deposited. Using a +45/-45 raster fill toolpath, ten layers were deposited, with a layer height of 2 mm being used for layers two through ten. This polymer machining stock was then machined to a height of 20.5 mm, and a 12.7 mm shoulder was machined to facilitate tensile testing (Figure 44c).

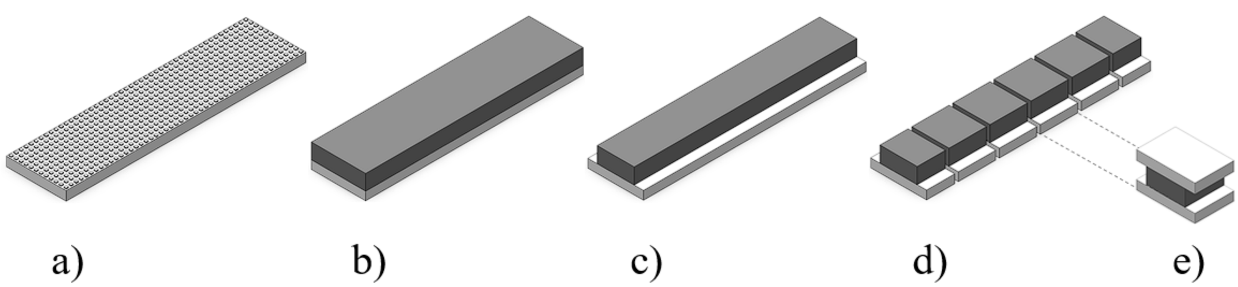

Figure 44. Test samples were prepared by a) machining dovetail features into the primary substrate, b) printing a machining stock of the secondary material, c) machining the surfaces, d) extracting tensile samples, and e) applying a tensile fixture.

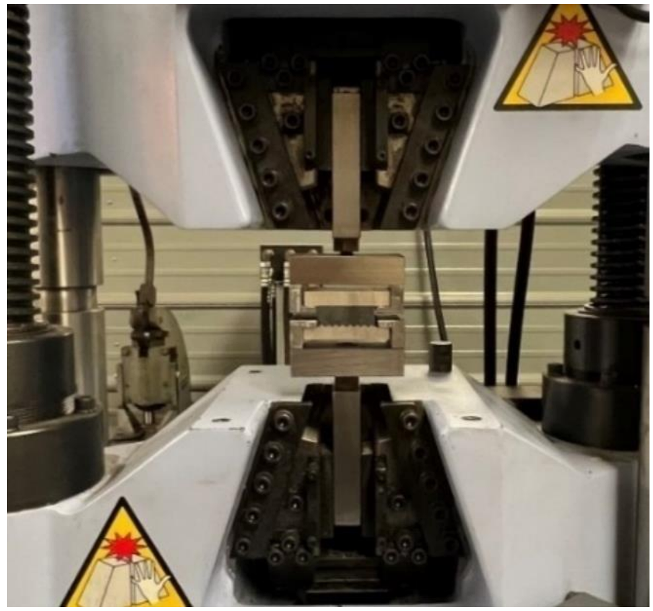

Figure 45. Custom fixture used to test the bond strength.

Tensile samples were extracted from the test piece, and a tensile fixture palate was attached to the top surface to facilitate tensile testing following a modified procedure based on ASTM D897-08. The interface between materials measured 50.8 x 50.8 mm. Samples were conditioned in the lab environment for a minimum of 24 hours before testing. Tensile specimens were tested using a custom fixture on a Shimadzu universal testing machine with a strain rate of 0.5 mm/min (Figure 45). The ultimate tensile strength of each specimen was recorded along with the failure mode.

4.4.2 Polymer-Polymer Bond Strength

A primary substrate of ABS-CF was used to determine how the same interlocking features perform when machined into a polymer substrate (Figure 46). A secondary substrate of composite polypropylene containing 20% chopped glass fiber fill (PP-GF) was used. Additionally, the same ABS-CF material was used as both a primary and secondary substrate in a sample set to determine if this approach can be used for interleaving the additive deposition and subtractive machining. Interleaving these processes can be challenging in polymers because they must cool before machining, which can result in reduced bond strength when depositing the following layers of material (Feldhausen, Heinrich, et al., 2022; Frank et al., 2019; Kishore et al., 2017).

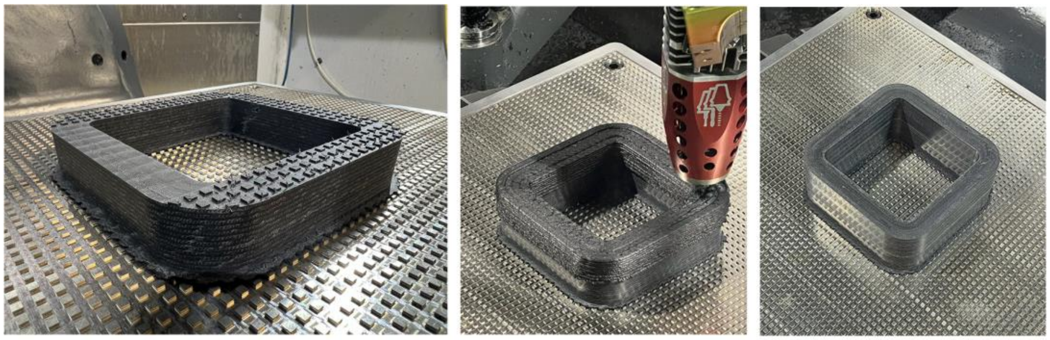

Figure 46. Polymer-polymer multi-material sample production involved a) depositing primary substrate and machining interlocking features, b) depositing secondary substrate, and c) final part machining.

A square was printed, and a different interface was machined into each of the four sides with dovetail and t-slot pin geometry matching those used in the metal-polymer experiments. Because there is a potential for thermal fusion in materials with similar processing temperatures, an additional control sample was included with straight wall pins having no undercut. Five tensile specimens measuring 63.5 x 22 x 16 mm were collected from each edge (Figure 47) and tested following ASTM D638 using a modified Type III geometry (Table 7). Samples were conditioned in the lab environment for 24 hours before testing on a universal testing machine.

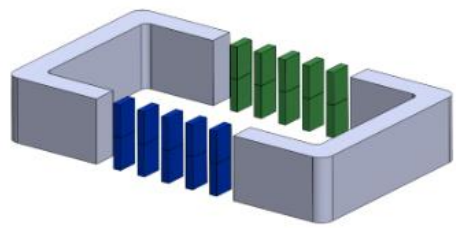

Figure 47. tensile samples cut from each edge of the square.

Table 7. Experimental matrix for polymer-polymer multi-material interfaces.

ID	Primary Material	Secondary Material	Interface	Quantity Tested
P1	ABS-CF	PP-GF	Control - Flat	0
P2	ABS-CF	PP-GF	Control - Pins	5
P3	ABS-CF	PP-GF	T-Slot Pins	5
P4	ABS-CF	PP-GF	Dovetail Pins	5
P5	ABS-CF	ABS-CF	Control - Flat	5
P6	ABS-CF	ABS-CF	Control - Pins	5
P7	ABS-CF	ABS-CF	T-Slot Pins	5
P8	ABS-CF	ABS-CF	Dovetail Pins	5

4.5 Results

4.5.1 Metal-Polymer Multi-Material Parts

To produce the tensile samples, dovetail and t-slot features were machined into aluminum and steel primary substrates (Figure 48). The depth of the undercut was measured using an optical microscope and a precision X-Y table. Five pin features spaced across the length of the sample were measured to determine how the achieved depth of undercut compared to the undercut of 0.17 mm in the 3D model.

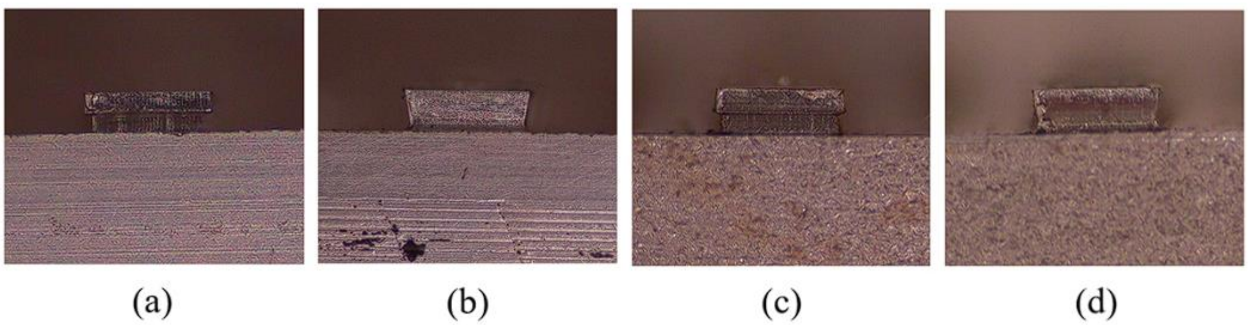

Figure 48. Optical microscope images of undercut pin features from each sample set geometries include a) t-slot in aluminum, b) dovetail in aluminum, c) t-slot in steel, and d) dovetail in steel.

Figure 49 shows that all samples achieved reduced undercut compared to the CAD model. The aluminum samples resulted in more undercut than the steel, and the t-slot cutting tool produced a greater undercut depth than the dovetail in both the aluminum and steel samples. This difference in undercut depth is likely due to tool deflection caused by cutting forces on the relatively small 3.2 mm diameter tools. Since the overhanging geometry generated by the undercut forms the mechanical interlocking, the differences in undercut may affect interfacial strength.

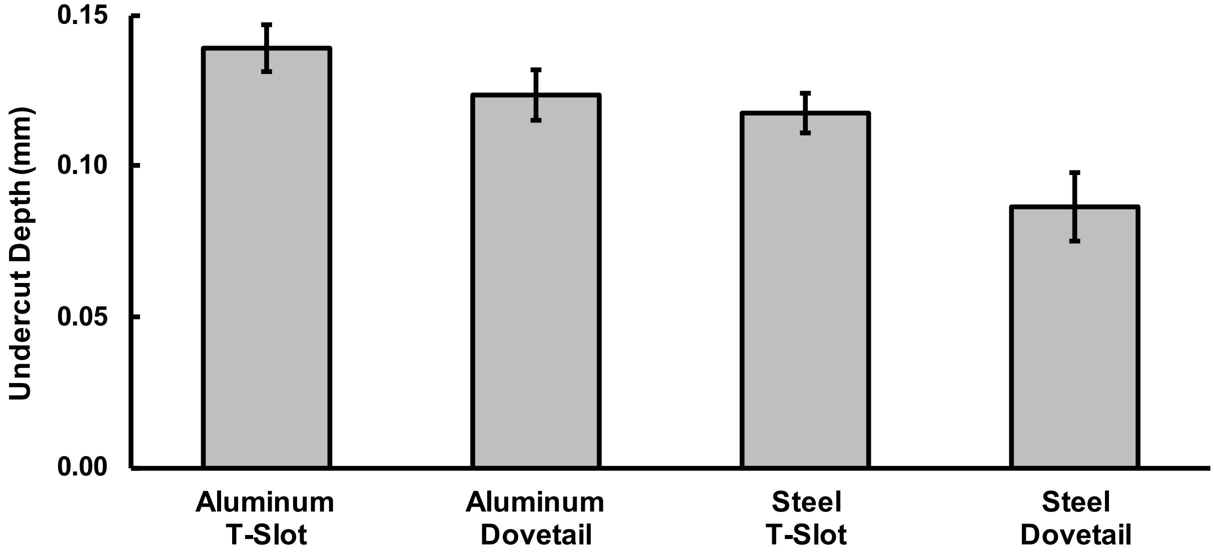

Figure 49. Maximum undercut dimension for each of the sample geometries. Error bars represent the standard deviation.

Production of the aluminum and steel control samples with a flat surface was impossible, as the bond strength was too low to resist the loads caused by processing and the build-up of residual stress (Figure 50). The inability of the bond to even support the loads during processing demonstrates the challenges faced when attempting to produce multi-material parts with dissimilar materials using current approaches. Even when an ABS film was solvent cast to the surface, there was a failure to achieve a sufficient bond to complete the printing process.

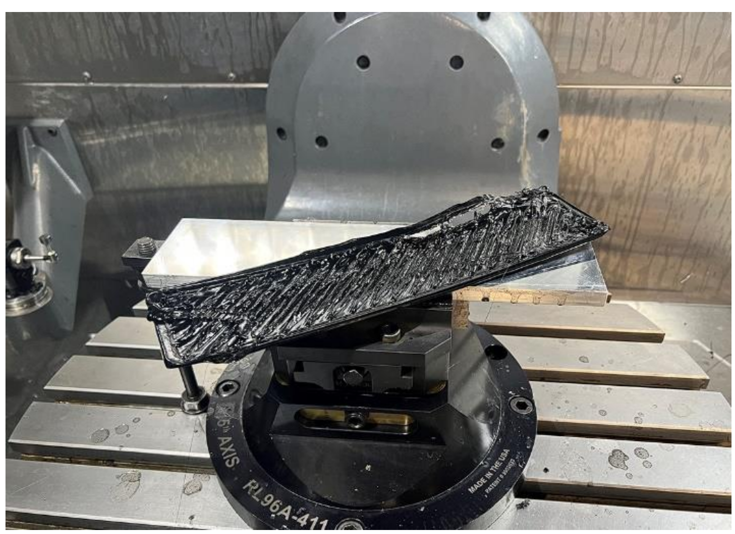

Figure 50. Bond failure on the control sample during processing.

The aluminum t-slot and dovetail samples produced with the unfilled ABS material experience a substantial bow of over 6 mm (Figure 51). While this deformation affected the quality of the printing process, it grew gradually over time and did not require the process to stop. Since the ends of the samples experienced a greater disruption in the printing process, they were discarded, and tensile specimens were collected from the center of the part. The degree of bowing in these samples demonstrated the large forces that can be generated due to the differential cooling rate caused by layer-by-layer deposition, and further demonstrate the importance of chopped carbon fiber or other filler materials in large-scale AM applications (Love et al., 2014).

Figure 51. Bow exhibited by samples produced with unfilled ABS.

The tensile testing results show that for both material systems, the t-slot geometry outperformed the dovetail geometry (Figure 52). This may suggest that for the formation of a permanent bond in a multi-material part, there may be a benefit of an aggressive interlocking geometry found in the t-slot samples. The aluminum/ABS samples exhibited higher strength than the steel/ABS-CF samples. This result may be due to the differing material properties or the reduced undercut in the steel samples. Comparing these results to the measured undercut dimension (Figure 49), it can be challenging to interpret these results alone what portion of the difference in bond strength can be attributed to undercut or to the different pin geometry.

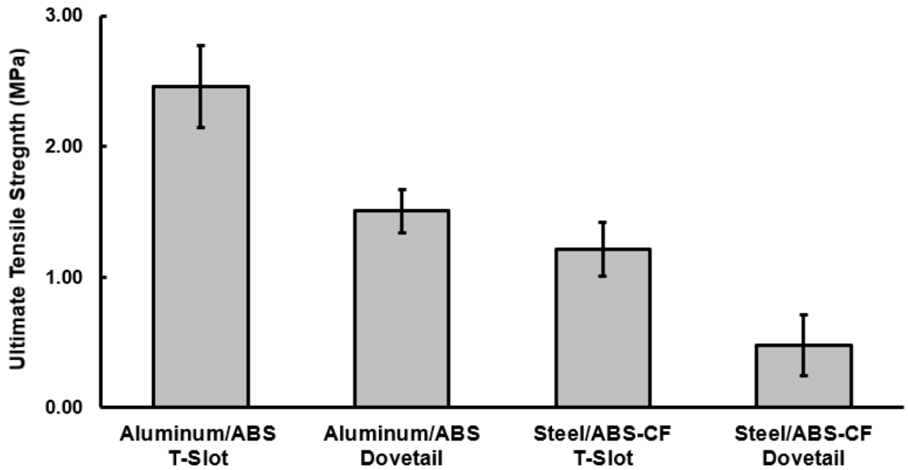

Figure 52.Ultimate tensile strength for ABS printed on aluminum and ABS-CF printed on steel t-slot and dovetail pin features. Error bars represent one standard deviation.

Typical failure modes for each sample set are shown (Figure 53). In all instances, the secondary polymer region is cleanly separated from the primary aluminum or steel material. In this failure mode, the undercut pin was pulled out of the polymer region instead of causing a delamination failure, which suggests that the mechanical bond strength was less than the inter-layer strength of the polymer. This type of failure indicates that an interlocking feature with more undercut may increase bond strength.

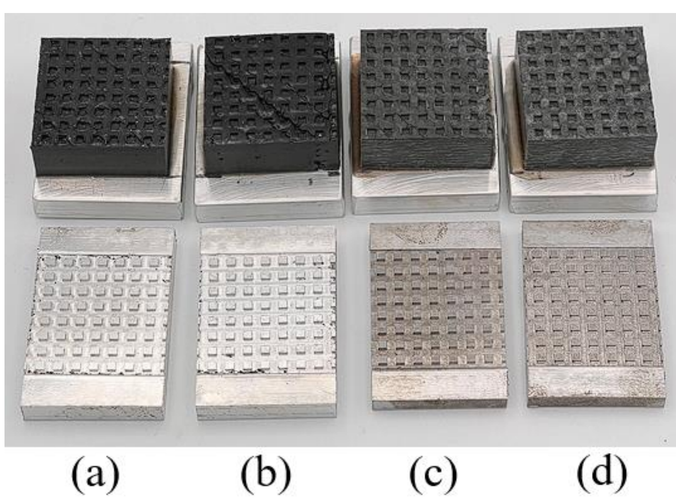

Figure 53. Typical tensile failures for sample sets a) M2 t-slot, b) M3 dovetail, c) M5 t-slot, and d) M6 dovetail.

4.5.2 Polymer-Polymer Multi-Material Parts

During sample production for the PP-GF polymer printed on the primary substrate of ABS-CF, the control interface was too weak to be formed into tensile samples. When compared to the secondary control set with straight pins lacking an undercut, the t-slot samples were 3.2x stronger, and the dovetail pins were 2.3x stronger (Figure 54). Again, the samples produced with the t-slot pins outperform the dovetail pins. In this instance, the t-slot geometry results in a bond that is 26% stronger than achieved by the dovetail pins. While the overall bond strength between the two materials is much lower than would typically be expected from either base substrate, a structural bond is still achieved that can be used to guide the design of a multi-material part consisting of these materials.

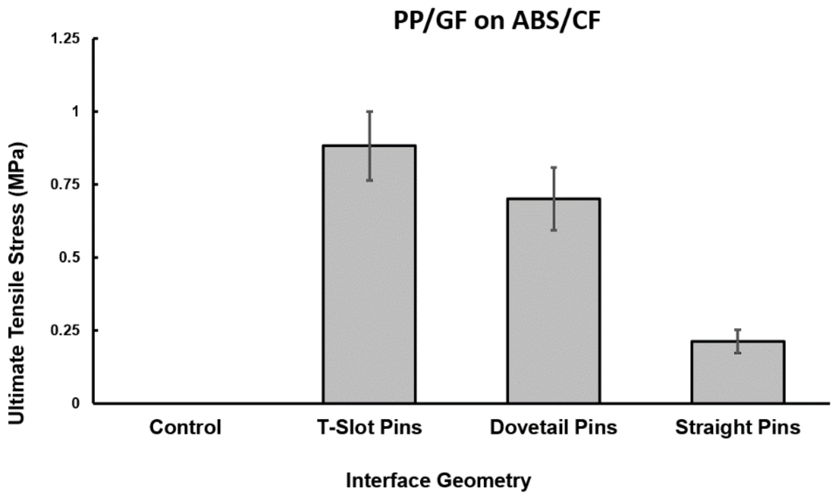

Figure 54. Ultimate tensile strength for PP-GF printed on ABS-CF.

The failure modes for the tensile samples show that samples with dovetail pins and straight pins experienced a clean separation. In contrast, the t-slot samples experienced a fracture of the overhanding features that create the mechanical interlocking (Figure 55). The same geometry was used for the t-slot pins in metal and polymer primary

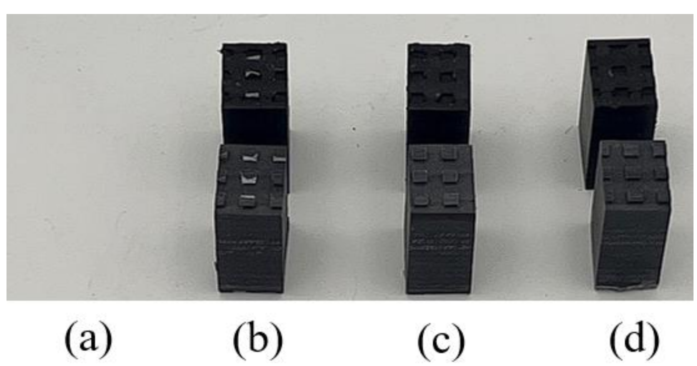

Figure 55. Typical failure modes for PP-GF to ABS-CF for a) no control samples tested, b) t-slot, c) dovetail, and d) straight pins.

substrates. When the weaker polymer material is used as the primary substrate, the design of the pin features may need to be modified to achieve the optimal bond strength.

Interleaving the additive deposition with subtractive machining can simplify processing and allow for the machining of high aspect ratio features with standard tooling. Interleaving can also enable the fabrication of parts that we would not otherwise be able to produce. Improving the bond strength achieved when depositing polymer on a cooled substrate is critical for interleaving in polymer hybrid systems. Tensile testing of the control samples shows that using the ABS-CF material as both the primary and secondary material achieves a bond strength above that of the PP-GF material deposited on the ABS-CF material (Figure 56). This difference is likely due to better material compatibility allowing for thermal fusion. However, this bond strength is still much lower than expected from ABS-CF material (Weflen & Frank, 2021). Still, the dovetail pins achieve a bond that is 68% stronger than the control, while the t-slot and straight pins show no significant difference. While below that of the ABS-CF substrate, or even the interlayer strength from ABS-CF produced using AM, this improved bond strength can help enable interleaving in applications where this strength is enough to achieve performance requirements.

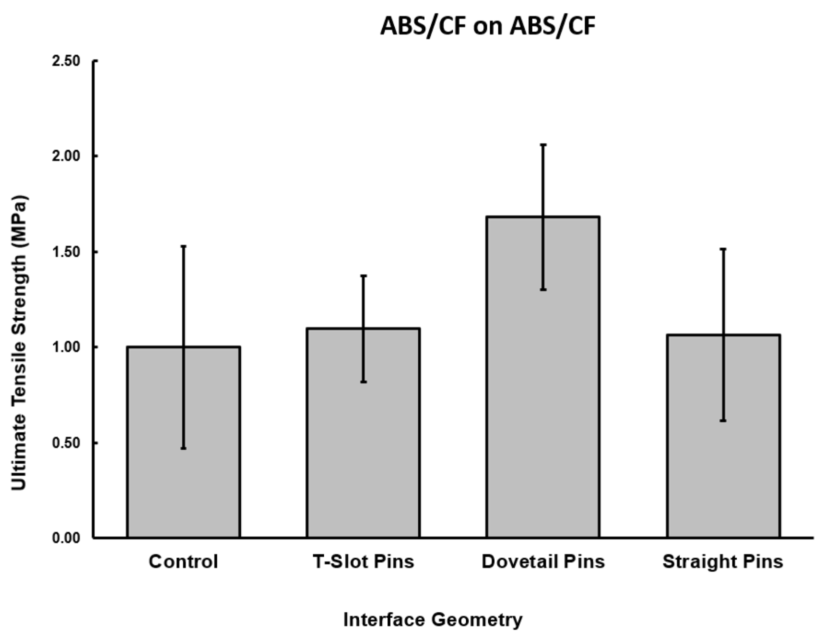

Figure 56. Ultimate tensile strength for ABS-CF to ambient ABS-CF tensile samples. Error bars represent one standard deviation.

For the first time, the t-slot geometry fails to show an improvement compared to the dovetail pin geometry or the control. Visual inspection of the failure surfaces reveals that the t-slot samples did not fracture as they did in the PP-CF samples (Figure 57). Furthermore, there does not appear to be polymer remaining under the t-slot geometry. It seems that the ABS-CF material did not flow into the overhanging region on these samples, which could explain the lack of improvement in strength.

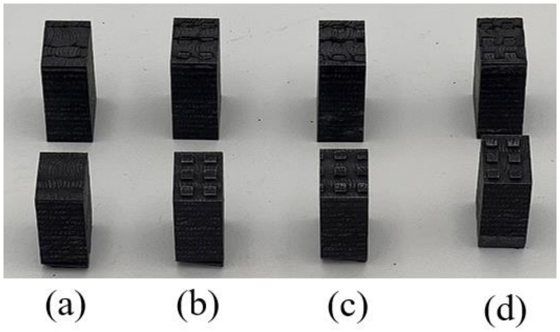

Figure 57. Typical failures for ABS-CF to ABS-CF samples a) control, b) t-slot, c) dovetail, d) straight pin.

A structural bond is achieved in both the case of printing with the same material on a cool interface and printing with a dissimilar secondary material, PP-GF. These results demonstrate the potential for mechanically interlocking features to achieve a structural bond in polymer systems. However, the data show that further research is needed to improve the design of the interlocking features when produced in a polymer primary substrate. Still, achieving a structural bond between these material systems can allow for interleaving AM and machining in a hybrid system while allowing the material properties to be tuned to meet the performance requirements.

4.5.3 Hybrid Manufacturing of Multi-Material and Large-Scale Parts

Two multi-material parts were produced using the method presented in this paper (Figure 58). The first is a duct that consists of an aluminum flange and an ABS-CF tube section. The primary aluminum substrate was machined with dovetail pin features nested in the interface between the material regions. ABS-CF material was deposited and machined. The part demonstrates the ability to transition between materials on various interface geometries. The second part is an aluminum primary substrate with unfilled ABS polymer turbine fins retained by dovetail pins. This part demonstrates how there may be multiple material regions in a single part.

Figure 58. Metal-polymer multi-material parts produced using hybrid manufacturing.

A casting pattern was produced using interleaved additive deposition (Figure 59a), machining of the surfaces (Figure 59b), and resuming additive deposition with the aid of interlocking dovetail pins (Figure 59c). Dovetail pins nested in the interface using a simple facing operation at 0/90 degrees, leaving an array of 3.2 mm pins (Figure 60). This part was produced using ABS-CF material. Because the print was stopped mid-way, simple 3-axis toolpaths could reach all part surfaces using a standard length, 75 mm cutting tool. The final machining of the part blends the two sections to achieve the required surface finish (Figure 59d). This part is produced on an aluminum build plate that temporarily retains the part during deposition using a grid of

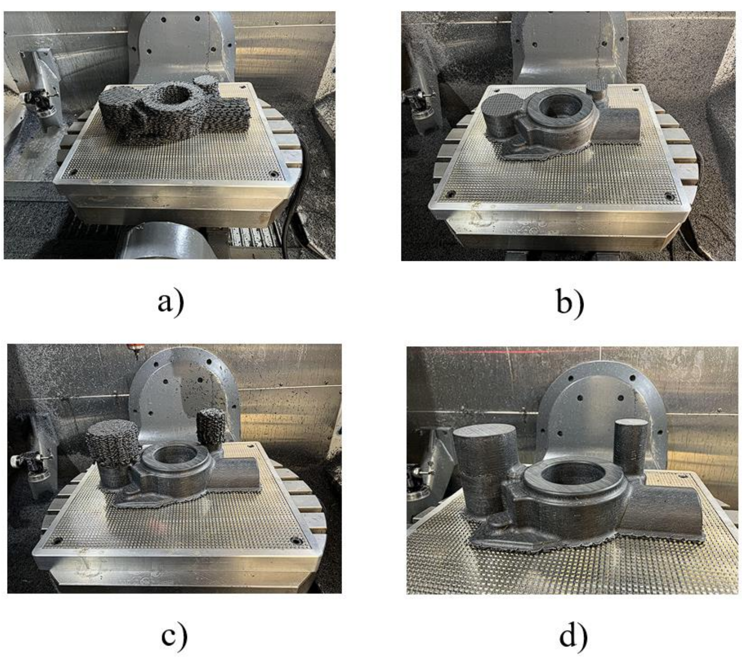

Figure 59. Production of a casting pattern using hybrid manufacturing by a) deposition a section of the part, b) machining primary section of the pattern and creating undercut features, c) depositing a second region of material, and d) final machining of the part.

dovetail pins. The mechanical bond between the build plate and the casting pattern is released by heating the build plate, resulting in softening of the polymer. The ability to remove the polymer regions of a multi-material part through heating could find applications for part features requiring frequent modification or customization. Applications may also include areas prone to wear or breakage. This process could allow for those regions to be removed and replaced.

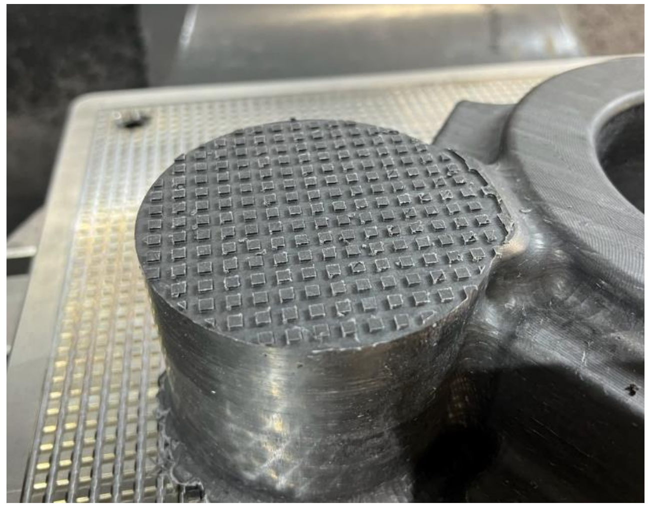

Figure 60. Dovetail pins machined in the interface between the primary ABS-CF and the secondary ABS-CF material.

While a small set of material combinations is presented in this work, there is a broad range of polymers, each with unique properties that could be beneficial if placed in regions of a part. For example, elastomeric materials like thermoplastic urethane (TPU) are often used in injection molding applications where a rigid material may be paired with a compliant material using over-molding. (Figure 61a) Low-friction polymers like high-density polyethylene (HDPE) are often used in assemblies as glide surfaces and for anti-marring (Figure 61b). Since this method relies on mechanical interlocking to join the regions of the material, a broad range of materials can be used. However, the findings of this study show that there may be additional benefits of designing the interface geometry for the properties of the materials being used. Still, many applications may not

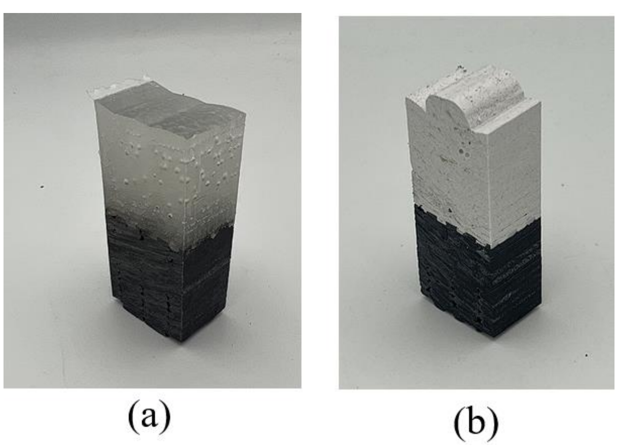

Figure 61. Polymer-Polymer multi-material parts consisting of a) ABS-CF and TPU, and b) ABS-CF and HDPE.

require optimal parameters to meet the functional requirements of the part, and this process may provide a route for the rapid implementation of various materials.

4.6 Conclusions

A method for producing multi-material parts consisting of dissimilar material regions was evaluated and implemented in the production of casting patterns and metal-polymer functional parts. By creating mechanical interlocking features using a hybrid additive and subtractive manufacturing approach, a range of materials can be used to meet a part's functional requirements. The bond strength for two metal-polymer and two polymer-polymer material combinations was evaluated. The effect of the interlocking geometry on the joint strength was quantified, with the more aggressive t-slot proving to be the most effective geometry in all applications except that of the ABS-CF to ABS-CF material combination. The results suggest an opportunity exists to further increase the size of the overhanging features to achieve a stronger bond.

A small set of material combinations was studied relative to the range of materials used in the machining and material extrusion AM processes. The suitability and compatibility of each material being considered for use with this process further warrants investigation. There is an opportunity to create a library of interfacial strengths for material combinations that could be used as a design guide. Furthermore, a limited range of mechanically interlocking features were investigated. Each pairing of materials could benefit from a design optimization of the interlocking features tuned to take advantage of their material properties. Tensile testing was used to determine the ability to produce a structural bond between material regions. However, tensile properties alone do not fully define the interfacial properties. Further investigation would be required to understand the structural performance of the joint for the loading conditions experienced by an end-use part.

The work described here demonstrates the potential for a mechanical bonding approach to be used with various materials in hybrid manufacturing. Further investigations will improve the interlocking structures presented here to improve the interfacial properties in multi-material parts. As the capabilities of hybrid manufacturing systems evolve, opportunities may emerge for new approaches for creating interlocking geometries. The added complexity brought by producing multi-material parts in a hybrid manufacturing system that combines multiple manufacturing processes into a single system will require the development of new automated design and manufacturing tools that will help the users realize the potential of these systems.

4.7 Acknowledgements

The authors thank Emma Bailey for the help producing test samples.

4.8 References

Albert, A., Werner, M., Landgrebe, D., Drossel, W.-G., Layer, M., Engelmann, U., & Kroll, L. (2019). Media Based Forming and Injection Molding Based on Fiber Reinforced Plastic Tubes. *Procedia Manufacturing*, *27*, 166–171. https://doi.org/10.1016/J.PROMFG.2018.12.060

Bapat, S., Sealy, M. P., Rajurkar, K. P., Houle, T., Sablon, K., Malshe, A. P., … Applications, ". (2022). Applications of Hybrid Manufacturing during COVID-19 Pandemic: Pathway to Convergent Manufacturing . *Smart and Sustainable Manufacturing Systems* , *6*(1), 12–22. https://doi.org/10.1520/SSMS20210022

Chueh, Y. H., Zhang, X., Ke, J. C. R., Li, Q., Wei, C., & Li, L. (2020). Additive manufacturing of hybrid metal/polymer objects via multiple-material laser powder bed fusion. *Additive Manufacturing*, *36*, 101465. https://doi.org/10.1016/J.ADDMA.2020.101465

Dávila, J. L., Neto, P. I., Noritomi, P. Y., Coelho, R. T., & da Silva, J. V. L. (2020). Hybrid manufacturing: a review of the synergy between directed energy deposition and subtractive processes. *The International Journal of Advanced Manufacturing Technology 2020 110:11*, *110*(11), 3377–3390. https://doi.org/10.1007/S00170-020-06062-7

Englert, L., Heuer, A., Engelskirchen, M. K., Frölich, F., Dietrich, S., Liebig, W. V., … Schulze, V. (2022). Hybrid material additive manufacturing: interlocking interfaces for fused filament fabrication on laser powder bed fusion substrates. *Https://Doi.Org/10.1080/17452759.2022.2048228*, *17*(3), 508–527. https://doi.org/10.1080/17452759.2022.2048228

Feldhausen, T., Heinrich, L., Saleeby, K., Burl, A., Post, B., MacDonald, E., … Love, L. (2022). Review of Computer-Aided Manufacturing (CAM) strategies for hybrid directed energy deposition. *Additive Manufacturing*, *56*, 102900. https://doi.org/10.1016/J.ADDMA.2022.102900

Frank, M. C., Croghan, J., Larson, S., & Beguhn, L. (2019). Integration Challenges with Additive/Subtractive In-Envelope Hybrid Manufacturing. *Proceedings of the 30th Annual International Solid Freeform Fabrication Symposium*. https://doi.org/10.26153/TSW/17258

Hiller, J. D., & Lipson, H. (2009). Multi material topological optimization of structures and mechanisms. *Proceedings of the 11th Annual Genetic and Evolutionary Computation Conference, GECCO-2009*. https://doi.org/10.1145/1569901.1570105

Jones, J. B. (2014). The synergies of hybridizing CNC and additive manufacturing. *Technical Paper - Society of Manufacturing Engineers*.

Kishore, V., Ajinjeru, C., Nycz, A., Post, B., Lindahl, J., Kunc, V., & Duty, C. (2017). Infrared preheating to improve interlayer strength of big area additive manufacturing (BAAM) components. *Additive Manufacturing*. https://doi.org/10.1016/j.addma.2016.11.008

Li, C., & Kim, I. Y. (2018). Multi-material topology optimization for automotive design problems. *Proceedings of the Institution of Mechanical Engineers, Part D: Journal of Automobile Engineering*, *232*(14), 1950–1969. https://doi.org/10.1177/0954407017737901/FORMAT/EPUB

Love, L. J., Kunc, V., Rios, O., Duty, C. E., Elliott, A. M., Post, B. K., … Blue, C. A. (2014). The importance of carbon fiber to polymer additive manufacturing. *Journal of Materials Research*, *29*(17), 1893–1898. https://doi.org/10.1557/JMR.2014.212

Martinsen, K., Hu, S. J., & Carlson, B. E. (2015). Joining of dissimilar materials. *CIRP Annals - Manufacturing Technology*. https://doi.org/10.1016/j.cirp.2015.05.006

National Academies of Sciences, E. and M. (2022). Convergent Manufacturing: A Future of Additive, Subtractive, and Transformative Manufacturing: Proceedings of a Workshop. *Convergent Manufacturing: A Future of Additive, Subtractive, and Transformative Manufacturing*. https://doi.org/10.17226/26524

Nazir, A., Gokcekaya, O., Md Masum Billah, K., Ertugrul, O., Jiang, J., Sun, J., & Hussain, S. (2023). Multi-material additive manufacturing: A systematic review of design, properties, applications, challenges, and 3D printing of materials and cellular metamaterials. *Materials & Design*, *226*, 111661. https://doi.org/10.1016/J.MATDES.2023.111661

Ribeiro, M., Sousa Carneiro, O., & Ferreira da Silva, A. (2019). Interface geometries in 3D multi-material prints by fused filament fabrication. *Rapid Prototyping Journal*, *25*(1), 38–46. https://doi.org/10.1108/RPJ-05-2017-0107/FULL/PDF

Weflen, E., & Frank, M. C. (2021). Hybrid additive and subtractive manufacturing of multi-material objects. *Rapid Prototyping Journal*, *27*(10), 1860–1871. https://doi.org/10.1108/RPJ-06-2020-0142/FULL/PDF

Zhang, C., Chen, F., Huang, Z., Jia, M., Chen, G., Ye, Y., … Lavernia, E. J. (2019). Additive manufacturing of functionally graded materials: A review. *Materials Science and Engineering A*. https://doi.org/10.1016/j.msea.2019.138209

CHAPTER 5. HYBRID ADDITIVE AND SUBTRACTIVE MANUFACTURING FOR AUTOMATING METALCASTING PRODUCTION WELDING

Eric Weflen, Matthew C. Frank, Frank, E. Peters

Industrial and Manufacturing Systems Engineering Department, Iowa State University,

Ames, Iowa 50011, USA

Modified from a manuscript to be submitted to the *Rapid Prototyping Journal*

5.1 Abstract

A method is presented for process parameter development and control for Wire Arc Additive Manufacturing (WAAM) for the production welding of anomalies found in steel castings. WAAM, sometimes referred to as Wire Arc Directed Energy Deposition (WA-DED), is used to rapidly produce large-scale metal parts and is often paired in-envelope with subtractive machining in a hybrid manufacturing system. However, industry adoption of WAAM is limited due to the need for the development of process parameters for different material systems. Process variation necessitates monitoring and control to ensure the deposited material meets the part requirements. WAAM process parameters are presented for low-carbon steel, a standard alloy used in steel foundries. A new metric is presented to support the data-driven evaluation of the step-over distance by evaluating 3D scan data. This metric consists of the ratio of the components of the surface waviness parallel and perpendicular to several adjacent weld beads. This new method provides either an automated agent or an operator of a hybrid manufacturing system with a quantitative metric that can be related to process parameter changes needed to resolve potential build issues. Operators of hybrid manufacturing systems currently lack adequate actionable process monitoring metrics. The presented method can help improve the monitoring and control of WAAM systems, reducing the occurrence of scrap.

5.2 Introduction

Wire arc additive manufacturing (WAAM) has gained popularity for producing large-scale parts out of various metals due to the high deposition rates and the ability to forgo tooling lead times and costs (Özel, Shokri, & Loizeau, 2023). Also referred to as Wire Arc Directed Energy Deposition (WA-DED), this process has also demonstrated potential for use in repairing and remanufacturing of metal parts (Hong, Xiao, Zhang, & Zhou, 2021; Lee et al., 2022). Welding is regularly used in the production of metalcastings to meet specification requirements (Figure 62) (Monroe, 2019). Regions of the casting that do not meet the customer's requirements are excavated and replaced by a skilled welder following a qualified welding procedure (Figure 63) (David et al., 2015).

Figure 62. Production welding of a metalcasting in a job shop steel foundry.

Foundry production welding can be challenging to automate because each excavation can be unique. There are also job shop foundries that specialize in low production volume castings, further complicating the automation. Low production volumes and mass customization are areas where additive manufacturing (AM) excels due to process planning automation. There is an opportunity to automate foundry production welding using WAAM. This study investigates the use of WAAM for the production welding of low carbon steel castings.

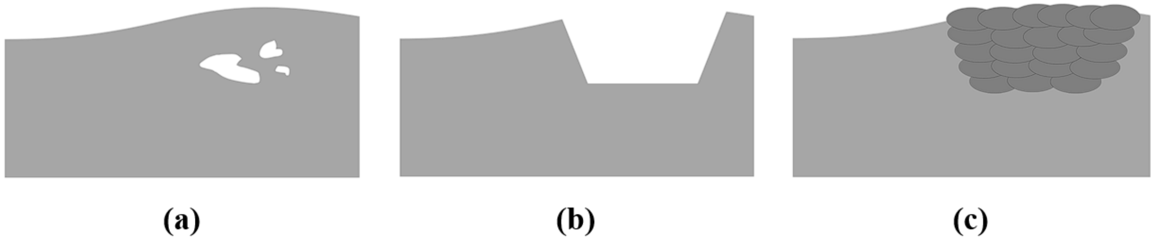

Figure 63. Production welding of a metalcasting involves a) identification of a production anomaly, b) excavation of the anomaly, c) filling the excavation with weld material.

Arc-welding has been used to deposit material to form geometry and add features to parts since early in its development (Patent No. US1533300A, 1920). However, advances in automation and AM automated process and motion planning have allowed for the creation of geometry with increasing complexity (Feldmann et al., 2019; Gardner, Kyvelou, Herbert, & Buchanan, 2020; Williams et al., 2016). High deposition rates on the order of 5 kg/h are used to produce objects on the scale of a meter cubed or more on a timescale of hours to days (Hagen et al., 2023; Nycz, Adediran, Noakes, & Love, 2016). Research and parameter development have often focused on reducing costs associated with the buy-to-fly ratio of aerospace materials such as titanium alloys and Inconel, though recently, there has been interest in applications using lower-cost materials such as stainless or carbon steel (Costello et al., 2023). WAAM and other directed energy deposition AM processes have been applied to remanufacturing and repairing large-scale parts that failed in service (Lee et al., 2022; Priarone, Campatelli, Catalano, & Baffa, 2021).

Hybrid manufacturing (HM) processes combine two or more unique manufacturing processes to create a synergistic effect that results in a system that is more capable than the processes individually (Lauwers et al., 2014; Zhu, Dhokia, Nassehi, & Newman, 2013b). These processes can be combined in-envelope, contained within a single device, or sequentially in an out-of-envelope approach (Frank et al., 2017a). Furthermore, the operations can take place simultaneously, one then the next in a serial fashion, or interleaved together to produce part geometry using an iterative approach (Feldhausen, Heinrich, et al., 2022; Lauwers et al., 2014). Subtractive machining has been demonstrated to pair well with AM due to each process possessing unique strengths that reduce weaknesses of the other to reduce cycle times while achieving required dimensional and material characteristics (Feldhausen et al., 2021; Jones, 2014). Hybrid AM and machining processes have also shown potential for remanufacturing parts that have failed to meet quality requirements or are in service (Feldhausen, Kannan, et al., 2022; Jones et al., 2012). Applications of this approach often focused on small or medium-scale parts (Hamilton, Sorondo, Li, Qin, & Rivero, 2023; Saleeby, Kurfess, Feldhausen, & Love, 2021; Zhang, Cui, Li, & Liou, 2019). Interleaving of additive and subtractive processes in a hybrid system may well suited for the removal and replacement of material and surface blending that occurs in production welding of a metalcasting.

Welding on a metalcasting requires qualified processes and quality control to ensure that weld material meets or exceeds requirements (David et al., 2015). Standardization and qualification of the parameters and conditions of the welding process are critical to ensure part quality (ASME-BPVC.IX, 2023; ASTM-A488, 2017). However, process monitoring and control are still needed to identify and prevent defects due to process variation (Zahidin et al., 2023). Numerous models have been studied for WAAM parameter development, which primarily center around modeling the bead geometry based on the width, height, and shape (Ding, Pan, Cuiuri, & Li, 2015a; Xiong, Zhang, Gao, & Wu, 2013). The flat top overlapping model (FOM) and the tangent overlapping model (TOM) have been used to predict the topology that results from adjacent weld beads with a given geometry (Ding et al., 2015a; Suryakumar et al., 2011). Despite this, the complexities of a unique part can still be challenging to predict and model, requiring methods to monitor changes in the weld bead geometry (Zahidin et al., 2023). In the end, the human operator of the hybrid system will need to develop intuitions of the physics involved with both the additive and machining processes to support time-constrained decision-making (Fillingim & Feldhausen, 2023). There is a need for understandable and actionable metrics for human–robot systems to build these intuitions and reduce the cognitive workload of the operators of advanced industry 4.0 manufacturing systems (Carvalho, Chouchene, Lima, & Charrua-Santos, 2020). This work presents a metric based on surface waviness that can help inform the user about the state of the bead geometry and the relation to the step over distance. This metric can support the operators as they develop an intuition an in their decision making process as they select the appropriate step over distance, or modify parameters that affect weld bead geometry. There is also an opportunity to use this approach for automated monitoring and control.

The surface topology of an intermediary layer has shown promise for evaluating whether deposited material falls within desired specifications and identifying potential defects (Shen, Zhang, Liao, & Li, 2022; Yonehara, Kato, Ikeshoji, Takeshita, & Kyogoku, 2021). Researchers have proposed several different surface topology approaches for evaluating intermediary layers in metal AM parts including methods for assessing the 2D and 3D roughness (R_a, R_q, S_a, S_q), skewness (R_{sk}, S_{sk}), kurtosis (R_{ku}, S_{ku}), and root mean square slope ($R_{\Delta q}$, $S_{\Delta q}$), yet, these methods have struggled to describe the output of the AM process and corresponding parameters (ASME-B46.1, 2019; Taylor, Jared, Koepke, Forrest, & Beaman, 2019). Gaussian filtering is an established method for separating short wavelength roughness from the underlying geometry and longer wavelength waviness (He, Zheng, Ding, Yang, & Shi, 2021; Raja, Muralikrishnan, & Fu, 2002; Schimpf & Peters, 2021). The average surface waviness (W_a) has been used to evaluate the surface topology of metal AM parts with various step-over distances (Khorasani, 2020; Peyre et al., 2012). However, 3D surface waviness may be limited in its ability to differentiate between the waviness of weld beads and the presence of peaks and valleys between weld beads. An alternative approach could involve dividing surface waviness into the component parallel (W_{a-y}) and perpendicular (W_{a-x}) to the weld beads. The parallel component primarily accounts for the baseline waviness caused by the rapid solidification during the welding process. The perpendicular component also contains the waviness caused by the peaks and valleys between adjacent weld beads. There is the potential for a ratio of the perpendicular waviness to the parallel component of the waviness to reduce the effects of the baseline waviness of the weld bead, allowing the waviness caused by the peaks and valleys caused adjacent weld beads to be quantified, even if that geometry is on a similar wavelength weld bead waviness.

This work presents the development of a HM system for the automation of metalcasting welding. Process parameters are developed for WAAM on low-carbon steel castings using an industrial robot. Single weld bead profiles are measured and modeled to evaluate the flat top and tangent overlap models. Experimental results of overlapping weld beads are compared to the modeled geometry through 3D scan data and evaluation of the surface waviness. The ratio of the perpendicular to parallel components of the surface waviness relative to the deposition direction of the weld beads shows potential as a new metric for measuring and monitoring overlap. This technique can differentiate between samples produced using step-over distances calculated using the flat top and tangent overlapping models. The parameters developed in this study and the methods for measuring and monitoring them can be applied broadly in WAAM and HM applications. Furthermore, bringing automation to metalcasting production welding can improve the harsh working conditions faced by workers in foundries and reduce production bottlenecks caused by a shortage of skilled labor.

5.3 Methodology

Process parameters were evaluated for the production of weld beads in low-carbon steel using a robotic welding system for WAAM (Figure 64). The geometry of a single weld bead is measured to calculate the appropriate step over distance using two different geometry models. The theoretical step-over distances are compared to experimental results produced on the Fanuc ArcMate welding robot. Test samples produced with varying step-over distances are 3D scanned and evaluated. To evaluate the resulting surface texture, a new parameter is developed to describe the directional surface waviness that results from the peaks and valleys between adjacent weld beads. Based on the experimental and theoretical results, a step over distance is selected and used in a subsequent study to evaluate the layer thickness parameter. Finally, the ability to transfer the resulting WAAM parameters to a constrained geometry application for remanufacturing castings is evaluated.

5.3.1 Single Bead Weld Geometry

The geometry of a single weld bead was measured as an input for the step-over distance models. A Fanuc ArcMate 50ic robotic welding system was used to produce single weld beads 150 mm long. Lincoln Electric SuperArc L-56 wire with a diameter of 1.14 mm was used to deposit low carbon steel onto a 101 x 203 x 19 mm section of 1020 steel substrate (Figure 64). The top surface was prepared by face machining before welding. The Lincoln Electric Powerwave R450 was set to Pulsed Spray Transfer mode (GMAW-P) with a trim

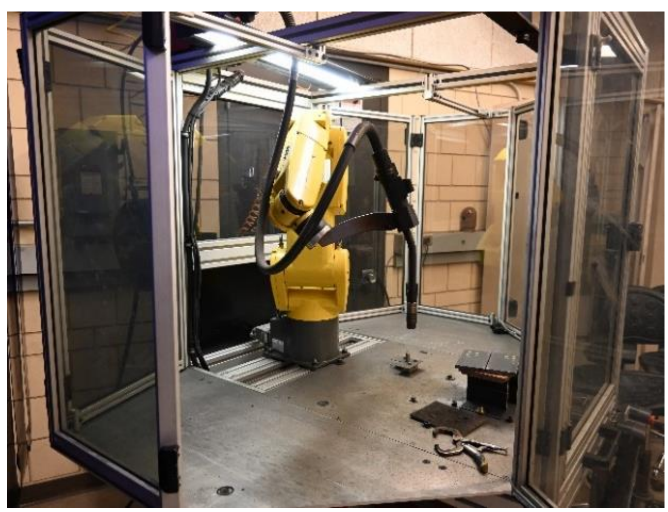

Figure 64. ArcMate 50iC welding robot used for wire arc additive manufacturing on castings.

value of 1.0 and a wire feed of 5.72 m/min. Welding shield gas with a 93% argon and 5% O_2 content with a flow rate of 18 L/min was used with a nozzle standoff distance of 19 mm. A torch travel speed of 0.41 m/min was used during deposition. The bead width and height were measured in four locations approximately 20 mm apart along the length of the bead, avoiding the first and last 45 mm of the sample to avoid irregular geometry at the start and end locations.

The single bead profile was modeled using the geometric form of a symmetric parabola with the general form $y = a + cx^2$. A detailed description of this model is provided by Suryakumar et al., though a brief description is provided here (Suryakumar et al., 2011). The algebraic parameters for this function are given in terms of the measured geometric parameters bead width (w) and height (h) in equations 1 and 2.

$$a = h \tag{1}$$

$$c = -\frac{4h}{w^2} \tag{2}$$

While some researchers have fit the geometric model to a cross-section of a weld bead (Ding et al., 2015a; Suryakumar et al., 2011), Suryakumar et al. 2011 have demonstrated that the measured geometric parameters can be used with a low level of error. The weld bead cross-sectional area can be calculated using the geometric parameters or using the welding process parameters of wire feed rate (v_w), wire diameter (d_w), and the welding torch velocity (v_t) using the equation they present (equation 3). Finally, an equation for the parabolic bead profile can be found using the process parameters (equation 4). The area predicted by the process parameters is compared to the section area calculated using the measured values for width and height to calculate the percent error.

$$A = \frac{2}{3}hw = \frac{\pi v_w {d_w}^2}{4v_t} \quad (3)$$

$$y = h\left[1 - \left(\frac{16hv_t}{3\pi v_w {d_w}^2}x\right)^2\right] \quad (4)$$

5.3.2 Modeling Step-Over distance

The critical step over distance, *d**, is calculated using the more conservative TOM and the more aggressive FOM approaches. Detailed descriptions of the TOM (Ding et al., 2015a) and FOM (Suryakumar et al., 2011) approaches can be found in the cited literature. The newer TOM approach sets *d** = 0.738*w*, while the FOM approach provides a *d** = 0.667*w*. Both models will be evaluated to determine if the narrower spacing of the FOM approach results in unstable deposition, where individual bead heights are inconsistent across the layer.

5.3.3 Experimental Step Over Distance

The step-over distances were evaluated using a raster fill tool path (Figure 35a) with six stringers each 150 mm long. The entire weld toolpath was deposited as a single continuous weld. The traditional flat-top overlapping model suggests that valleys indicate that the step-over is too large while bulging indicates a step-over that is too small (Figure 65b). This approach was used to evaluate the step-over distance samples to find the appropriate step-over distance; however, the TOM approach was also considered, which suggests that

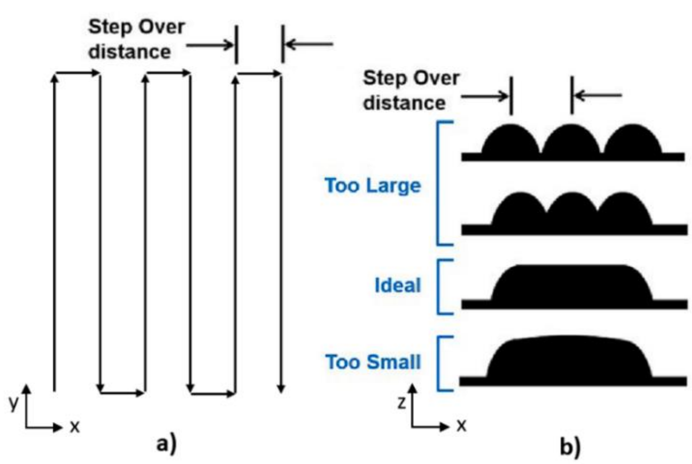

Figure 65. Step over distance was evaluated using a) raster toolpath with variable step over distance that b) resulted in inter-bead valleys or bulging.

valleys may still be present with an ideal step-over distance (Ding et al., 2015a). To validate the step-over distances modeled using the flat and tangent overlapping models, single-layer raster samples were produced with step-over distances of 4.5, 5.0, 5.5, 6.0, and 6.5 mm. Samples were also produced with step-over distances of 5.6, 5.7, 5.8, and 5.9 mm to further investigate the region between the modeled step-over distances.

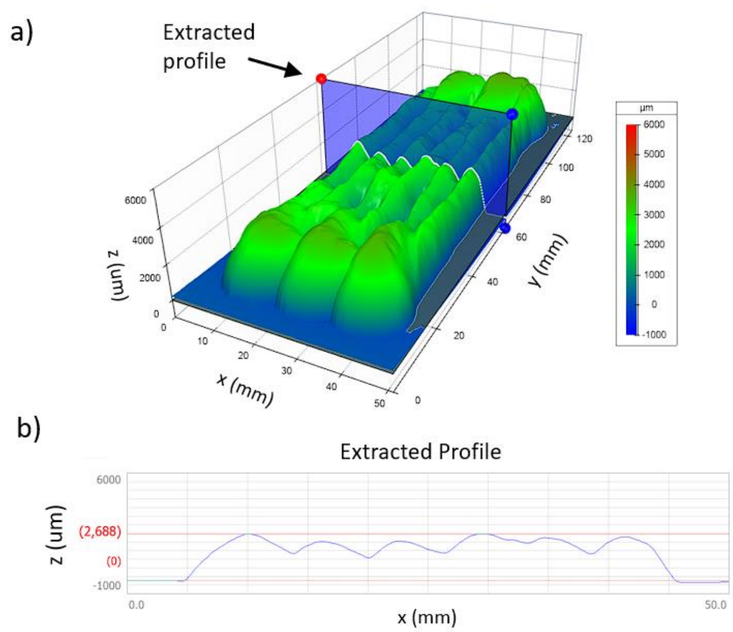

Figure 66. Visualizing the a) 3D surface scan of the step over weld sample and the b) extracted 2D profile.

The weld sample surface was captured using a laser 3D scanner (FARO Technologies, Lake Mary, United States) and analyzed using OmniSurf3D (Digital Metrology, Columbus, Indiana, United States). A profile is extracted from the weld area (Figure 66) to view the cross-section's resulting peaks, valleys, and potential bulging. Surface waviness (W_a) was used to evaluate the presence of peaks and valleys (Khorasani, 2020). Following the AMSE B46.1 standard, a second-order high-pass Gaussian filter was used with a short cutoff wavelength (λ_{cw}) of 0.8 mm (ASME B46.1 2019). This high-pass filter separates the longer wavelength surface geometry representing the underlying geometry and surface waviness (Figure 67a) from the shorter wavelength geometry representing the surface roughness (Figure 67b).

To better differentiate the baseline waviness of the weld beads from the peaks and valleys caused by overlapping weld beads, the component parallel ($W_{a\text{-}y}$) and perpendicular ($W_{a\text{-}x}$) to the weld beads was calculated. The ratio of the perpendicular waviness (W_{a-x}) to the parallel component of the waviness (W_{a-y}) is taken. A new waviness ratio metric (W_{a-x} / W_{a-y}) is evaluated for its ability to quantify the magnitude of peaks and valleys and to differentiate between the samples produced using the FOM, and TOM approaches.

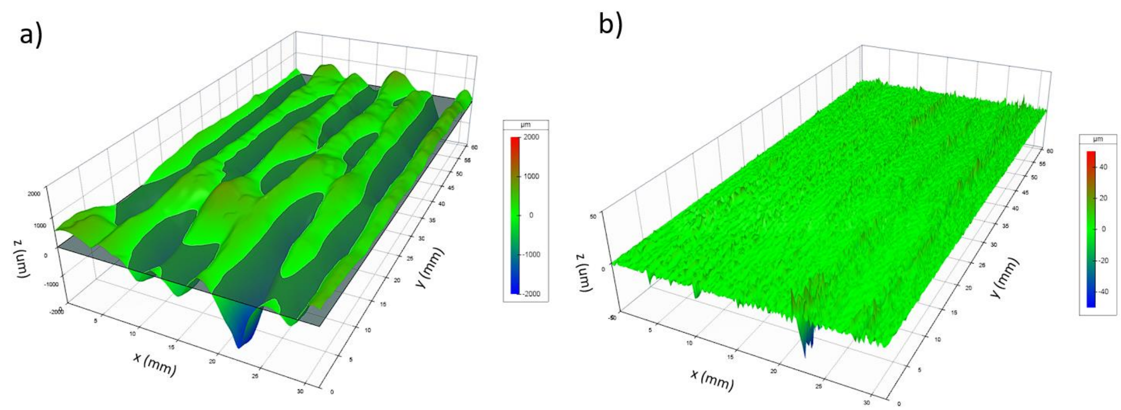

Figure 67. Visualizing the a) surface waviness and the b) surface roughness components of the 3D scan post-filtering.

5.3.4 Layer Height

The incremental height increase caused by stacking layers in the z-direction (Figure 68) was found by taking a 3D laser scan of the surface after each layer was printed and fitting a plane to the surface. Three samples were produced, each with ten layers stacked in the z-direction, using a step-over distance of 5.6 mm and a weld length of 150 mm. The samples are allowed to cool to achieve an inter-pass temperature of 130° C or less, measured using an inferred thermometer. For each layer, the mean and standard deviation of the change in height is taken. One-way analysis of variance (ANOVA) is used to evaluate if the incremental height

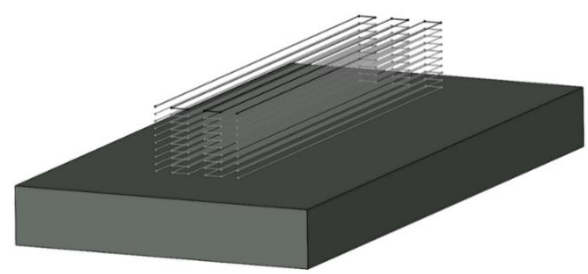

Figure 68. Stacked welding toolpaths used to evaluate the incremental height increase per

change significantly differs on the first layer when no sample pre-heating is used. Sections of the sample were machined to check for signs of welding defects or anomalies.

5.3.5 Filling a Constrained Excavation

Cavities were machined into the 1020 steel substrate to simulate a casting excavation using a 12.7 mm diameter cutting tool with a 3.175 corner radius on a HAAS UMC750 machining center. A cavity sized for a single layer (Figure 69a) of weld beads was produced with a length of 101.6 mm, a width of 17.1 mm, and a depth of 1.2 mm. This excavation cavity was filled with a raster fill tool path similar to that used on the step-over distance testing but with only three weld passes. This dimension was selected because the cavity would fit the lowest integer multiple of weld beads that could be produced using the 12.7 mm cutting tool. The geometry of the excavation was designed to achieve overfilling of the cavity, allowing for a subsequent grinding operation to reproduce the original surface even with the presence of surface abnormalities. This process was repeated with a 3-layer deep v-groove (Figure 69b), adding one additional weld bead for each subsequent layer. This results in approximately a 98.8° included angle of the v-groove, allowing welding torch access on larger samples. A layer depth of 2.4 mm was used for the first two layers, matching the average layer height from the prior experiment. The top layer was again 1.2 mm, allowing for overfilling of the excavation.

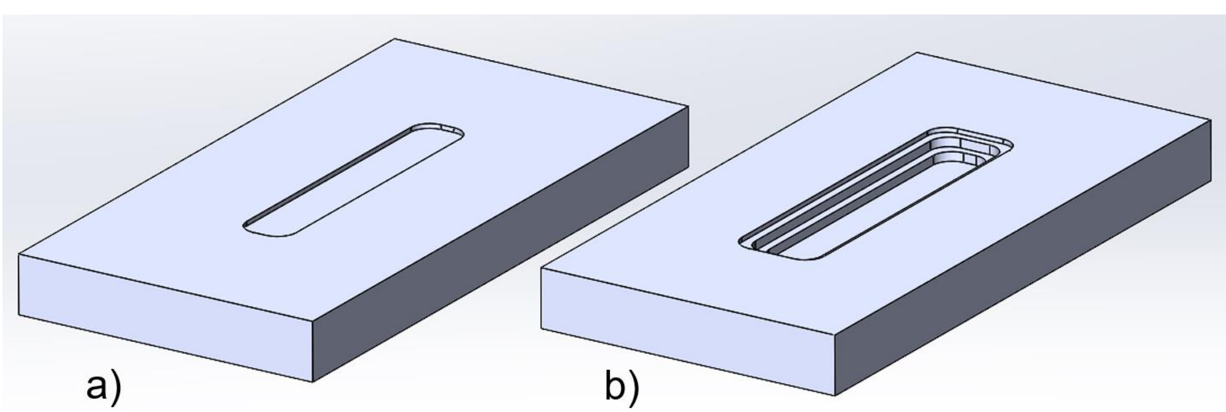

Figure 69. Simulated excavation models used for the a) single layer and b) triple layer cavity.

5.4 Results and Discussion

To develop a prototype process for the evaluation of critical or new automated tasks, process parameters are needed for the WAAM system in low-carbon steel. The process parameter development study aims to build a relationship between the process parameters and the resulting geometry. This was completed by evaluating individual weld bead cross sections, the resulting cross sections from a series of welds with different step-over distances, and the incremental height increase when multiple layers are stacked, and evaluating these parameters in an excavated cavity in a steel casting. A new metric based on surface waviness is also developed to quantitatively assess the surfaces resulting from different step-over distances. This metric is used to select the appropriate step over distance in this study and is proposed as a method for automated monitoring and control of the weld bead geometric parameters.

5.4.1 Single Bead Geometry and Critical Overlap Distance

The two single-bead test samples had an average width (*w*) of 8.12 and 8.31 mm with standard deviations of 0.21 and 0.02 mm, respectively, when measured at four locations each along their length. The two samples also had 2.69 and 3.00 mm heights, with standard deviations of 0.09 and 0.08 mm. The process parameters, calculated algebraic parameters, and measured geometric parameters are presented in Table 8. The algebraic parameters *a* and *c* that define the parabolic geometry of the singular weld bead are calculated using equations 1 and 2 from the measured geometric parameters.

Table 8. Measured and calculated parameters of the deposited single weld bead samples.

Sample No.	Process Parameters			Algebraic Parameters		Geometric Parameters	
	d_w (mm)	υ_w (m/min)	υ_t (m/min)	a	c	h (mm)	w (mm)
1	1.14	5.72	0.41	2.69	-0.16	2.69	8.12
2	1.14	5.72	0.41	3.00	-0.17	3.00	8.31

The predicted and measured cross-sectional areas are calculated using Equation 4. These areas and the error between the predicted and measured values are presented in Table 9. The error between measured and predicted areas is similar to those found by Suryakumar et al. 2011, which suggests that this model is appropriate for the process parameters used in this study, even though they vary from those used in the original research. The geometric variation between samples indicates a substantial degree of process variability, emphasizing the need for methods to monitor and control the geometry produced by WA-DED systems (Costello et al., 2023).

Table 9. The predicted and measured cross-sectional areas

Sample No.	Area		Error (%)
	Predicted	Measured	
1	14.30	14.56	-1.82
2	14.30	16.62	-13.98

Using the geometric models of the single weld beads, the critical step over distances, *d**, between parallel weld beads can be calculated using the FOM and TOM approaches to achieve a stable layer height. The FOM approach results in a step-over distance of *d** = 5.48 mm, while the newer TOM approach results in a step-over distance of *d** = 6.06 mm between weld beads. Step-over distance experiments were conducted with distances of 4.5, 5.0, 5.5, 6.0, and 6.5 mm to validate the theoretical step-over distances provided by these models. In addition, samples with a finer increment of 0.1 mm were produced between the two modeled step-over distances from the TOM and FOM calculations.

5.4.2 Experimental Step Over Distance

A 3D scan and 2D section profile are presented for each weld of the coarse step over weld samples (Figure 70). Beads were deposited starting on the right and moving to the left. A visual comparison of the 3D scan for the sample produced using a large 6.5 mm (Figure 70a) step-over distance to the sample with a narrow 4.5 mm step-over distance (Figure 70e) was conducted. The visual inspection shows clear peaks and valleys when the larger step-over distances of 6.5 and 6.0 mm are used, while slight bulging can be seen with the smaller step-over distances of 5.0 and 4.5 mm. The crowning in the 4.5 mm sample is also seen by the increase in the peak height in the z-direction in the 2D profile, as predicted by the TOM model (Ding et al., 2015a). The sample with a 5.5 mm distance between adjacent weld beads shows a representation of a flat surface achieved by using what would be considered an appropriate step over distance using a flat top model, aligning with the calculated values found using the FOM (Suryakumar et al., 2011). This sample shows the characteristic increase in height when comparing the first and second weld beads that the TOM predicts; however, the subsequent weld beads do not maintain the increased layer height in this instance. While the sample with the FOM step-over distance of 5.5 mm achieves an approximately flat top surface that lacks the clear valleys between weld beads, the sample with the 6.0 mm step-over distance suggested by the TOM model still shows clear valleys. It is expected that the TOM model developed by D. Ding et al. 2015 would result in a slightly less flat surface than the FOM model under visual inspection. However, this visual comparison approach is not a precise or quantifiable method for selecting the best step over distance for a WAAM system, which can put the human operator of a hybrid manufacturing system into a situation where they must make an ambiguous judgment call based on qualitative data and their prior experience. Process variation can drive geometric variability in the weld beads, requiring the parameters to be tuned. A quantitative approach to support operator decision-making or closed-loop control of the step-over distance based on data captured during processing may reduce instances of unstable deposition rates.

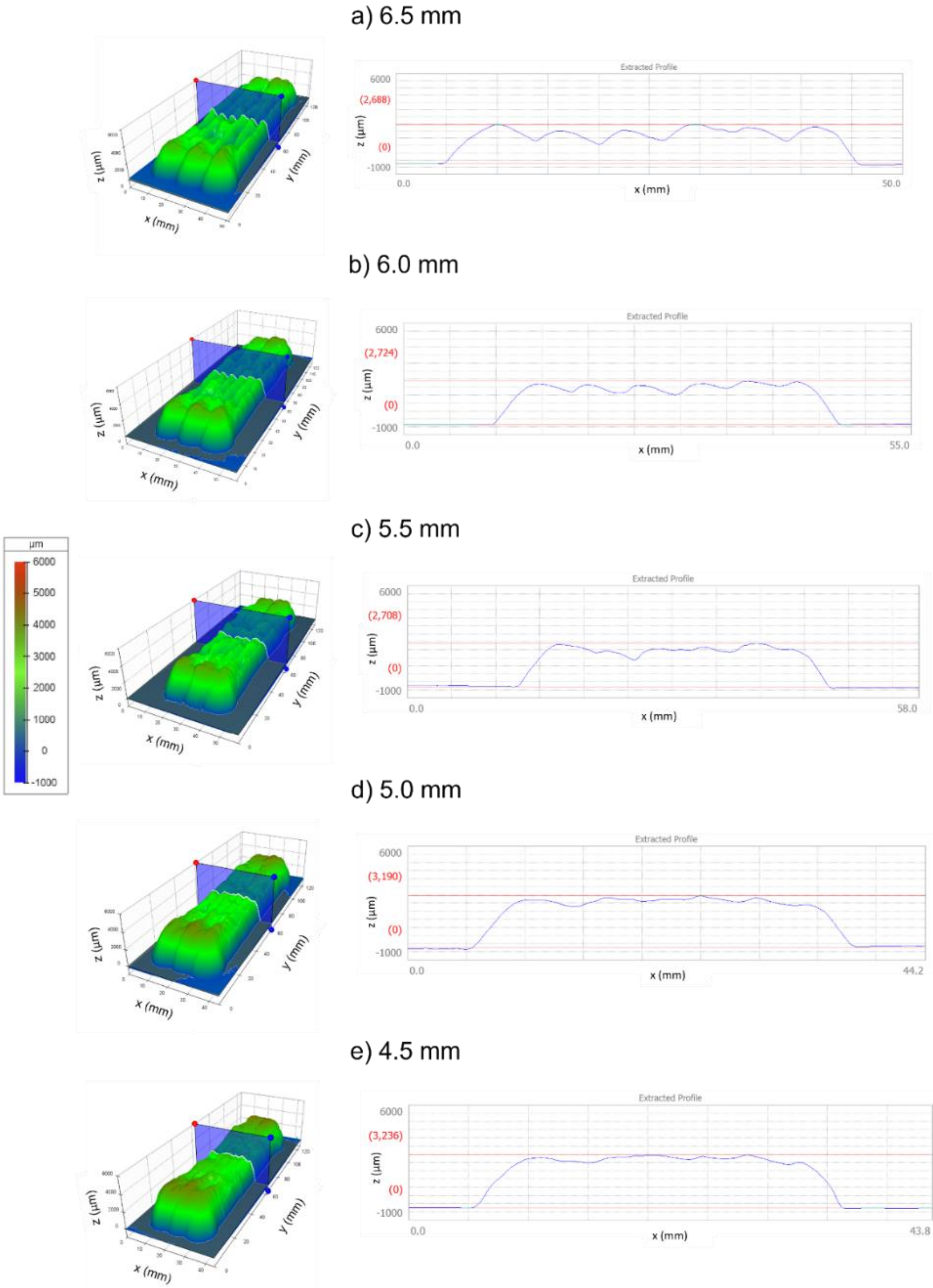

Figure 70. 3D scans, cross-section plane, and the resulting cross-section are shown for layer samples consisting of six weld beads and step-over distances between beads of a) 6.5 mm, b) 6.0 mm, c) 5.5 mm, d) 5.0 mm, and e) 4.5 mm

A measure of the surface waviness is used to quantify the change in surface peaks and valleys as the step over distance changes. Waviness is a measure of the part surface texture geometry at a wavelength scale longer than what is typically considered surface roughness (ASME B46.1 2019). By filtering the surface to remove wavelengths below the 0.8 mm threshold, the resulting surface waviness is calculated using the same equations used to calculate 3D surface roughness, S_a, resulting in the average surface waviness, W_a (Figure 71). While the average surface waviness, W_a, appears to show a slight general trend of increasing as the step-over distance increases, there is not a clear signal that can be used to select the correct step-over distance. Looking at the component of the surface waviness parallel to the weld beads, $W_{a\text{-}y}$, there does not appear to be a clear trend in the data. This result is expected, as the primary driver of waviness parallel to the weld bead is likely the baseline surface irregularities caused by the welding process. The component of surface waviness perpendicular to the weld bead, $W_{a\text{-}x}$, aligns with the values for $W_{a\text{-}y}$ when lower step-over values are present, then diverges for larger step-over distances. On their own, the metrics W_a, $W_{a\text{-}y}$, and $W_{a\text{-}x}$ do not appear to be reliable methods for quantifiably identifying the best step over distance.

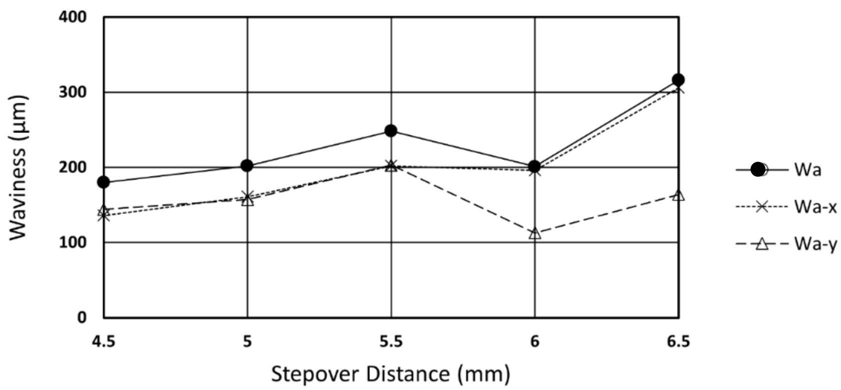

Figure 71. Average surface waviness and the x and y component of surface waviness for weld samples consisting of six parallel weld beads with varying step over distances between beads.

An attempt to remove the baseline waviness caused by welding irregularities leads to the creation of a new metric, the perpendicular-parallel waviness ratio consisting of the component that contains the waviness of the peaks and valleys, W_{a-x}, to the component that does not capture the peaks and valleys, W_{a-y} (Figure 72). The samples with narrow step-over distances of 4.5, 5.0, and 5.5 mm that do not show clear signs of valleys between weld beads (Figure 70c, d, & e) result in a waviness ratio of approximately one. This finding indicates that the waviness perpendicular to the weld beads is similar to the baseline waviness parallel to the weld beads. However, the samples with larger step-over distances of 6.0 and 6.5 mm that show clear peaks and valleys between weld beads (Figure 70a & b) result in an increase in the waviness ratio. This demonstrates the ability of this metric to detect the presence of the peaks and valleys caused by an increasing step over distance. By adding in data from additional test samples at the finer step-over distance increments of 0.1 mm, the transition from the flat top to a tangent top can be visualized. These data suggest that the waviness ratio calculated from a 3D scan of the part surface can be used to quantitatively measure the effect of the step-over distance on the resulting inter-bead valleys. This metric can be used as an operator aid to signal that a parameter change may be required or as the input to a closed or open loop control system to prevent unstable and inconsistent deposition caused by a step-over distance that is too great or too small.

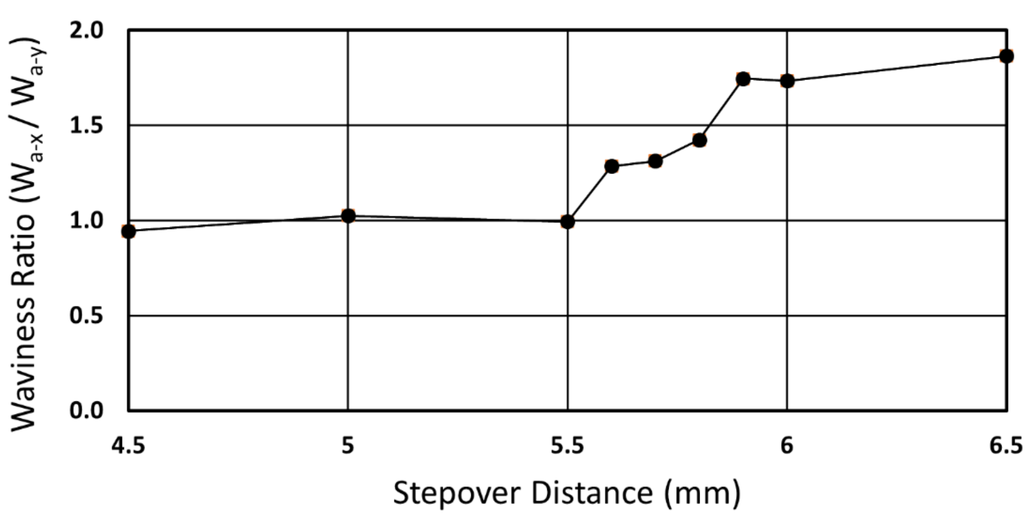

Figure 72. The ratio of the perpendicular (W_{a-x}) to parallel (W_{a-y}) components of waviness for samples consisting of six parallel weld beads with various step-over distances between welds.

While it may be possible to use the aggressive step-over distance of 5.5 mm, which results in a waviness ratio of approximately one, variation in the process could lead to a situation where surface bulging could occur. Bulging or crowning of the surface during the production of a 3D object using WAAM would continue to build up each layer until the print could not continue, potentially resulting in a part that does not meet customer requirements. Such process variation could be caused by several sources, including the part's thermal history, the standoff distance of the welding torch, welding torch travel speed, gas flow rate, or geometry. The decision was made to pull back slightly from the potentially unstable deposition of the flat-top model and use a step-over distance of 5.6 mm, which falls between those suggested by the FOM and TOM. However, this method of quantifying the valleys of the surface could be used whether a more or less aggressive step-over distance of the FOM or TOM model is implemented in production.

5.4.3 Layer Height

The toolpath used to produce the 5.6 mm step-over distance single-layer sample was used to evaluate the incremental increase in z-height when multiple layers are stacked (Figure 73). Machining of the sample did not reveal signs of welding porosity or other defects. The average layer height of each layer on the three samples is plotted (Figure 74) with error bars representing one standard deviation. The average layer thickness across all samples and layers was 2.4 mm, slightly greater than the average for the first layer, which only

Figure 73. Layer height test samples as printed and with machined faces for weld inspection.

increased by 2.2 mm. Since the first layer was deposited on an ambient substrate, while the following layers were deposited on warm material, there is a potential to achieve a difference in the bead geometry for this layer. An evaluation of the data using a one-way analysis of variance (ANOVA) with a significance level (alpha) of 0.05 resulted in an F-statistic slightly below the critical level and a P-value of 0.051. Thus, we fail to reject the null hypothesis that there is a significant difference between the means of the different groups. However, the sample sizes for each group were small, and the P-value fell just outside of the threshold, suggesting a more in-depth analysis may be warranted. This difference could be critical for developing parameters, as the single bead samples used to define the bead geometry were deposited on the ambient substrate and then used to predict the geometry for the entire production process. Since this analysis suggests no significant difference in the means of the sample sets, the average layer height of 2.4 mm will be used for all layers.

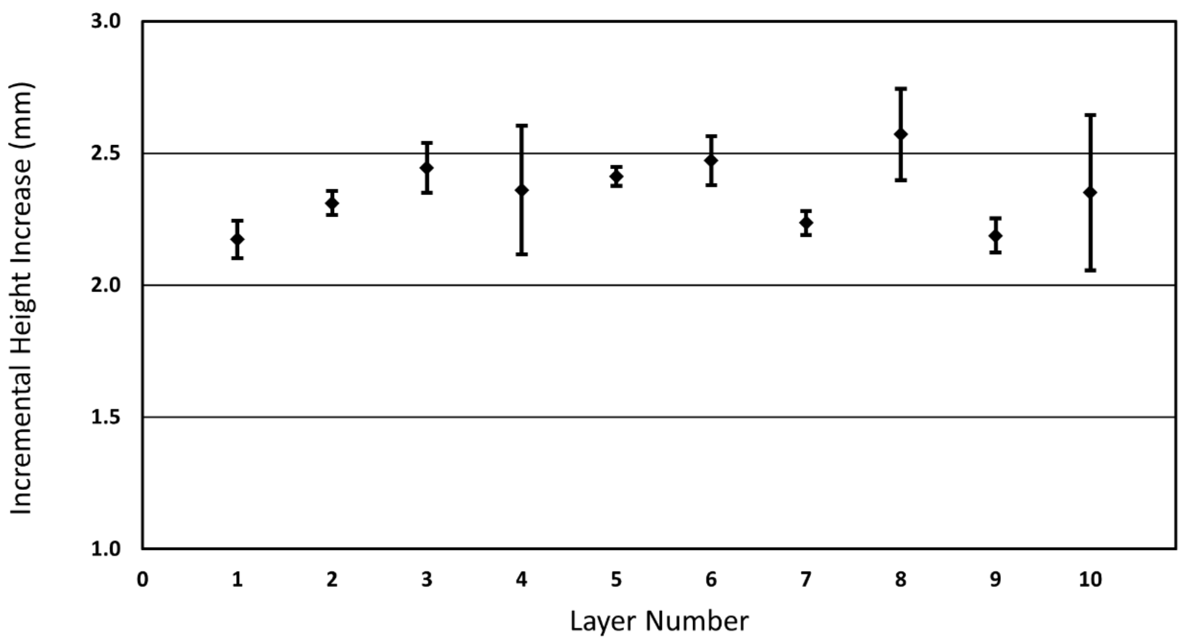

Figure 74. The incremental increase in z-height for each layer. The error bars represent one standard deviation.

5.5 WAAM in an Excavation

After the layer height of welds deposited using traditional WAAM toolpaths was established, toolpaths were developed for filling excavations in a metalcasting. Slight overfilling of the excavation is required to blend the filled excavation with the surrounding surface using a grinding operation post-weld. Overfilling was achieved by reducing the excavation depth of the top layer in the machining process to 1.2 mm, or half of the anticipated weld height of 2.4 mm. This resulted in layer heights of 1.2 mm for the single-layer excavation and 1.2 mm, 2.4 mm, and 2.4 mm for the three-layer deep excavation (Figure 75). The bottom layer width of 17.1 mm was filled with four weld beads, with the first weld bead centerline aligning with the edge of the weld preparation cavity to ensure wall penetration and prevent undercut.

The excavation width of each layer was increased to make room for one additional weld bead. This approach resulted in an excavation included angle of 98.8°, which allowed for torch reach and access for any excavation more extensive than the one presented here. However, excavations with smaller included angles are used in industry. Welding toolpaths with more complex torch control may need to be developed to fill excavations with this narrower included angle to reduce the need for excessive machining around manual casting excavations. Angling of the torch may also improve weld penetration and fusion to the side wall of excavations with smaller included angles. A simple approach to filling these narrower cavities may be adding an additional weld bead every two layers instead of every layer. Several iterations of excavation geometry were tested to arrive at the geometry presented here. The goal of the iterative process was to ensure the complete filling of the cavity. Feedback from welding professionals and industry experts suggests that the sharp edges between layers caused by the bullnose endmill could affect weld quality and wall penetration (Figure 75). Future iterations should include an additional step to remove these features, and a more in-depth metallurgical study should be conducted to evaluate the material properties achieved by the welding operation. There are opportunities for further process parameter refinement of the weld preparation geometry for applications of WAAM to repair sub-surface defects and production anomalies.

Figure 75. Single and triple-layer machined v-grooves used to simulate the weld preparation of an indication excavation for parameter development.

Complete filling of the machined weld preparation geometry was achieved for both the one- and three-layer deep samples (Figure 77). The etched cross-section of the three-layer sample clearly shows that adequate filling was achieved, though further refinement may reduce excess material that would drive grinding time and cost (Figure 76). The section also exhibits a weld interface geometry that could have been influenced by the sharp scalloped features produced by forming the v-groove geometry using a bullnose endmill. This finding reinforces the need to remove the scalloped features through an additional milling step. Initial testing showed incomplete filling of the

Figure 76. Etched cross section of a three-layer filled excavation.

cavity on the trailing edge of the final layer caused by the formation of an undercut. This challenge was overcome through an additional weld bead at the trailing edge of the top layer in the process plan. However, further development and tuning of the welding toolpaths and process parameters may remove the need for this extra pass on the top layer.

Figure 77. Single and triple-layer v-grooves filled using the WAAM process parameters developed in this study.

The Developed process parameters for filling low-carbon steel casting excavations using a robotic WAAM system can be used for a prototype implementation of the automated system design presented. The approach to parameter development can be applied to other applications, such as repairing service parts or modifying tooling. Furthermore, the quantitative approach for tuning the step-over distance between weld beads presented that uses 3D scan data, filtering, and directional surface waviness calculations can be applied to parameter development for new WAAM systems and alloys or process monitoring and control.

5.6 Conclusions

This study investigated WAAM geometric process parameters for low-carbon steel to enable the remanufacture of large-scale metalcastings produced from low-carbon steel. It also presented a novel method for quantitative analysis of surface topology that results when the step-over distance between weld beads is modified. The ability to quantitatively differentiate between parts produced using two well-established step-over distance models, FOM and TOM shows that the presented approach is sensitive enough to potentially be useful for monitoring and controlling WAAM process parameters. The ability to transfer the process parameters developed for typical WAAM production of freeform geometry into a constrained v-groove geometry was shown, though the bounds of the v-groove excavation geometry required adjustment.

Establishing process parameters for high deposition rates in low-carbon steel using WAAM further expands the capabilities of this process into the space of remanufacturing. This work also contributes to the expansion of hybrid manufacturing remanufacturing applications to those using a hybrid WAAM + machining system. The qualitative approach to measuring the step over distance using 3D surface data can help accelerate process parameter development and has the potential for process monitoring and control applications. This simple metric may give a human operator a simple and actionable metric that they can use to ensure a quality part is produced. The directional surface waviness ratio may find applications in monitoring and controlling other AM processes.

While this investigation presented parameter development for an HM approach for remanufacturing large-scale metalcastings, further work is needed to develop the broader manufacturing process, including integrating the human operator and creating a user interface. Further development of automated process planning, including toolpath generation and orientation, is needed to develop a flexible automated system. A more in-depth investigation into the resulting material properties when an excavation is filled is required. Metalcastings are produced using a wide range of materials, each requiring a clear understanding of the process parameters and material properties before remanufacturing work can proceed.

5.7 Acknowledgement

This research is sponsored by the DLA-Troop Support, Philadelphia, PA and the Defense Logistics Agency Information Operations, J68, Research & Development, Ft. Belvoir, VA.

5.8 Disclaimer

The publication of this material does not constitute approval by the government of the findings or conclusion herein. Wide distribution or announcement of this material shall not be made without specific approval by the sponsoring government activity.

5.9 References

ASME-B46.1. (2019). *Surface Texture (Surface Roughness, Waviness, and Lay) ASME B46.1-2019*. 144. Retrieved from https://www.asme.org/codes-standards/find-codes-standards/b46-1-surface-texture

ASME-BPVC.IX. (2023). ASME BPVC. IX-2023. In *ASME International*. Retrieved from https://www.asme.org/codes-standards/find-codes-standards/bpvc-ix-bpvc-section-ix-welding-brazing-fusing-qualifications

ASTM-A488. (2017). *Standard Practice for Steel Castings, Welding, Qualifications of Procedures and Personnel*. https://doi.org/10.1520/A0488_A0488M-06

Baker, R. (1920). *Patent No. US1533300A*. Retrieved from https://patents.google.com/patent/US1533300A/en

Carvalho, A. V., Chouchene, A., Lima, T. M., & Charrua-Santos, F. (2020). Cognitive manufacturing in industry 4.0 toward cognitive load reduction: A conceptual framework. *Applied System Innovation*, *3*(4), 1–14. https://doi.org/10.3390/ASI3040055

Costello, S. C. A., Cunningham, C. R., Xu, F., Shokrani, A., Dhokia, V., & Newman, S. T. (2023). The state-of-the-art of wire arc directed energy deposition (WA-DED) as an additive manufacturing process for large metallic component manufacture. *Https://Doi.Org/10.1080/0951192X.2022.2162597*, *36*(3), 469–510. https://doi.org/10.1080/0951192X.2022.2162597

David, D., Monroe, R., & Thomas, E. (2015). Exploring the Need to Include Cast Carbon Steels in Welding Procedure Specifications. *Welding Journal*, *94*(10), 56–58.

Ding, D., Pan, Z., Cuiuri, D., & Li, H. (2015a). A multi-bead overlapping model for robotic wire and arc additive manufacturing (WAAM). *Robotics and Computer-Integrated Manufacturing*, *31*, 101–110. https://doi.org/10.1016/J.RCIM.2014.08.008

Ding, D., Pan, Z., Cuiuri, D., & Li, H. (2015b). A multi-bead overlapping model for robotic wire and arc additive manufacturing (WAAM). *Robotics and Computer-Integrated Manufacturing*. https://doi.org/10.1016/j.rcim.2014.08.008

Feldhausen, T., Heinrich, L., Saleeby, K., Burl, A., Post, B., MacDonald, E., … Love, L. (2022). Review of Computer-Aided Manufacturing (CAM) strategies for hybrid directed energy deposition. *Additive Manufacturing*, *56*, 102900. https://doi.org/10.1016/J.ADDMA.2022.102900

Feldhausen, T., Kannan, R., Saleeby, K., Fillingim, B., Kurfess, R., Nandwana, P., & Post, B. (2022). Hybrid Manufacturing Approaches for the Production and Repair of Industrial Tooling. *International Conference on Nuclear Engineering, Proceedings, ICONE*, *1*. https://doi.org/10.1115/ICONE21-16472

Feldhausen, T., Raghavan, N., Saleeby, K., Love, L., & Kurfess, T. (2021). Mechanical properties and microstructure of 316L stainless steel produced by hybrid manufacturing. *Journal of Materials Processing Technology*, *290*, 116970. https://doi.org/10.1016/J.JMATPROTEC.2020.116970

Feldmann, M., Kühne, R., Citarelli, S., Reisgen, U., Sharma, R., & Oster, L. (2019). 3D-Drucken im Stahlbau mit dem automatisierten Wire Arc Additive Manufacturing. *Stahlbau*, *88*(3), 203–213. https://doi.org/10.1002/STAB.201800029

Fillingim, K. B., & Feldhausen, T. (2023). Operator 4.0 for Hybrid Manufacturing. *INTERNATIONAL CONFERENCE ON ENGINEERING DESIGN*, 24–28. https://doi.org/10.1017/pds.2023.284

Frank, M. C., Harrysson, O., Wysk, R. A., Chen, N., Srinivasan, H., Hou, G., & Keough, C. (2017). Direct Additive Subtractive Hybrid Manufacturing (DASH) – An Out of Envelope Method. *Proceedings of the 28th Annual International Solid Freeform Fabrication Symposium*. https://doi.org/10.26153/TSW/16910

Gardner, L., Kyvelou, P., Herbert, G., & Buchanan, C. (2020). Testing and initial verification of the world's first metal 3D printed bridge. *Journal of Constructional Steel Research*, *172*, 106233. https://doi.org/10.1016/J.JCSR.2020.106233

Hagen, L., Yu, Z., Clarke, A., Clarke, K., Tate, S., Petrella, A., & Klemm-Toole, J. (2023). High deposition rate wire-arc directed energy deposition of 316L and 316LSi: Process exploration and modelling. *Materials Science and Engineering: A*, *880*, 145044. https://doi.org/10.1016/J.MSEA.2023.145044

Hamilton, J. D., Sorondo, S., Li, B., Qin, H., & Rivero, I. V. (2023). Mechanical behavior of bimetallic stainless steel and gray cast iron repairs via directed energy deposition additive manufacturing. *Journal of Manufacturing Processes*, *85*, 1197–1207. https://doi.org/10.1016/J.JMAPRO.2022.12.029

He, B., Zheng, H., Ding, S., Yang, R., & Shi, Z. (2021). A REVIEW OF DIGITAL FILTERING IN EVALUATION OF SURFACE ROUGHNESS. *METROLOGY AND MEASUREMENT SYSTEMS*, *28*(2), 217–253. https://doi.org/10.24425/mms.2021.136606

Hong, X., Xiao, G., Zhang, Y., & Zhou, J. (2021). Research on gradient additive remanufacturing of ultra-large hot forging die based on automatic wire arc additive manufacturing technology. *International Journal of Advanced Manufacturing Technology*, *116*(7–8), 2243–2254. https://doi.org/10.1007/S00170-021-07424-5/FIGURES/17

Jones, J. B. (2014). The synergies of hybridizing CNC and additive manufacturing. *Technical Paper - Society of Manufacturing Engineers*.

Jones, J., Mcnutt, P., Tosi, R., Perry, C., & Wimpenny, D. (2012). Remanufacture of turbine blades by laser cladding, machining and in-process scanning in a single machine. *Proceedings of 23rd Annual International Solid Freeform Fabrication Symposium*, 821–827.

Khorasani, A. B. (2020). *A theoretical and experimental study of geometry, microstructure and mechanical properties of 316l stainless steel manufactured by direct energy deposition-based hybrid manufacturing*. Iowa State University.

Lauwers, B., Klocke, F., Klink, A., Tekkaya, A. E., Neugebauer, R., & McIntosh, D. (2014). Hybrid processes in manufacturing. *CIRP Annals - Manufacturing Technology*. https://doi.org/10.1016/j.cirp.2014.05.003

Lee, J. H., Lee, C. M., & Kim, D. H. (2022). Repair of damaged parts using wire arc additive manufacturing in machine tools. *Journal of Materials Research and Technology*, *16*, 13–24. https://doi.org/10.1016/J.JMRT.2021.11.156

Monroe, R. (2019). Welding Steel Castings. *Steel Founders' Society of America*.

Nycz, A., Adediran, A. I., Noakes, M. W., & Love, L. J. (2016). Large Scale Metal Additive Techniques Review. *Proceedings of Teh 27th Annual International Solid Freeform Fabrication Symposium*. Retrieved from http://energy.gov/downloads/doe-public-access-plan

Özel, T., Shokri, H., & Loizeau, R. (2023). A Review on Wire-Fed Directed Energy Deposition Based Metal Additive Manufacturing. *Journal of Manufacturing and Materials Processing 2023, Vol. 7, Page 45*, *7*(1), 45. https://doi.org/10.3390/JMMP7010045

Peyre, P., Gharbi, M., Gorny, C., Carin, M., Morville, S., Carron, D., … Fabbro, R. (2012). Surface finish issues after Direct Metal Deposition. *Materials Science Forum*, *706–709*, 228–233. https://doi.org/10.4028/WWW.SCIENTIFIC.NET/MSF.706-709.228

Priarone, P. C., Campatelli, G., Catalano, A. R., & Baffa, F. (2021). Life-cycle energy and carbon saving potential of Wire Arc Additive Manufacturing for the repair of mold inserts. *CIRP Journal of Manufacturing Science and Technology*, *35*, 943–958. https://doi.org/10.1016/J.CIRPJ.2021.10.007

Raja, J., Muralikrishnan, B., & Fu, S. (2002). Recent advances in separation of roughness, waviness and form. *Precision Engineering*, *26*(2), 222–235. https://doi.org/10.1016/S0141-6359(02)00103-4

Saleeby, K. S., Kurfess, T., Feldhausen, T., & Love, L. (2021). Production of Medium-Scale Metal Additive Geometry With Hybrid Manufacturing Technology. *ASME 2020 15th International Manufacturing Science and Engineering Conference*, *MSEC 2020*, *1*. https://doi.org/10.1115/MSEC2020-8391

Schimpf, D. W., & Peters, F. E. (2021). Variogram Roughness Method for Casting Surface Characterization. *International Journal of Metalcasting*, *15*(1), 17–28. https://doi.org/10.1007/s40962-020-00451-0

Shen, W., Zhang, X., Liao, Y., & Li, B. (2022). Real-Time Structured Light Scanning Characterization of Surface Topography of Direct Energy Deposited 316L Stainless Steel. *Proceedings of ASME 2022 17th International Manufacturing Science and Engineering Conference, MSEC 2022*, *1*. https://doi.org/10.1115/MSEC2022-85783

Suryakumar, S., Karunakaran, K. P., Bernard, A., Chandrasekhar, U., Raghavender, N., & Sharma, D. (2011). Weld bead modeling and process optimization in Hybrid Layered Manufacturing. *Computer-Aided Design*, *43*(4), 331–344. https://doi.org/10.1016/J.CAD.2011.01.006

Taylor, S., Jared, B., Koepke, J., Forrest, E., & Beaman, J. (2019). Investigating Applicability of Surface Roughness Parameters in Describing the Metallic AM Process. *Proceedings of the 30th Annual International Solid Freeform Fabrication Symposium*, 1651–1664. https://doi.org/10.26153/TSW/17388

Williams, S. W., Martina, F., Addison, A. C., Ding, J., Pardal, G., & Colegrove, P. (2016). Wire+ Arc Additive Manufacturing. *Materials Science and Technology*, *32*(7), 641–647. https://doi.org/10.1179/1743284715Y.0000000073

Xiong, J., Zhang, G., Gao, H., & Wu, L. (2013). Modeling of bead section profile and overlapping beads with experimental validation for robotic GMAW-based rapid manufacturing. *Robotics and Computer-Integrated Manufacturing*, *29*(2), 417–423. https://doi.org/10.1016/J.RCIM.2012.09.011

Yonehara, M., Kato, C., Ikeshoji, T. T., Takeshita, K., & Kyogoku, H. (2021). Correlation between surface texture and internal defects in laser powder-bed fusion additive manufacturing. *Scientific Reports 2021 11:1*, *11*(1), 1–10. https://doi.org/10.1038/s41598-021-02240-z

Zahidin, M. R., Yusof, F., Abdul Rashid, S. H., Mansor, S., Raja, S., Jamaludin, M. F., … Syahriah Hussein, N. I. (2023). Research challenges, quality control and monitoring strategy for Wire Arc Additive Manufacturing. *Journal of Materials Research and Technology*, *24*, 2769–2794. https://doi.org/10.1016/J.JMRT.2023.03.200

Zhang, X., Cui, W., Li, W., & Liou, F. (2019). A Hybrid Process Integrating Reverse Engineering, Pre-Repair Processing, Additive Manufacturing, and Material Testing for Component Remanufacturing. *Materials 2019, Vol. 12, Page 1961*, *12*(12), 1961. https://doi.org/10.3390/MA12121961

Zhu, Z., Dhokia, V. G., Nassehi, A., & Newman, S. T. (2013). A review of hybrid manufacturing processes – state of the art and future perspectives. *International Journal of Computer Integrated Manufacturing*, *26*(7), 596–615. https://doi.org/10.1080/0951192X.2012.749530

CHAPTER 6. ROBOTIC HYBRID ADDITIVE AND SUBTRACTIVE MANUFACTURING IN JOB SHOP MANUFACTURING ENVIRONMENTS

Eric Weflen, Matthew C. Frank, Frank, E. Peters

Industrial and Manufacturing Systems Engineering Department, Iowa State University,

Ames, Iowa 50011, USA

Modified from a manuscript to be submitted to *The International Journal of Advanced Manufacturing Technology*

6.1 Abstract

Challenges filling manufacturing roles requiring skilled labor in harsh working conditions have left an opportunity for automated systems that improve working conditions. However, robotic automation can fail to meet project objectives in environments with high product mix and low production volumes. It is critical to consider the abilities of automated systems and human users. This work presents a case study implementing robotic hybrid additive and subtractive (machining) manufacturing in a job shop steel foundry considering human factors. System development involved conducting a work task analysis and then classifying work into the areas of information gathering, information analysis, decision making, and action taking. An appropriate level of automation is applied to each task, defining the division of labor between the automated system and the human operator. This approach to automation is demonstrated by developing an assistive automation system for the in-process welding of low carbon steel castings to remove production anomalies. This is achieved through process hybridization of robotic Wire Arc Additive Manufacturing (WAAM), robotic machining, robotic grinding, and a user interface employing physical markings and computer vision. Improving the success rate and adoption of industrial automation implementations in low volume manufacturing can improve the working conditions in applications where automation was considered too challenging.

6.2 Introduction

Robotic systems have been used to automate repetitive and dangerous tasks for decades and have gained traction due to a tightening labor market (Grau, Indri, Lo Bello, & Sauter, 2017). However, automated systems often lack the versatility and resilience to succeed in job-shop manufacturing environments with high product mix and lower production volumes (Johansen, Rao, & Ashourpour, 2021). Traditional approaches may not have succeeded because they did not appropriately consider the human-machine system, leveraging their abilities while avoiding their weaknesses (Romero Díaz et al., 2016). As the skilled labor shortage increases (Figure 78), filling positions with harsh working conditions becomes increasingly challenging. However, there is a lack of methods for developing next-generation manufacturing systems with the flexibility and adaptability needed in a job shop environment that requires ambiguous decision-making. This challenge may be due to the difficulty and cost of developing traditional expert systems that could account for the large variety of situations that could arise and the relatively low value generated due to the low production volumes and infrequent occurrences. This work presents a method for implementing robotic automation in a job shop foundry environment that integrates the human operator to augment the system's adaptability and act as an indispensable mediator that allows the team to achieve a common goal despite ambiguity present in the process (Ekbia & Nardi, 2014; Johannsmeier & Haddadin, 2017). The operator will handle ambiguous situations that are common when working on tasks with a one-off nature, like found in production welding. A task

Figure 78. Production welding in a steel foundry.

analysis is used to define the process steps, which are then evaluated for their affinity for automation, their fit for a human operator, or the ability to modify the task to better suit for either. Tasks with high ambiguity preferentially remain with the human or are modified for automation, while those with repetitive content are candidates for automation (Lee & Seppelt, 2009). Key aspects of a user interface are developed for communication between humans and the automated system using physical markings and computer vision. This approach to automation is presented as a case study for developing a human-robot hybrid system for the production welding process in job shop steel foundries. The system employs robotic wire arc additive manufacturing (WAAM), machining, grinding, and a computer vision-based user interface. There are opportunities to apply this collaborative and assistive automation approach to processes in other harsh environments that have been difficult to automate using traditional approaches, such as job shop welding, grinding, and arc-air cutting. This hybridized manufacturing system integrating multiple manufacturing processes, advanced sensing, and the human operator is a step towards convergent manufacturing in the metalcasting industy (National Academies of Sciences, 2022).

Figure 79. Welded casting ready for the surface to be blended.

In a steel foundry, the production welding process (Figure 79) is used for the crucial role of rectifying indications of anomalies in a part that occur during the casting process, such as porosity, cracks, or inclusions that are identified using Nondestructive Evaluation (NDE) (Monroe, 2019). This process involves highly skilled workers utilizing various artisanal manual techniques while making complex decisions. Arc-Air gouging removes the anomaly by excavating in the NDE-identified site (Figure 80). The excavation site is prepared for a quality check and welding by grinding the surface. Then, an arc welding technique such as Flux Cored Arc Welding (FCAW) or Gas Metal Arc Welding (GMAW) deposits metal into the excavation to refill the void. This process requires ambiguous decision-making by the welder about the economics, feasibility, and best approach for welding, which may evolve during the excavation and welding processes. The procedure taken is supported by documentation including a Welding Procedure Specification (WPS) and Procedure Qualification Record (PQR) that ensures the final part meets the customers' requirements and specifications as well as industry standards (David et al., 2015). Each casting will pose a unique challenge to the operator due to variability in anomaly location, type, and size, and the difficulty is compounded in low production volume facilities with a high product mix and the need to deliver a product that is free from defects (Babalola, Mishra, Dutta, & Murmu, 2023). While industrial robotic systems are effective at automating repetitive tasks in high-volume manufacturing environments, tasks with high process variability and requiring ambiguous decision-making in a job shop environment can be particularly challenging to implement while meeting project success metrics.

Figure 80. Harsh working conditions are present during the arc-air gouging process.

Difficulty in hiring skilled labor to work in manufacturing environments with harsh working conditions (Figure 80) and an increasing labor rate have driven demand for automation in job shop manufacturing facilities (Kanike & Robinson, 2023). Groover 2019 provides a comprehensive overview of traditional automation approaches targeting high-volume and repetitive tasks. Research into flexible automation techniques aims to bring automation to applications with increased process variability and product lines with lower production volumes (J. D. Lee & Seppelt, 2009; Salvendy, Spath, Braun, & Meinken, 2012). Flexible systems can incorporate networking, advanced sensing, and artificial intelligence, often called Industry 4.0 or smart factory technologies (Javaid, Haleem, Singh, & Suman, 2021). Bringing these technologies into a factory environment does not replace the human function but transforms the work being conducted by the operator and the way they interact with the machines and the parts being produced (Parasuraman & Riley, 1997; Díaz et al., 2016).

Automated systems can be classified by their degree or level of automation, with a higher value indicating an increase in autonomy and authority of the system or agent (Endsley, Kaber, & Ica, 1999; Frohm, Lindström, Winroth, & Stahre, 2008; Vagia, Transeth, & Fjerdingen, 2016). The tasks of an automated system can be classified by their function as a) information acquisition, b) information analysis, c) decision and action selection, and d) action implementation (Parasuraman, Sheridan, & Wickens, 2000). For each of these areas, a range of levels of automation can be assigned that describe the level of system autonomy and authority held by the human and the machine. Division of labor between the human operator and automation should leverage the strengths of the human and system while avoiding their weaknesses. Humans are fit for tasks that require ambiguous decision-making or tasks with a high degree of variability, while automated systems and robotics are well suited for repetitive and physically demanding tasks (Lee & Seppelt, 2009). Job shop automation for high variability tasks that include ambiguous decision-making requires careful consideration of human factors and the interaction between humans and robotic systems.

Hybrid Manufacturing (HM), which integrates multiple complementary processes to leverage their strengths while mitigating their weaknesses to create a system with unique capabilities, is gaining attention in industry and academia (Bapat et al., 2022; Jones, 2014). A notable combination involves Additive Manufacturing (AM) and Subtractive Manufacturing, with the former offering high material utilization and the latter ensuring high dimensional accuracy and surface quality (Feldhausen, Heinrich, et al., 2022). HM has begun to gain traction in the production of aerospace and the repairing of components (Feldhausen, Kannan, et al., 2022; Dezaki et al., 2022). Wire Arc Additive Manufacturing (WAAM) is a manufacturing process that has been paired with machining to produce an HM system (Figure 81) (Li et al., 2017). In WAAM, Arc welding technologies like GMAW are paired with robotic or gantry-style motion control systems to enable the rapid production of large parts using a layer-by-layer approach (Patent No. US1533300A, 1920; Greer et al., 2019; Zhang & Li, 2001; Zhang et al., 2003). Applying WAAM and HM to the production welding process in job shop steel foundries has the potential to automate repetitive welding tasks and improve working conditions (Plotkowski, Knapp, Feldhausen, Nycz, & Li, 2023; Weflen et al., 2021). However, process parameter development is still needed to to ensure WAAM material meets performance requirements since WAAM has traditionally focused on high-cost materials (Benedetti et al., 2023). In addition, proper evaluation of operator burden and human factors considerations is critical to successfully integrating these technologies into an advanced hybrid manufacturing

Figure 81. Example of Wire Arc Additive Manufacturing (WAAM)

system (Elliott & Love, 2016; Fillingim & Feldhausen, 2023). However, a solution does not exist to address the high degree of variability and ambiguity in production welding in a job shop foundry, holding industry adoption back.

This work presents a method for leveraging the unique skills of the user when developing an industrial automation system. The method is presented as a case study for the implementation of job shop foundry welding automation that incorporates NDE, arc-air gouging, robotic additive (WAAM), and subtractive (machining and grinding) manufacturing, along with 3D vision and advanced sensing. A system architecture is developed, and the system's key components are implemented to demonstrate feasibility. Process parameters for WAAM of low carbon steel components previously developed are used for the filling of an excavation on a casting larger than previously demonstrated in the literature. While the automated manufacturing system presented in this study has the potential to relieve the labor shortage in foundries, the user integrated approach that was developed has broader applications in developing assistive automation and convergent manufacturing systems for other challenging to automate tasks.

6.3 Methodology

6.3.1 Documenting the Current State

The current state of the production welding process was documented using a task analysis. Data was collected through a literature review, facility visits to foundries, and expert elicitation. The individual tasks were documented in a process flowchart. The tasks in the flow chart were then categorized as being focused on Information Acquisition, Information Analysis, Decision Making, and Action Taking. Tasks requiring frequent ambiguous decision-making or external input from other operators, supervisors, or documentation were marked by shading them gray. Tasks with high degrees of product or process variability were also marked.

6.3.2 Division of Labor

The tasks were also decomposed into a hierarchical structure with the bottom-level tasks matching those in the sequential flow task analysis. Tasks where operators often face uncertain, unanticipated, or ambiguous situations were marked by shading them gray. If most tasks in a grouping of the hierarchy were shaded, the parent task level was also shaded. The hierarchical structure reveals groupings of tasks and sub-tasks with lower levels of ambiguity, which are strong candidates for automation. By focusing automation efforts on clusters of tasks, it is possible to reduce the frequency at which control is transitioned, and information is passed between the operator and the machine.

The tasks were then divided into those remaining with the operator and those assigned to the automated system. Since switching between the human operator and the robotic system requires additional user interaction steps that take time and can be a source of errors, an emphasis was placed on reducing the frequency of switching responsibility to reduce the magnitude and frequency of information that would need to be communicated between the operator and the system. This method could lead to instances where a task that was a good candidate for automation may be assigned to the human operator because the burden of the user interface may outweigh the benefit of automation. Alternatively, if a single task is not suitable for automation in a cluster of other tasks that are well suited, research was conducted into alternative methods of completing that task to take advantage of the strengths of the robotic system while avoiding weaknesses in the areas of ambiguity and uncertainty. Changing the approach to the work can make it more suitable for robotic automation.

6.3.3 System Design and Automation Levels

Tasks suitable for automation were designated, and an automation approach was determined. This work evaluates critical aspects of the approach as a proof-of-concept evaluation to ensure the feasibility of the system design. Implementation was streamlined by using the process planning simplifications used in WAAM systems and a machining weld preparation operation to expand the manual excavation to a known geometry.

6.3.4 Prototype System Implementation

A prototype system was developed for proof-of-concept testing of individual tasks to evaluate the feasibility of novel aspects of the system design. Individually, the inspection, excavation, weld preparation, welding, and grinding tasks were evaluated. A section of a steel casting with a production anomaly identified using phased array ultrasonic testing (PAUT) was used to evaluate the system. Manual Arc-Air gouging was used to excavate the location and depth of the anomaly as identified using PAUT. A 3D scan of the excavation was taken to fit the geometry to a standard weld preparation geometry based on an integer multiple of weld beads to simplify the WAAM process planning. In place of robotic machining, a 5-axis HAAS UMC750 machining center was used to simulate the automated weld preparation. The ArcMate 50ic welding robot was used to fill the excavation, which was blended with the surface using grinding.

6.4 Results and Discussion

This section presents the approach to developing an automated system in a job shop foundry for the production welding process that requires skilled workers to navigate complex and uncertain decisions. The approach involved the creation of a normative model of the system in the form of a sequential flow task analysis. Additional information is integrated into the task analysis by marking tasks best suited for the human operator and those with a strong potential for automation. An hierarchical structure is also used to visualize the work content to reveal the clustering of tasks suitable for automation. By focusing the automation efforts on clusters of similar work, it may be possible to reduce the frequency that information needs to be passed between the operator and the machine, reducing the complexity of the user interface requirements. This article presents this approach as a case study of the welding process, including the system implementation.

6.4.1 Current Production Welding Process

The sequential flow task analysis (Figure 82) represents the ordered work tasks for the production welding process in a steel foundry. In this flowchart, rectangles represent tasks, diamonds for decisions, parallelograms for inputs and outputs, and circles for the result of a decision. Arrows are used to describe the typical flow through the process. The sequential flow task analysis was created with input from industry experts at several different foundries and represented the union of operations at the various facilities.

The current state production welding process begins with the operator looking up the customer specifications for a given production casting to understand the inspection and quality requirements (Figure 82). The operator may have experience with the requirements for that casting, or there may be notes from previous production runs that give the operator an idea of the typical type of production anomaly and critical locations. The operator then selects the appropriate nondestructive evaluation (NDE) inspection technique for casting soundness, which the customer may specify. Standard inspection methods used in steel foundries include visual inspection, magnetic particle inspection (MPI), liquid penetrant testing, radiographic testing, and ultrasonic testing (Lau, 2022; Lau, Eisenmann, & Peters, 2021). The inspector then compares the anomalies with the customer's requirements. The operator must decide whether the discovered anomaly must be resolved by excavating the site and refilling using arc welding. Locations where excavation and welding are required are marked by the operator. Often, these steps of the NDE process are not quantitative, instead relying on trained operators to make a judgment call.

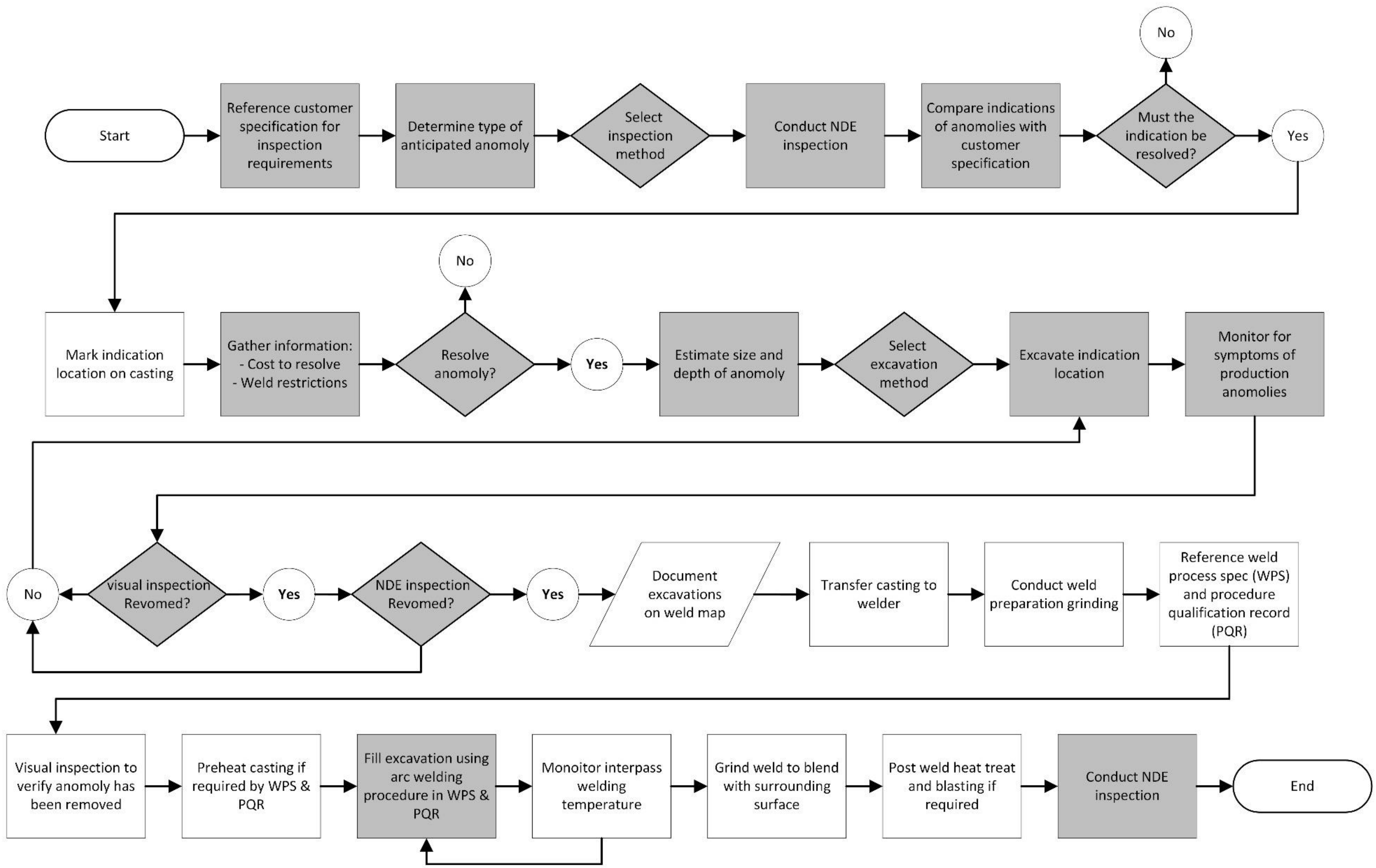

Figure 82. Sequential flow task analysis for the steel foundry production welding process.

Once the indications of an anomaly have been identified and marked, a third decision must be made in the process. This decision is whether to continue with the remaining steps in the production welding process or scrap the part. To make this decision, the operator must consider the cost and lead time for completing the production welding process with the cost and lead time of melting down the part and casting a new one. This decision is critical and may include multiple stakeholders and involves uncertainty in the factors that influence the decision, such as the actual size of the production anomaly. For example, it is often considered that the operator excavating the indication site is “exploring” as they remove material, where further unplanned issues may be uncovered. Because of this uncertainty, it can be a challenging decision to make for an inexperienced operator who has yet to develop an intuition about the casting process. Furthermore, at any point throughout the process, the decision may be reversed if it is decided that it is no longer worthwhile continuing the production welding process, and the casting may be scrapped.

The task of “Estimate the size and depth of the anomaly” moves the process into the excavation phase. The operator will estimate the size and depth of the area that must be excavated, which supports the following decision: determining the excavation method. The excavation is often conducted using arc-air or carbon-arc gouging, though grinding or other processes can also be used. Once an excavation method has been determined, the operator enters a loop where they gouge into the casting, watch for signs of an anomaly, and continue gouging. They will conduct a visual inspection to verify removal once they believe the anomaly has been entirely removed. They will loop back and continue excavating if the anomaly is not wholly removed. Once the visual inspection is passed, the operator will inspect the excavation site using an NDE method to uncover any indications of defects that would not be caught using visual inspection alone. The operator will return to the excavation step if the NDE inspection reveals additional indications. Suppose no further indications of production anomalies are found. In that case, the operator will move on to a documentation step where the sizes and locations of excavations are recorded to create a weld map for the part that will be stored for reference or supplied to the customer. The casting is then transferred to the welder.

The welder begins work by adjusting the shape of the excavation site to give them access for the welding torch and to meet the geometry requirements for the welding procedure. This weld preparation process is carried out by the welder, who has expert knowledge of appropriate geometry requirements for achieving a weld that will meet the specifications for that casting. The welder will reference the Welding Process Specification (WPS) and the Procedure Qualification Record (PQR) for additional information about the welding requirements for that part that were developed by following section IX of the boiler and pressure vessel code (ASME-BPVC.IX, 2023). The welder will also conduct a visual inspection to ensure no signs of additional casting anomalies are uncovered by the weld preparation before they continue with welding. If the welding procedure requires, the casting will be pre-heated before welding. The operator then fills the excavation site using arc welding while monitoring the inter-pass temperature to meet the specifications. The welder will overfill the excavation site and then grind the weld site to blend the surface with the surrounding casting surface. If a post-welding heat treatment or media blast is required, that step is conducted next. Finally, the same NDE procedure that uncovered the original production anomaly is used to reinspect the site to ensure that the indication of a production defect has been rectified.

Tasks with high variability, uncertainty, or ambiguity were shaded in gray (Figure 82). In this case, the authors made a judgment call based on input from industry experts and facility visits. However, there is an opportunity for further research into an appropriate classification method for tasks. The shaded tasks are those that are likely to be a good fit for the human operator, who will be well-equipped to handle these ambiguous situations. The remaining tasks are left in white, representing those that may be a good fit for automation. These non-shaded tasks are those that require primarily repetitive and consistent to be completed. Limiting task switching between the human operator and the automated system is desirable to minimize errors and reduce the user interface's complexity. Shading of tasks in the sequential flow task analysis helps visualize a series of tasks that are candidates for automation (Figure 82). However, a sequential flow task analysis does not represent clusters of similar work that segment the process.

6.4.2 Division of Labor

An hierarchy of tasks is constructed on the workflow to cluster similar tasks and find natural breaking points where it may make sense to transition tasks between the operator and the automated system (Figure 83). Since a sequential flow task analysis was completed and contained all individual tasks, a bottom-up approach was used to develop the hierarchy, where tasks were clustered and labeled. This clustering process resulted in a top level of the hierarcy that consisted of six high-level operations: 1) inspection, 2) excavation, 3) weld preparation, 4) welding, 5) grinding, and 6) re-inspection (Figure 83). Operation 2, excavation, was divided into three sub-groups: 2.1) gather information, 2.2) excavation, and 2.3) documentation. Below these tasks are the bottom-level tasks that match the sequential flow task analysis. A similar structure was produced for each top-level work item in the hierarchy.

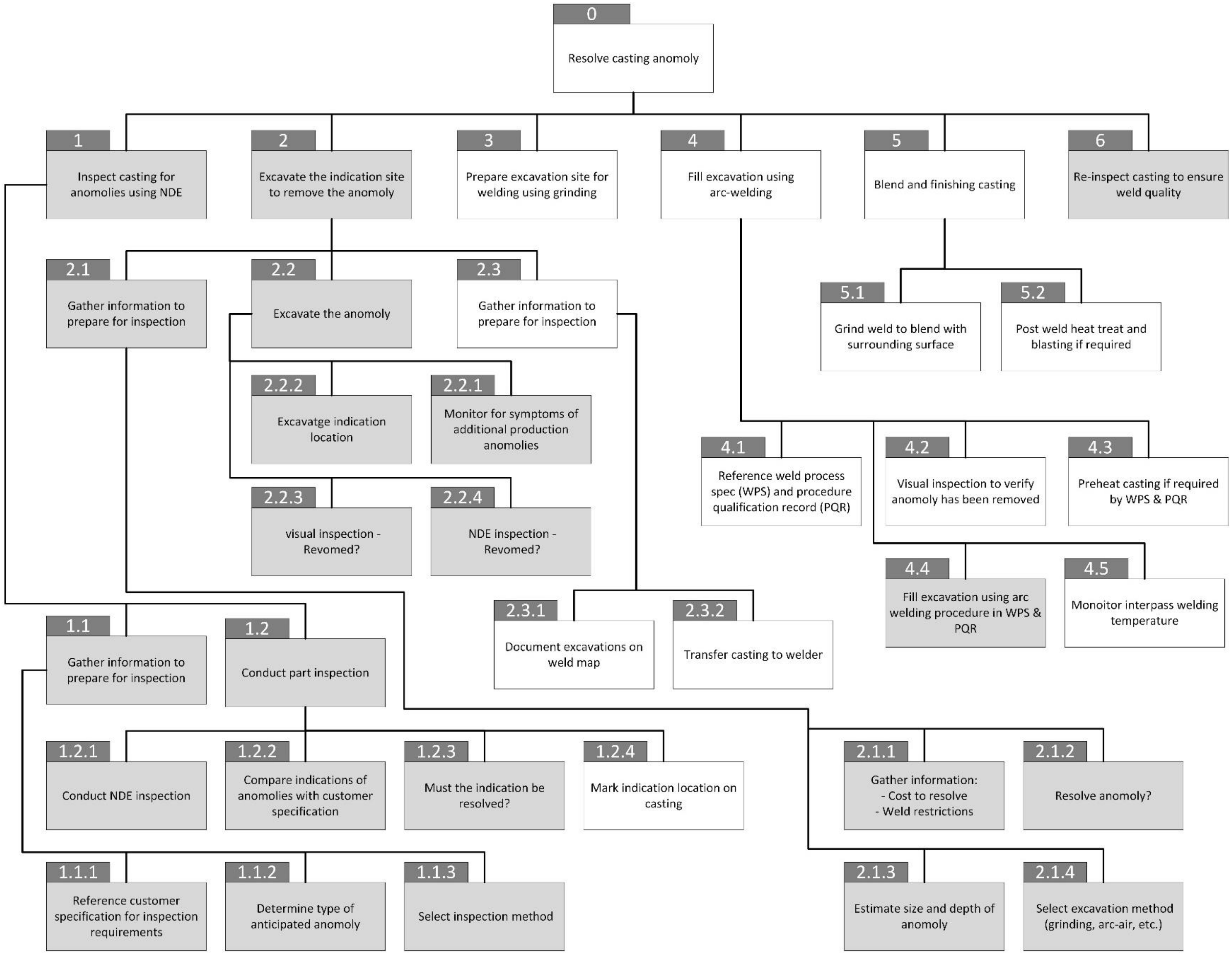

Figure 83. Hierarchical visualization of tasks for the production welding process.

While the hierarchical visualization clearly shows clustering, the sequential flow task analysis format provides additional information about the type of task through the task shape. For example, the decision tasks are marked in the sequential flow task analysis, and the reader can understand the order of tasks along with process loops. For these reasons, there may be value in creating each representation of the process.

The shading of ambiguous tasks on the bottom level is transferred to the HTA from the sequential flow task analysis. The higher-level tasks that were shaded due to most of their lower-level sub-tasks being shaded included 3) weld preparation, 4) welding, and 5) grinding/blending. There may also be value in automating some or all of the work related to sub-task 2.3, which is related to documenting the location of the excavations so that the welder knows where to weld and for the customers' reference. Task 4.4 is particularly interesting because it is the lone shaded task in a group with tasks suitable for automation. This task could be managed by having the human operator handle just that task while attempting to automate the other aspects of that work collaboratively. However, that may require additional complexity in the user interface, and may affect the coherence of work conducted by the operator. Furthermore, in this instance, the task represents welding the casting, which puts the operator in a harsh working environment. Since a primary desired outcome of this automation implementation is to improve working conditions in this process, an alternative approach will be taken with that task. Instead, that task will be changed to make it more suited for automation through simplification and removing the ambiguous aspects. While it can often be attractive to copy a manual operation when implementing robotic automation, the unique capabilities of the automation may open opportunities to improve the process by modifying the work. However, this approach may require additional research.

Tasks assigned to the human operator may change due to changing requirements of the human-robot system. For example, the quality requirements for task 2.3.1, document excavations on weld map, will need to be modified because the markings are now meant to communicate locations to a computer vision system instead of another human operator. Currently, that task consists of marking locations on the casting, typically by circling the area with a paint marker or chalk (Figure 84). However, the exact marking may be different between operators or foundries. A computer vision system can identify these markings, but the color, shape, and quality must be standardized. In addition, the operator will need to receive feedback from the vision system to verify that the markings were correctly identified and that the robotic system will make appropriate movements for the weld preparation and welding operations. Once these items are verified, the operator will approve the plan to move forward with automatic completion tasks in groups three, four, and five. An operator will also need to monitor the system during operation and, depending on customer requirements may need to stop the process for part inspection or documentation. Future research will be needed to develop user interface elements, which are anticipated to be accomplished through a video display and button input.

(a) (b)

Figure 84. Excavations marked for transition to the welder using a) circling or b) marking

6.4.3 System Design and Level of Automation

After documenting the current state process and identifying the areas for automation, the next step is to use those findings to design the system. The future state high-level system architecture is presented with tasks marked for those assigned to the human operator and those assigned to the robotic system (Figure 85). Two additional tasks are included here that were not in the original hierarchical representation of the tasks. Those tasks include the human operator "programming" the robot by marking the casting locations and the 3D vision aspects of the automated system that will take the operator's input to generate a process plan. This section will discuss the essential features of the automated procedure and the user interface.

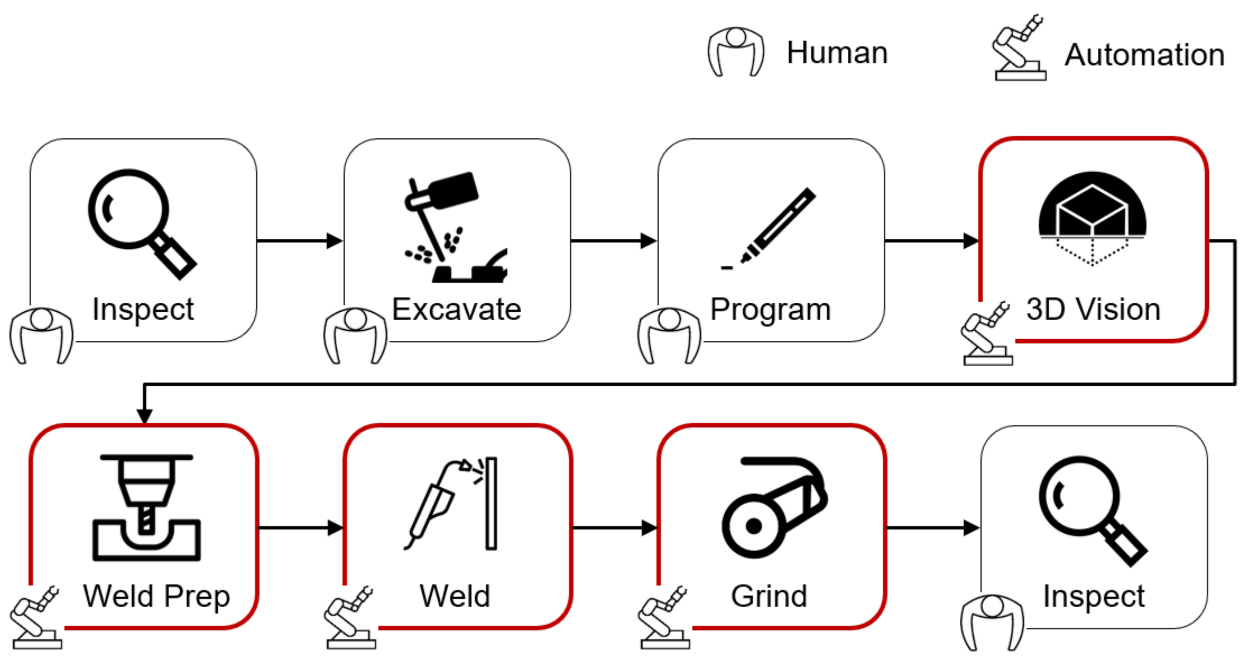

Figure 85. High-level architecture of the proposed human-automation system.

First, the casting is manually inspected using an NDE approach, typically including visual inspection, magnetic particle inspection (MPI), radiography, or ultrasonic testing, and anomalies that do not meet the specifications are documented. This inspection process will remain a manual step conducted by the operator due to the high degree of ambiguous decision-making and the wide variety of specifications encountered. Those anomalies are excavated from the casting using arc-air gouging or grinding. While this step may appear to be a good candidate for automation, the operators conduct an exploratory excavation based on in-situ visual observations and a challenging to document decision-making process so that it will remain a manual step. The operator will then program the robot by communicating the desired geometry using physical markings on the casting. The automated system will use a 3D vision system to extract the part geometry and operator markings, from which it will prepare the excavation for welding using a machining operation, fill the excavation using WAAM, and use grinding to blend the surface. The operator will conduct a post weld inspection process in the final step.

Figure 86. Process qualification test coupon used in a steel foundry.

If toolpath planning for a WAAM filling operation were attempted on a manual arc-air excavation, it would require complex toolpaths that would increase the difficulty in developing robust planning algorithms and risk the potential to produce a weld that did not meet the required material properties. The layer-by-layer 2.5D process planning used in AM systems is used to circumvent this complexity. To further simplify the process, the weld preparation step will be standardized to be a v-groove geometry similar to those used to develop the WPS and PQR in a foundry (Figure 86). The weld preparation material removal will be conducted using a spindle on the robot with an endmill. This material removal will expand the manual excavation using arc-air to form a standard v-groove geometry. The standard v-groove will be paired with the additive process to match the dimensions of each layer to an integer multiple of weld beads in width, length, and depth. The sharp edges created by the bullnose endmill will be cleaned using a chamfer mill. This approach ensures reach and access for the robot welding torch, eliminating the need for complex collision avoidance to be considered in the toolpath generation process or for adjusting the torch angle on the fly during welding. Additionally, by setting the cavity geometry to a pre-defined multiple of weld beads, the filling of the cavity can be simplified (Figure 87). By streamlining the process, it becomes more feasible that the welds produced meet customer specifications. A standard library of toolpaths can be created and tested to ensure they meet customer requirements. This standard library of toolpaths will be located on the surface of the casting based on the markings provided by the operator that are picked up by the computer vision system. The robotic system can define the location and geometry with length, width, depth, and location information collected from a 3D scan of the operator markings and the associated excavation geometry (Figure 88a).

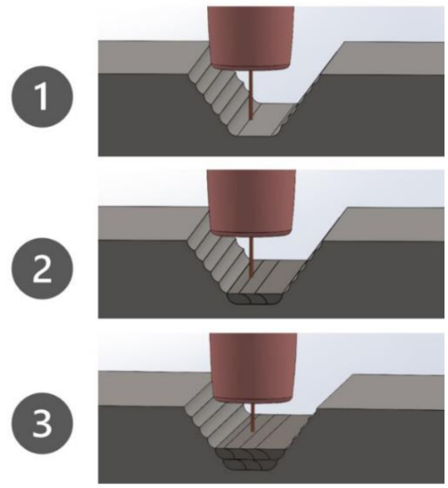

Figure 87. Cross section view of a standard weld geometry, welding torch access, and fitting a multiple of weld beads.

An algorithm will be needed to fit this standard weld preparation geometry to the manual arc-air excavation. The operator will mark the location on the casting where the excavation was conducted to trigger the system to take a 3D scan and to help segment the resulting point cloud. This information can be used to calculate the smallest v-groove that will fully contain the excavation (Figure 88 b & c). Surface reconstruction can be used to interpolate the desired surface. Welding toolpaths will be driven by the selected weld preparation geometry, and the grinding operation will blend weld material down to the interpolated surface to blend with the surrounding casting surface.

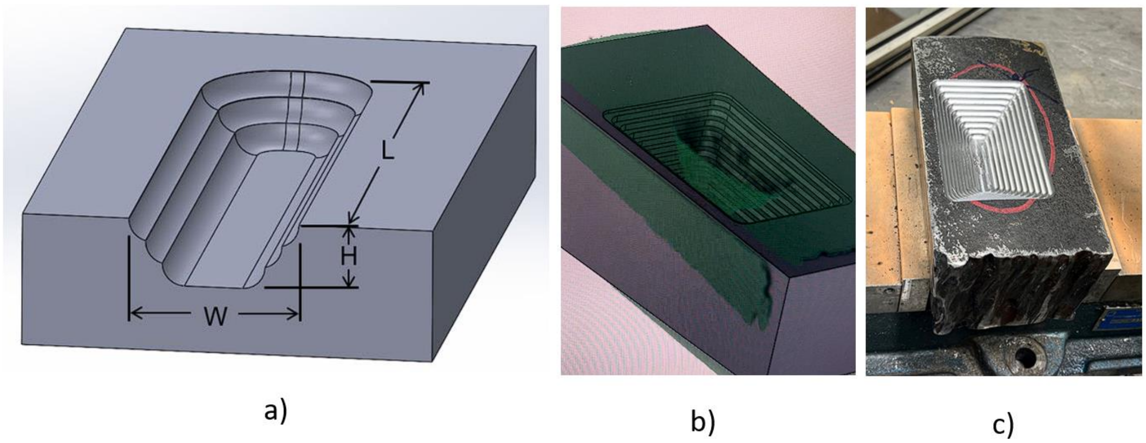

Figure 88. The standard weld prep geometry a) can be defined by a length, width, and depth parameter b) which can be fit to a 3D scan of the manual arc-air gouge c) weld preparation allowing for process planning simplification.

The level of automation (LOA) is commonly used to represent the level of autonomy and authority in the system (Frohm et al., 2008). This work evaluated LOA by layering automation information on the and the sequential flow task analysis and hierarchical visualization of tasks, which can be summarized in a chart showing the system's areas and levels of automation (Li & Burns, 2017). This tool can help develop a user’s mental model of the system by creating a visual representation of the tasks and division of labor to improve transparency and achieve an appropriate level of operator trust, reliance, and compliance (Lee & Seppelt, 2009). The level of automation in the four areas of information gathering, information analysis, decision making, and taking action are presented for the system developed in this study (Figure 89). The automation focuses on the action-taking area for this system, while much of the information gathering, analysis, and decision-making remains with the human. This approach was taken because those areas have a high degree of ambiguity and a process variation that would make developing an expert system that could interpret inputs and arrive at a result a challenging exercise. In addition, there was a desire to focus automation efforts on the tasks that resulted in a harsh working environment for the operator, which were primarily the action steps. A limitation of this presentation method is that in a process such as the one presented, numerous tasks fall within each category, each with different levels of automation. However, this visualization of the automation can be limited. For example, the arc-air excavation action step remains with the human operator, but this representation cannot present the automation to that level of granularity. For that reason, there may be limited value in this data representation method for complex systems.

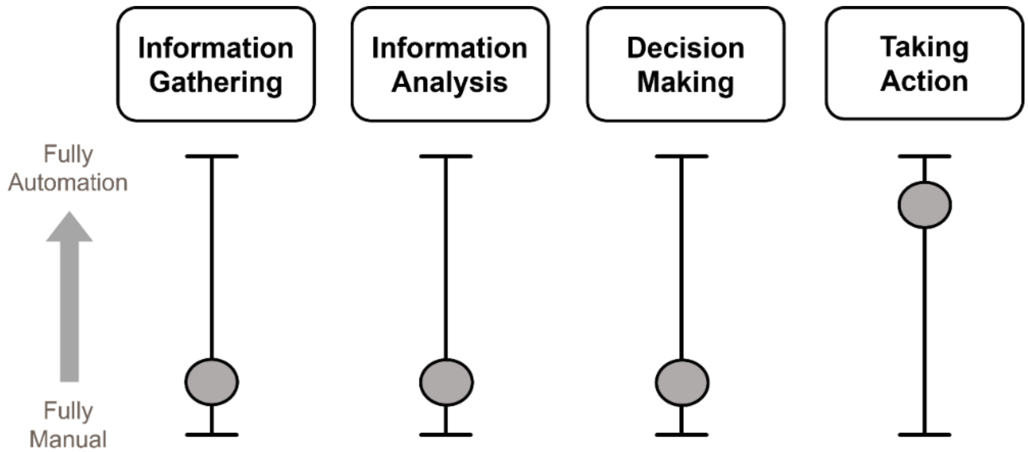

Figure 89. Areas and levels of automation for the steel casting production welding system.

6.4.4 System Prototype Evaluation

Novel sub-tasks of the designed automation system were tested individually as a proof of concept before broader system implementation (Figure 90). Evaluating new aspects of the system using prototype systems can increase confidence in the ability of the fully automated system to successfully achieve the desired outcomes. This will help achieve the objective of improving working conditions in the job shop steel foundry cleaning room by automating repetitive tasks and tasks that place the operator in harsh environments.

Figure 90. The process steps were evaluated on a real casting anomaly through a) finding an anomaly using PAUT, b) excavating the anomaly with Arc-Air gouging, c) marking the location for 3D scanning, d) fitting and machining a standard weld preparation v-groove, e) filling the cavity using WAAM, f) blending the surface by grinding, and g) inspecting the part.

A large steel casting, with extents on a cubic meter scale, had a section removed with dimensions approximately 100 x 200 x 75 mm. This section was used to evaluate the system. PAUT was used to find a production anomaly indication with the location, boundary, and depth marked on the casting (Figure 90a). Manual arc-air gouging was used to manually excavate the anomaly (Figure 90b). The computer vision approach used to identify the excavation location marked manually by the operator (Figure 90c) will be borrowed from an existing automated system used in the steel casting industry for the grinding of riser and gating locations, details of which can be found in (Schimpf, 2021). The process of fitting the weld preparation geometry to the excavation was conducted manually by taking a 3D scan of the excavated part and designing a weld preparation geometry using Computer-Aided Design (CAD) software (Figure 91). Machining of the 10-layer deep weld preparation took place in a machining center as a stand-in for a robotic machining center that would be used in a full implementation (Figure 90d).

However, other researchers have demonstrated robotic milling of steel materials in similar applications where high geometric variability is acceptable (Tratar & Kopač, 2013). During the machining process, the arc-air gouge surface was found to have the potential to be differentiated from the milled surface through visual inspection, which can be used to ensure that the fitting succeeded in removing the entire manual excavation and suggests that an automated computer vision monitoring approach may be feasible. A parametric robotic welding program was created to take the length, width, and depth parameters of the weld preparation v-groove and automatically generate WAAM toolpaths to fill the cavity (Figure 90e). The weld material was manually blended with the surrounding surface geometry (Figure 90f), though other researchers have presented automated robotic grinding systems, demonstrating their feasibility (Schimpf, 2021). Typically, a foundry will reinspect the part using the same process that identified the anomaly to ensure removal (Figure 90g).

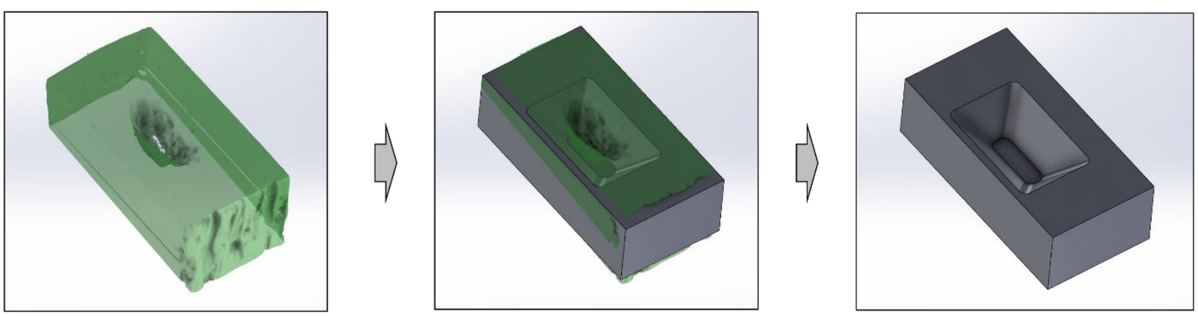

a) Scanning b) Fitting c) Weld Preparation

Figure 91. Transforming the manual arc-air gouge to a standard geometry through a) taking a 3D scan of the surface, fitting a standard geometry to the scanned excavation, and c) machining the surface to achieve the weld preparation geometry.

This prototype system shows the potential feasibility of the automated system for the production welding of steel castings using a hybrid additive (WAAM) and subtractive (machining) approach. Since this prototype focused on technical feasibility, additional user interface design work is needed to integrate the user and automated system. In addition, further user research is required in order to elucidate the effectiveness of the division of labor. User feedback can be regularly integrated into the design process by taking an iterative development approach to designing the manufacturing system.

6.5 Conclusions

As a shortage of skilled labor increases the motivation to implement automated solutions into new applications, it will become progressively more important to consider how to integrate the user's abilities into the broader system to achieve the desired outcomes. This work presented an approach to implementing industrial automation for the production welding of steel casting that leverages the user's and robotic system's strengths. This approach was demonstrated through the case study of a human-robot system designed to automate the production welding process in job shop steel foundries with low production volumes and high product mix. By defining the current state process steps and categorizing them based on their suitability for automation, a level of automation could be determined for the areas of information gathering, information analysis, decision making, and taking action. An approach was defined to pass information between the human and the robot through computer vision and markings on the part surface. A demonstration system applied process parameters previously developed for low carbon steel WAAM to excavations in large-scale steel components. Critical aspects of the system were prototyped to determine their feasibility by identifying, removing, and repairing a casting anomaly.

The presented approach may be able to expand applications where industrial robotic automation can be applied to tasks with higher process variability, low production volumes, and requiring ambiguous decision-making. These are areas where traditional automation approaches that attempt to automate all aspects of the process have struggled to take hold but have become increasingly important in the context of convergent manufacturing. By keeping the human in the loop when developing the human-robot automated system, ambiguous tasks can be handled by the human who is not only well suited for that type of work but takes pride in their ability to apply their skills in this area. Improving working conditions in steel foundries can help attract skilled labor to these facilities. The labor-intensive production environment in job shop foundries can increase throughput and become more competitive through automation. Expanding the production capacity through expanded labor availability and productivity improvements in the production welding process will remove a bottleneck that slows the flow of in-process products. This can reduce the production lead time, the work in process, and the need for working capital. The approach presented in this study can be applied to other applications that have traditionally struggled to adopt automation due to high process or product variability or require complex decisions that can be challenging to develop into an expert system.

Further research is needed to evaluate the performance of the proposed system and user interface through additional user research. While this work presented an approach and identified tasks suitable for automation, and user interface elements were proposed, the evaluation of the design and implementation of the complete user interface and robotic system may still face challenges that require modification of the system design presented or evolution of the approach taken in this study. However, the feasibility analysis suggests that the critical aspects of the system show promise and warrant further investigation and development toward implementation in a production environment. The WAAM process parameters for low carbon steel will guide the implementation of a production welding system. Still, the implementation must be tuned to the welding equipment, performance requirements, and alloy used in that application. There is an opportunity to integrate advances in simulation and real-time process monitoring into the WAAM aspects of the system to ensure quality requirements are achieved.

6.6 Acknowledgement

This research is sponsored by the DLA-Troop Support, Philadelphia, PA and the Defense Logistics Agency Information Operations, J68, Research & Development, Ft. Belvoir, VA.

6.7 Disclaimer

The publication of this material does not constitute approval by the government of the findings or conclusion herein. Wide distribution or announcement of this material shall not be made without specific approval by the sponsoring government activity.

6.8 References

ASME-BPVC.IX. (2023). ASME BPVC. IX-2023. In *ASME International*. Retrieved from https://www.asme.org/codes-standards/find-codes-standards/bpvc-ix-bpvc-section-ix-welding-brazing-fusing-qualifications

Babalola, S. A., Mishra, D., Dutta, S., & Murmu, N. C. (2023). In-situ workpiece perception: A key to zero-defect manufacturing in Industry 4.0 compliant job shops. *Computers in Industry*, *148*, 103891. https://doi.org/10.1016/J.COMPIND.2023.103891

Baker, R. (1920). *Patent No. US1533300A*. Retrieved from https://patents.google.com/patent/US1533300A/en

Bapat, S., Sealy, M. P., Rajurkar, K. P., Houle, T., Sablon, K., Malshe, A. P., … Applications, ". (2022). Applications of Hybrid Manufacturing during COVID-19 Pandemic: Pathway to Convergent Manufacturing . *Smart and Sustainable Manufacturing Systems* , *6*(1), 12–22. https://doi.org/10.1520/SSMS20210022

Benedetti, M., Hu, L., Nguyen, V.-T., Minh, P. S., The Uyen, T. M., Do, T. T., … Nguyen, T. (2023). WAAM Technique: Process Parameters Affecting the Mechanical Properties and Microstructures of Low-Carbon Steel. *Metals 2023, Vol. 13, Page 873*, *13*(5), 873. https://doi.org/10.3390/MET13050873

David, D., Monroe, R., & Thomas, E. (2015). Exploring the Need to Include Cast Carbon Steels in Welding Procedure Specifications. *Welding Journal*, *94*(10), 56–58.

Ekbia, H., & Nardi, B. (2014). Heteromation and its (dis)contents: The invisible division of labor between humans and machines. *First Monday*, *19*(6). https://doi.org/10.5210/FM.V19I6.5331

Elliott, A. M., & Love, L. J. (2016). Operator Burden in Metal Additive Manufacturing. *Proceedings of the 27th Annual International Solid Freeform Fabrication Symposium*, 1890–1899. Retrieved from http://energy.gov/downloads/doe-public-

Endsley, M. R., Kaber, D. B., & Ica, M. (1999). Level of automation effects on performance, situation awareness and workload in a dynamic control task. *Ergonomics*, *42*(3), 462–492. https://doi.org/10.1080/001401399185595

Feldhausen, T., Heinrich, L., Saleeby, K., Burl, A., Post, B., MacDonald, E., … Love, L. (2022). Review of Computer-Aided Manufacturing (CAM) strategies for hybrid directed energy deposition. *Additive Manufacturing*, *56*, 102900. https://doi.org/10.1016/J.ADDMA.2022.102900

Feldhausen, T., Kannan, R., Saleeby, K., Fillingim, B., Kurfess, R., Nandwana, P., & Post, B. (2022). Hybrid Manufacturing Approaches for the Production and Repair of Industrial Tooling. *International Conference on Nuclear Engineering, Proceedings, ICONE*, *1*. https://doi.org/10.1115/ICONE21-16472

Fillingim, K. B., & Feldhausen, T. (2023). Operator 4.0 for Hybrid Manufacturing. *INTERNATIONAL CONFERENCE ON ENGINEERING DESIGN*, 24–28. https://doi.org/10.1017/pds.2023.284

Frohm, J., Lindström, V., Winroth, M., & Stahre, J. (2008). Levels of automation in manufacturing. *Ergonomia*.

Grau, A., Indri, M., Lo Bello, L., & Sauter, T. (2017). Industrial robotics in factory automation: From the early stage to the Internet of Things. *Proceedings IECON 2017 - 43rd Annual Conference of the IEEE Industrial Electronics Society*, *2017-January*, 6159–6164. https://doi.org/10.1109/IECON.2017.8217070

Greer, C., Nycz, A., Noakes, M., Richardson, B., Post, B., Kurfess, T., & Love, L. (2019). Introduction to the design rules for Metal Big Area Additive Manufacturing. *Additive Manufacturing*, *27*, 159–166. https://doi.org/10.1016/J.ADDMA.2019.02.016

Groover, M. P. (2019). *Automation, production systems, and computer-integrated manufacturing* (Fifth edition.) [Book]. NY NY: Pearson Education, Inc.

Javaid, M., Haleem, A., Singh, R. P., & Suman, R. (2021). Substantial capabilities of robotics in enhancing industry 4.0 implementation. *Cognitive Robotics*, *1*, 58–75. https://doi.org/10.1016/J.COGR.2021.06.001

Johannsmeier, L., & Haddadin, S. (2017). A Hierarchical Human-Robot Interaction-Planning Framework for Task Allocation in Collaborative Industrial Assembly Processes. *IEEE Robotics and Automation Letters*, *2*(1), 41–48. https://doi.org/10.1109/LRA.2016.2535907

Johansen, K., Rao, S., & Ashourpour, M. (2021). The Role of Automation in Complexities of High-Mix in Low-Volume Production – A Literature Review. *Procedia CIRP*, *104*, 1452–1457. https://doi.org/10.1016/J.PROCIR.2021.11.245

Jones, J. B. (2014). The synergies of hybridizing CNC and additive manufacturing. *Technical Paper - Society of Manufacturing Engineers*.

Kanike, U. K., & Robinson, J. M. (2023). Factors disrupting supply chain management in manufacturing industries. *Journal of Supply Chain Management Science*, *4*(1–2), 1–24. https://doi.org/10.18757/JSCMS.2023.6986

Lalegani Dezaki, M., Serjouei, A., Zolfagharian, A., Fotouhi, M., Moradi, M., Ariffin, M. K. A., & Bodaghi, M. (2022). A review on additive/subtractive hybrid manufacturing of directed energy deposition (DED) process. *Advanced Powder Materials*, *1*(4), 100054. https://doi.org/10.1016/J.APMATE.2022.100054

Lau, S. (2022). *Reducing measurement error in magnetic particle inspection through the optimization of process parameters and artificially intelligent solutions*. Iowa State University.

Lau, S. M. Y., Eisenmann, D., & Peters, F. E. (2021). Development of an Image Analysis Protocol to Define Noise in Wet Magnetic Particle Inspection. *International Journal of Metalcasting*, *15*(4), 1317–1325. https://doi.org/10.1007/S40962-020-00566-4/METRICS

Lee, J. D., & Seppelt, B. D. (2009). Human Factors in Automation Design. *Springer Handbook of Automation*, 417–436. https://doi.org/10.1007/978-3-540-78831-7_25

Li, F., Chen, S., Shi, J., Tian, H., & Zhao, Y. (2017). Evaluation and Optimization of a Hybrid Manufacturing Process Combining Wire Arc Additive Manufacturing with Milling for the Fabrication of Stiffened Panels. *Applied Sciences 2017, Vol. 7, Page 1233*, *7*(12), 1233. https://doi.org/10.3390/APP7121233

Li, Y., & Burns, C. M. (2017). Modeling Automation With Cognitive Work Analysis to Support Human-Automation Coordination. *Journal of Cognitive Engineering and Decision Making*. https://doi.org/10.1177/1555343417709669

Monroe, R. (2019). Welding Steel Castings. *Steel Founders' Society of America*.

National Academies of Sciences, E. and M. (2022). Convergent Manufacturing: A Future of Additive, Subtractive, and Transformative Manufacturing: Proceedings of a Workshop. *Convergent Manufacturing: A Future of Additive, Subtractive, and Transformative Manufacturing*. https://doi.org/10.17226/26524

Parasuraman, R., & Riley, V. (1997). Humans and automation: Use, misuse, disuse, abuse. *Human Factors*, *39*(2), 230–253. https://doi.org/10.1518/001872097778543886

Parasuraman, R., Sheridan, T. B., & Wickens, C. D. (2000). A model for types and levels of human interaction with automation. *IEEE Transactions on Systems, Man, and Cybernetics Part A:Systems and Humans*. https://doi.org/10.1109/3468.844354

Plotkowski, A., Knapp, G., Feldhausen, T., Nycz, A., & Li, M. (2023). Hybrid Al Casting + AM Components for Automotive Applications. In *United States*. https://doi.org/10.2172/1971032

Romero Díaz, D., Stahre, J., Wuest, T., Noran, O., Bernus, P., Fast-Berglund, Å., & Gorecky, D. (2016). Towards An Operator 4.0 Typology: A Human-Centric Perspective On The Fourth Industrial Revolution Technologies. *46th International Conference on Computers & Industrial Engineering 2016 (CIE46)*. Retrieved from https://research-repository.griffith.edu.au/handle/10072/341888

Salvendy, G., Spath, D., Braun, M., & Meinken, K. (2012). Handbook of Human Factors and Ergonomics: Fourth Edition. In *Handbook of Human Factors and Ergonomics: Fourth Edition* (pp. 1643–1665). https://doi.org/10.1002/9781118131350/FORMAT/EPUB

Schimpf, D. W. (2021). *Objective surface inspection and semi-automated material removal for metal castings* (Iowa State University). Retrieved from https://www.proquest.com/dissertations-theses/objective-surface-inspection-semi-automated/docview/2552137001/se-2?accountid=10906

Tratar, J., & Kopač, J. (2013). Robot milling of welded structures. *Journal of Production Engineering*, *16*(2), 29–32.

Vagia, M., Transeth, A. A., & Fjerdingen, S. A. (2016). A literature review on the levels of automation during the years. What are the different taxonomies that have been proposed? *Applied Ergonomics*, *53*, 190–202. https://doi.org/10.1016/J.APERGO.2015.09.013

Weflen, E., Black, M., Frank, M., & Peters, F. (2021). Wire Arc Additive Manufacturing of Low Carbon Steel for Casting Applications. *Proceedings of the 33rd Annual International Solid Freeform Fabrication Symposium*, 170–177.

Zhang, Y M, & Li, P. J. (2001). MODIFIED ACTIVE CONTROL OF METAL TRANSFER AND PULSED GMAW OF TITANIUM. *Welding Journal*, *80*(2), 54–61.

Zhang, Yu Ming, Chen, Y., Li, P., & Male, A. T. (2003). Weld deposition-based rapid prototyping: a preliminary study. *Journal of Materials Processing Technology*, *135*(2–3), 347–357. https://doi.org/10.1016/S0924-0136(02)00867-1

CHAPTER 7. GENERAL CONCLUSIONS

7.1 Summary of Contributions

In this dissertation, hybrid additive/subtractive manufacturing processes were studied for the purpose of removing manufacturing limitations on the fabrication of large-scale and multi-material parts. The research aimed to address the problem that current manufacturing methods for producing large-scale and multi-material parts are limited by manufacturing process capabilities. This research achieved the four research objectives: Studying interlocking features to create a model for the design of metal-polymer interface forming a mechanical bond and thermally releasing print surface for production of large-scale polymer parts, investigating mechanically interlocking interfacial features for bonding dissimilar materials in multi-material parts produced using hybrid manufacturing, developing a process and parameters for hybrid manufacturing in steel foundries, and creating an approach for integrating hybrid manufacturing into a production environment to automate tasks with complex decisions and low production volumes.

The first objective was achieved by improving the large-scale AM process by creating a build plate capable of fixturing a part during production and releasing it when production is completed. This was accomplished through mechanical interlocking features on the print surface that form a bond to the deposited polymer material upon solidification. The part is released through rapid heating to soften the polymer material, reducing the mechanical interlocking force so the part can be easily removed. A model was produced to explain how interlocking feature height and undercut angle parameters affect the bond strength in the ambient (locked) and elevated temperature (released) conditions. To evaluate the versatility of the print surface, two demonstration parts were printed, machined, and removed from the print surface. One demonstration part was produced using carbon fiber-filled ABS, and the other from HDPE. This switchable level of adhesion contrasts the single adhesion level for production and part removal from current print surface technologies for large-scale additive manufacturing systems. The results from this study can help expand the material capabilities of large-scale additive manufacturing systems and streamline the post-print part processing time while improving the rate of successful prints by avoiding unintended in-process delamination.

The second research objective evaluated approaches of forming mechanically interlocking bonds between dissimilar materials for the production of multi-material parts in hybrid additive and subtractive (machining) manufacturing environments. Interfaces for transitions from polymer to dissimilar polymer regions and metal-to-polymer regions in parts were evaluated using a dovetail feature and a more aggressive t-slot feature geometry. Two combinations of polymer materials were verified to create a structural bond with ABS/CF material: PP-GF and ABS-CF. In addition, two metal-polymer material combinations were investigated: ABS to aluminum and ABS-CF to steel. The variety of approaches for producing mechanical interlocking bonds between regions of dissimilar materials in multi-material parts helps expand the ability to better optimize part designs by enabling new material combinations. Product designers or generative design and optimization approaches can leverage the increased design space created by expanding the manufacturing capabilities of multi-material parts in hybrid manufacturing systems.

The third research aim was achieved by developing a hybrid process for the production welding or repair of steel castings. Process parameters were established for WAAM in low carbon steel and demonstrated in filling excavations in a casting. Subtractive machining was used for weld preparation of the manual excavation, and grinding was used to blend the surface after processing. This work demonstrates how using industrial robotics and advanced sensing can allow for hybridizing several manufacturing processes to meet an industry need.

The fourth component of the research presented an approach to transition hybrid additive/subtractive manufacturing and other robotic automation processes into a high mix and low volume production environment. Key aspects of this approach were to identify the tasks, categorize them as those pertaining to a) information acquisition, b) information analysis, c) decision and action selection, and d) action implementation, then analyze the tasks for the level of ambiguity to find those suitable for the human or the robotic system. This resulted in a level of automation for each task category in the system. As a case study, this approach was applied to the production welding of steel castings in job shop steel foundries. A system design was completed, with novel aspects of that system being tested to evaluate their feasibility. While traditional automation approaches have succeeded in automating high-volume, repeatable tasks, this operator-focused approach can help expand the applications where automation can be applied to increasingly challenging enigmatic applications due to elevated variation.

7.2 Broader Impacts

This work has extended the body of knowledge in manufacturing large-scale and multi-material parts produced using hybrid manufacturing. These contributions toward developing interfaces between processes, materials, and between the operator and the manufacturing system is a step toward a convergent manufacturing system. By investigating the methods with which mechanically bonding interfaces can be formed between dissimilar materials, this work has enabled higher-performance multi-material parts to be produced. Higher-performing parts that meet functional requirements at reduced weight can substantially impact energy consumption in aerospace applications and are becoming increasingly important in automotive applications with expanding electrification. The ability to select the material within a single part can optimize the design to reduce cost by only using high-cost materials like titanium where needed and meeting other functional requirements using composite or polymer materials. Lowering the cost of high-performance parts can expand the applications where they can be put into service.

This approach to mechanical bonding can be tuned to solve the challenge of build plate adhesion for large-scale parts. Prior attempts failed at solving the competing print surface requirement of high bond during production and releasing the part when processing is complete because they attempted to use either chemical bonding or thermal fusion, which were material-specific and resulted in a single bond strength for both situations. Mechanical bonding paired with thermal release has resulted in a print surface that can meet production needs during processing while reducing the cost of part removal and post-print processing by releasing the object. The presented model describes the influence of crucial mechanical interlocking feature parameters on the resulting bond strength in both the cool (locked) and heated (unlocked) states, which will allow for the design to be tuned in production to meet the specific requirements of individual applications in industry.

Fundamental research in manufacturing automation can struggle to transition from academia into industry as they move up the technology readiness level (TRL) ladder. One reason may be a lack of focus on the appropriate division of labor between the operator and the automated system. These challenges are even more pronounced in job shop manufacturing environments with low production volumes and high product mix. The presented approach for transitioning manufacturing automation into job shop environments, demonstrated by bringing hybrid manufacturing technologies into job shop steel foundries, will help improve the reach of automation into manufacturing environments that have struggled to adopt these systems in the past. This work expands the body of knowledge around large-scale WAAM in low-carbon steels.

Additionally, it will improve working conditions in the steel foundry production welding process by taking the skilled operator out of the harsh welding and grinding environment while utilizing the operator's experience and judgment to deal with ambiguous situations that would cause a failure if encountered by a traditional robotic system. By integrating the operator into the manufacturing processes, there is a potential to achieve a synergistic effect where the system can perform beyond the capabilities of either on its own. The application of this approach is much broader than just steel foundries, WAAM, or hybrid manufacturing. This approach can be applied to other job shop manufacturing environments typical in the forging, machining, and non-ferrous casting industries. By integrating the operator in this approach to managing ambiguous and variable situations into the design of manufacturing automation systems, there is the potential to increase the success rate and adoption of automation, which is critical as the industry faces a shortage of skilled labor and an aging workforce.

7.3 Limitations and Opportunities for Further Research

While this work has extended the knowledge base on multi-material and large-scale part production using hybrid manufacturing, there are still numerous opportunities for further research in this space. Large-scale additive and hybrid manufacturing are relatively new processes, gaining expanded interest and adoption over the past decade. There are many potential applications for multi-material parts that have not been explored. As the possibility of producing parts in new material combinations is demonstrated and more data is gathered on the mechanical performance of these types of parts, new applications will emerge. These new applications will face challenges during implementation that must be explored and solved.

Similarly, the production of large-scale parts using hybrid manufacturing has been limited to a small set of materials despite the rapid adoption of the technology over the past decade. As these technologies mature, data will be captured on part performance in the field, which will help build the confidence needed for broader adoption. Broader adoption will lead to improved tools for designing and process planning for the parts, which can still be more challenging than traditional part design.

Several limitations and opportunities for further development on the proposed mechanically interlocking print surface exist. The primary material used for evaluating the print surface was ABS-CF. While this is one of the most common materials used in large-scale part hybrid manufacturing, several other materials are used. Still, the mechanical bonding may be less sensitive to the material used to produce the part than other print surface materials. However, there are opportunities to improve the interlocking feature design further to account for a broader range of materials that can be printed. A model could be developed for these different material systems that could help guide the design of a print surface tuned to perform best on the materials primarily used in a specific application. Manufacturing the interlocking features requires extensive machining time due to the small and specialty tooling required. Several potential methods could produce a similar interlocking effect at a lower production cost. The ability to switch off the mechanical bond between the metal print bed and the polymer part may find other applications, such as remanufacturing wear or serviceable aspects in a multi-material part.

Various material combinations were evaluated for their performance with the mechanically interlocking interface. However, this represents a small fraction of the material combinations that could exist. These material combinations would need to be evaluated, and the design of the interlocking features would be optimized to maximize part performance and manufacturability. At the same time, the broad range of material combinations tested led to a smaller subset of the performance characteristics being measured. The tensile strength of an interface is just one of many mechanical properties needed to design a part adequately. While tensile properties can provide valuable information for screening material combinations, more work is required to fully characterize the interfacial properties of any material combination that will be implemented. Developing a simulation model to predict performance can accelerate the optimization process for these different materials. As increasing levels of test data are gathered to verify model accuracy, confidence in the model's ability to predict performance will improve. There are also opportunities for further research into methods for creating multi-material parts consisting of materials that are challenging to bond, like PP, HDPE, or even ultra-high molecular weight polyethylene. While structural bonds for multi-material parts were achieved with these materials for the first time in a hybrid manufacturing environment, there are further opportunities to improve the bond performance.

One approach may be to add carbon fiber or other reinforcement material to help control the material contraction during solidification. This may also improve the printability of these materials in the open environment often used on large-scale BAAM systems. Using DED or other AM approaches to engineering porous structures or using foamed metal may present an opportunity to scale down the interlocking feature size without incurring the increased challenges with micro-machining. Additionally, depositing materials that are challenging to mill, like titanium, may present a more economical approach to producing interlocking features. There are opportunities to explore the space of multi-material parts made from foamed metals and UHMWPE for biomedical applications.

The operator-focused approach to transitioning hybrid manufacturing automation into job shop manufacturing environments presents several opportunities for further research. While the approach presented is based on HCI and HRI research found in the literature and implemented in a manufacturing environment through the case study presented here, this research does not quantify the effect this approach has on the outcome in production. Further research is needed to measure the effectiveness of this approach to quantify the impact on adoption, satisfaction, and performance in a production environment. A full implementation of the system designed in the case study would further support the approach presented. While this work presented WAAM parameters developed for low carbon steel, there are opportunities to improve productivity through full implementation of pulse spray transfer or high deposition rate technologies like Hyperfill Twin Mig from Lincoln Electric. Arc-welding technologies with multiple wires allow for alloying on the fly during deposition and may provide opportunities for adding features to castings in addition to simply filling excavations. However, switching to these processes would require adjusting the parameters. In addition, job shop steel foundries frequently adjust the alloy being cast, which could require changing the welding wire on the automated welding system and adjusting process parameters. The welds must also be certified to meet the appropriate standards and specifications, which could require tuning the parameters and toolpaths.